DEPARTMENT OF ELECTRONIC AND ELECTRICAL ENGINEERING

Performance Analysis and Centralised Optical Processing in Next Generation Access Networks

A thesis submitted for the degree of Doctor of Philosophy

Bowen Cao

Department of Electronic and Electrical Engineering

University College London

December 2011

Statement of Originality

I, Bowen Cao confirm that the work presented in this thesis is my own. Where information has been derived from other sources, I confirm that this has been indicated in the thesis.

Signed: _____

Date: _____

Acknowledgements

I would like to express my sincere appreciation to my supervisor Dr. John Mitchell for his guidance, encouragement, patience and advice that he provided me throughout the course of this PhD and during my undergraduate years at UCL. Besides learning his engineering techniques and understanding of the subject, I enjoyed the work and discussions on various issues in this study with him, which proved invaluable. I would also like to express my gratitude to Professor Izzat Darwazeh, Dr. Darren Shea and Dr. Manoj Thakur for their advice and support along the way. It is been a great pleasure to work with Dr. José Manuel Delgado Mendinueta and Dr. Benn Thompson in our collaboration. I would like to give special thanks to all members and colleagues in the Communications and Information System Group and Optical Networks Group of UCL Electronic and Electrical Engineering department for their friendship, support, as well as creating the most enjoyable research environment.

On a personal level I would like to extend special thanks to my parents and friends for their encouragement, support and understanding.

Abstract

The Next Generation Passive Optical Network (NG-PON) is currently being standardised and developed, with a goal to achieve higher bandwidth at 10Gb/s, greater capacity at thousands of users and longer backhaul reach at 60km or 100km. The aim is to provide cost effective solutions for telecom operators to vastly deploy optical access networks, enabling customers with the benefit of the greater bandwidth and wider range of services.

This thesis presents research that has identified and addressed various design issues relating to next generation access networks. Interferometric noise may be present in future, ring based, access networks which utilise WDM and OADMs. Simulation and experiment results are presented which studies the performance tolerance to not-precisely-defined wavelength, in the presence of interferometric noise. The impact of receiver electrical filtering was also investigated.

The next generation access network will, in the upstream direction, use burst transmission and are likely to need a large tolerance to wavelength drift due to the low cost equipment used at the customer's premises. A demonstration of optical burst equalisation was presented, based on SOAs. This study also explores the possibility of reducing the SOA saturation induced non-linear distortions through simulations and experiments.

As an extension to the optical burst equaliser and to remedy the saturation induced distortions, an intermediate site optical processing system was proposed. This solution not only performs burst-mode wavelength conversion at 10 Gb/s, but also pre-chirps the signal to allow long-reach transmission and suppressed level fluctuation to ease the requirements on the burst-mode receiver. As a result, a proof

of concept 10Gb/s Wavelength Converting Optical Access Network (WCOAN) with up to 62km DWDM backhaul is experimentally demonstrate. It is designed to consolidate drifting wavelengths, generated with an uncooled laser in the upstream direction, into a stable wavelength channel for DWDM long backhaul transmission.

Table of Content

List of Figures

List of Abbreviations

2R	-	Regeneration & Reshaping
3R	-	Regeneration, Reshaping and Retiming
ADSL	-	Asymmetrical Digital Subscriber Line
ASK	-	Amplitude Shift Keying
ATM	-	Asynchronous Transfer Mode
AWG	-	Arrayed Waveguide Grating
BER	-	Bit Error Rate
BERT	-	Bit Error Rate Tester
BM	-	Burst Mode
BMR	-	Burst Mode Receiver
BPON	-	Broadband Passive Optical Network
CDM	-	Code Division Multiplexing
COPU	-	Centralised Optical Processing Unit
CW	-	Continuous Wave
CWDM	-	Coarse Wavelength Division Multiplexing
DBMRx	-	Digital Burst-Mode Receiver
DCA	-	Digital Communications Analyser
DFB	-	Distributed Feedback (Laser)
DUT	-	Device Under Test
DWDM	-	Dense Wavelength Division Multiplexing
EAM	-	Electro-Absorption Modulator
ED	-	Error Detector
EDFA	-	Erbium Doped Fibre Amplifier
EPON	-	Ethernet Passive Optical Network
ER	-	Extinction Ratio
ESA	-	Electro Spectrum Analyser
FEC	-	Forward Error Correction
FFT	-	Fast Fourier Transform
FPGA	-	Field-Programmable Gate Array
FTTC	-	Fibre to the Curb
FTTH	-	Fibre to the Home
FTTX	-	Fibre to the Node, Curb, Building, or Home
FWHM	-	Full Width at Half Maximum
FWM	-	Four-Wave Mixing
GPON	-	Gigabit Passive Optical Network
HDTV	-	High Definition Television
IEEE	-	Institute of Electrical and Electronics Engineers
IFFT	-	Inverse Fast Fourier Transform
IN	-	Interferometric Noise

ISI	-	Inter-Symbol Interference
ITU	-	International Telecommunication Union
IPDR	-	Input Power Dynamic Range
LAN	-	Local Area Network
LCA	-	Light-wave Component Analyser
MZ	-	Mach-Zehnder
MZI	-	Mach-Zehnder Interferometer
MZM	-	Mach-Zehnder Modulator
NG-PON	-	Next Generation Passive Optical Network
NRZ	-	Non-Return to Zero
OADM	-	Optical Add-Drop Multiplexer
ODN	-	Optical Distribution Network
OEO	-	Optical-Electrical-Optical
OFDM	-	Orthogonal Frequency-Division Multiplexing
OLT	-	Optical Line Terminal
ONU	-	Optical Network Unit
OOK	-	On-Off Keying
OSA	-	Optical Spectrum Analyser
OSNR	-	Optical Signal-to-Noise Ratio
PCB	-	Printed Circuit Board
PDF	-	Probability Density Function
PIN	-	Positive-Intrinsic-Negative (as in p-i-n junction)
PLANET	-	Photonic Local Access Network
PMD	-	Polarisation Mode Dispersion
PON	-	Passive Optical Network
PRBS	-	Pseudo Random Bit Sequence
Pre-amp	-	Pre-Amplifier
PPG	-	Pulsed Pattern Generator
RF	-	Radio Frequency
RN	-	Remote Node
Rx	-	Receiver
RZ	-	Return to Zero
SMF	-	Single Mode Fibre
SNR	-	Signal-to-Noise Ratio
SOA	-	Semiconductor Optical Amplifiers
SOA-MZI	-	SOAs in a Mach-Zehnder Interferometer configuration
SPM	-	Self Phase Modulation
SSMF	-	Standard Single Mode Fibre
TDM	-	Time Division Multiplexing
TDMA	-	Time Division Multiple Access
TIA	-	Trans-Impedance Amplifier

Tx	-	Transmitter
WC	-	Wavelength Converter
WC-PON	-	Wavelength Converting Passive Optical Networks
WCOAN	-	Wavelength Converting Optical Access Network
WDM	-	Wavelength Division Multiplexing
WDMA	-	Wavelength Division Multiple Access
WDM-PON	-	Wavelength Division Multiplexing Passive Optical Networks
XGM	-	Cross-Gain Modulation
XG-PON	-	10 Gb/s Passive Optical Network
XPM	-	Cross-Phase Modulation

Chapter 1. Introduction

Passive Optical Networks (PONs) are currently being trialled and deployed around the world while next generation access network technologies are in the process of being developed and standardised, driven by new bandwidth hungry application and services in both the upstream and downstream direction such as three-dimensional ultra-high definition television delivery, user generated content, video-on-demand and peer-to-peer unicast services [1].

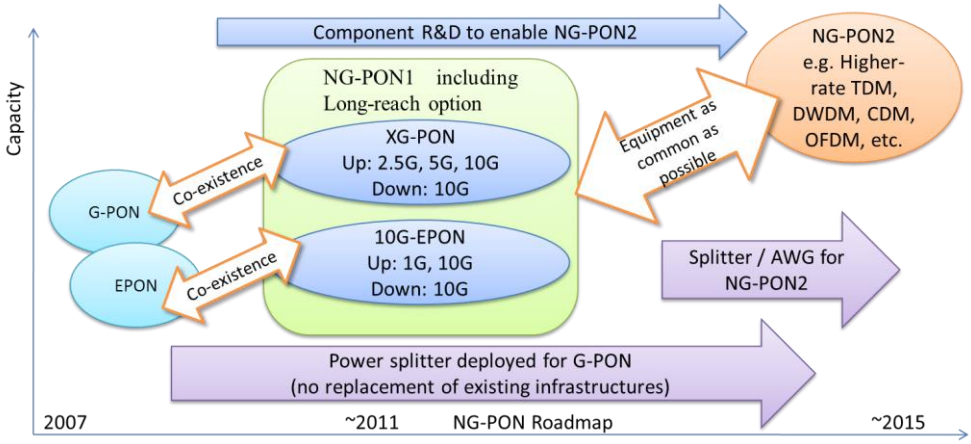

Figure 1.1 NG-PON current status and roadmap, based on [2, 3]

The international standard development organisation ITU-T is drafting Next Generation Passive Optical Network (NG-PON) standards. In the development road map for PON [4], as shown in Figure 1.1, two generations of the NG-PON systems were proposed by the ITU-T, the first generation is the 10Gb/s PON (XG-PON), focus on co-existing with currently deployed Gigabit PON (GPON), which could deliver much higher data rate at 10Gb/s while maintaining the same optical distribution network (ODN). At present, there are still debates about what technology will be adopted by NG-PON2, which considers a variety of technologies, which includes, but not limited to: higher line rate TDM, DWDM, CDM, and OFDM [5, 6]. These new systems are either not compatible with the existing PON distribution architecture or would require a significant change in the optical infrastructure that are not yet commercially available or viable to deploy at the time of this investigation. It was expected that full WDM-PON will be a highly possible candidate[7] for NG-PON2 and hybrid TDM/WDM PON will be a logical upgrade path for bridging the deployed TDM-PONs and future WDM-PONs [8]. Since 2006, the IEEE P802.3av task force have also been working on their next generation of Ethernet PON (EPON) called the 10G-EPON [9], this standard has now been published and the project so far has been driving progress in developing burst mode and more sensitive receivers, as well as high power sources research and development. It has been suggested that the NG-PON and 10G-EPON may eventually converge, at least at the physical level, further reducing the capital cost at deployment by the increase of manufacturing volume [10].

The key challenge for next generation access technologies such as Wavelength Converting Optical Access Network (WCOAN) and hybrid TMD/WDM PON is to offer diverse upstream wavelengths available for each PON

segment while having a single customer's Optical Network Units (ONU) type, or "colourless" ONUs that use low-cost, non-temperature controlled components that are subject to temperature dependent wavelength drifts within a standard defined ±10nm window. The cost can be further reduced by stacking multiple TDM point-to-multipoint PON links onto a WDM backhaul, forming a hybrid TDM/WDM PON for increased equipment sharing and consolidation of the access/metro network.

The topologies of a TDM/WDM PON can be ring based or tree based. A ring access network [11, 12] is where multiple PON ODNs are linked by optical add drop multiplexers (ODAM) in remote nodes, forming a WDM ring which is connected to central office Optical Line Terminal/Termination (OLT). There are important differences between this type of access network and the core, as a result of the desire to minimise capital expenditure in deployment, wavelength tolerance and filter leakage are expected due to the low cost components used. The lower isolation of the OADM will lead to increased crosstalk, between the dropped wavelength passing through the filter leakage and the added signal. This can cause unwanted interferometric noise (IN) when the leaked and added channels are at the very closely tuned wavelength. Although system performance in the presence of IN has been analysed for the core, where wavelengths are typically well defined, in the access network, where lasers wavelengths are not so well defined, the issue is slightly different and an investigation of the effects of closely (but not precisely) tuned wavelengths is needed.

Alternatively, the multiple PON ODNs can be aggregated via an intermediate or exchange site, in order to seamlessly integrate them into a DWDM backhaul. Core networks achieve this by making use of stable wavelengths, high gain fibre

amplifiers and optical switches, while in access, passive power splitters are currently used for cost considerations. In the downstream direction, the signal is multicast to all users as this adds the ability to transmit a separate wavelength for the video broadcast overlay. In the upstream, however, the aggregation of multiple PON becomes complicated. The wavelengths of the ONUs will need to be consolidated so that each PON segment can have a WDM wavelength assigned to it, therefore, one physical backhaul can have multiple logical point-to-point links. A potential solution is to use all-optical wavelength conversion [13] or some form of optical processing for transparent integration. Such a system can avoid the need for electronic signal processing in an optical-electrical-optical conversion stage, keeping the system simple. In addition, processing in the optical domain allows multi-rate PON segments to be supported. Such a proposed concept system is illustrated in Figure 1.2, the inclusion of intermediate site optical processing capabilities means that the transmitter wavelength drift due to the un-cooled laser has no effect on system performance as it is converted to a stable wavelength. Furthermore, the unequal received burst power due to the passive optical splitters and near-far ranging is levelled by the burst equalisation part of the optical processing unit. As a final point, the chirp and dispersion limited backhaul reach at 10 Gb/s line-rate can be addressed by negatively chirping the wavelength stabilised and power levelled output signal, which is also accomplished in the optical processing unit.

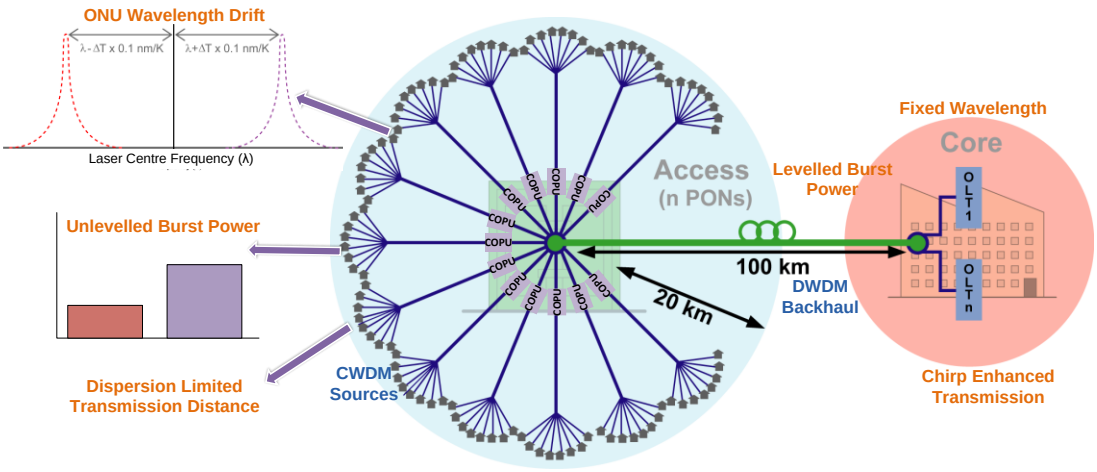

Figure 1.2 Wavelength conversion optical access network (WCOAN) with intermediate optical processing to stack multiple PON segments onto a DWDM backhaul

The challenges and performance considerations of these novel optical access network architectures are different from that of the core network. The temperature dependent ONU wavelengths with a possible drift of ±10nm, limited and uneven optical power levels, power and dispersion limitations to backhaul distance and the bursty nature of the upstream transmission have to be taken into account when studying the next generation access network. Additionally, these systems are required to operate at 10Gb/s in both upstream and downstream, with up to 60 or 100 km long backhaul distance while being dispersion tolerant for transmission. In both 10Gb/s ring and wavelength converting access network scenarios, optical amplification is required to increase the power budget of the overall system for long-reach [14], optical burst equalisation based on these amplifiers may be used to reduce the burst-to-burst power dynamic range requirement in 10Gb/s burst mode receivers.

Ultimately, the major factors that are key to the successful deployment and operation of the optical access networks are still the same, they include: the cost-efficiency of the technology; the consumer demand for bandwidth and the bandwidth available; the service framework telecom operators able to offer on the transmission

medium and solutions to various technical challenges. These factors are applicable to both the ring and tree type network topologies of next generation access, and the problems to be solved in these next generation networks are outlined below.

In ring access networks, WDM is achieved using OADMs at the remote nodes, which are connected via fibre rings to the central office. This type of network is considered in Chapter 3, also taking into account imperfections in devices (e.g. filter leakage) and component tolerance (e.g. source wavelength tolerance) common in cost-sensitive access networks. As a result of these new considerations, the impact of interferometric noise in access network need to be re-evaluated, because closely but not precisely tuned wavelength need to be considered, not as in core network where the wavelength is strictly defined.

From the network operator's point of view [7] of classic tree topology PON, it is highly desirable to fully exploit and re-use the existing, investment in fibre infrastructure to fully exploit existing ODN, as well as enabling the use of low cost components. This is the main motivation for investigating optical processing at the exchange site, which is carried out in Chapter 4 & 5. The intermediate site centralised optical processing capability does much more than just optical amplification, the wavelength conversion stabilises ONU laser wavelength drift due to temperature change, enabling low cost ONU lasers to be used at the customers' premises. The burst equalisation capability lowers the power difference (dynamic range) of the bursts arriving at the OLT, which enables low cost BMRx to be used at the OLT site. Overall, the intermediate optical processing architecture also allows the consolidation of access and metro nodes and addition of new services, which are achieved through consolidation of PONs and adding DWDM wavelengths to the

backhaul. This new architecture can potentially lead to significant operational savings by reducing power consumptions and the footprint of the network [15].

Studies and experimental demonstrations have been carried out to solve the technical challenges presented with the next generation access network outlined above. This thesis identified the issues and challenges in NG-PON and addresses them using system designs that co-exist with deployed distribution architectures, at the same time trying to increase system performance and extend reach. The details of the thesis structure and the contributions of this work are presented in the following sections.

1.1 Thesis Organisation

Chapter 2 explains the current status of PON and where the next generation of access network is heading. Literature is reviewed on the topics of SOA modelling, burst equalisation, optical wavelength conversion and the areas of optical access network integration.

In Chapter 3, a theoretical description of the interferometric noise phenomenon in access network is presented. How interferometric crosstalk can be a performance limiting factor in future hybrid TDM/WDM ring based access networks is discussed. Through experiment and validated simulation, the relationship between the BER performance and the electrical filter bandwidth is investigated in terms of varying interferer power and source-to-interferer frequency difference. The chapter concludes with a numerical analysis of the filtering bandwidth on interferometric noise, when the source-to-interferer frequency is more than 5GHz.

Chapter 4 reviews the SOA saturation characteristics and non-linear phenomenon that occur at deep saturation. A theoretical dynamic model of the SOA was constructed and compared, in order to explore the possibility of using the non-

linear saturated SOA as a limiting amplifier to equalise bursts for future access networks, to enable low cost receivers to be used. Spectral broadening and output signal distortion due to chirping is predicted through simulation and confirmed via experimental demonstration. The performances of optical filtered chirped signals are investigated through simulation and experiment.

Chapter 5 begins by describing the need for integrating multiple Coarse-WDM (CWDM) PONs into a Dense-WDM (DWDM) long-reach backhaul to form a wavelength converting optical access network (WCOAN) with all-optical centralised processing at the intermediate exchange site to consolidate wavelength, equalise burst and regenerate signals long distance dispersion tolerant transmission. Then a characterisation of the centralised optical processing unit was given, followed by a experimental demonstration of the long-reach WCOAN and the performance of such a system under continuous- and burst- mode operations were analysed.

Chapter 6 concludes the thesis and gives suggestions for future work.

1.2 Contributions and Publications

The research reported in this thesis has presented demonstrations and analysis on various performance related issues that are present in next generation access networks. The main contributions of the thesis can be categorised in two main areas and are summarised below:

Interferometric noise in hybrid WDM TDM ring based access networks

- Evaluation through experiment and simulation the relationship between BER performance and filtered interferometric noise for various levels of interferer power, in the context of 10Gb/s ring based access network, where not strictly defined wavelength as a factor is being considered for the first time.

- Developed an analytical model to assess the impact of receiver filter bandwidth on interferometric noise, where frequency/wavelength separations between the interferer and data signals are subject to wavelength drift. Key parameters for choosing the receiver filter bandwidth were identified.

Centralised optical processing for burst power equalisation, wavelength conversion and reach extension in next generation access network with a long DWDM backhaul

- Created and implemented a SOA model for the dynamic simulation of both time and frequency domain signal characteristics that operated into the deeply gain saturated region, based on comparisons, analysis and adjustment of two existing SOA theories. The simulated gain characteristics of the SOA were also verified by experiment.
- Analysed the performance of burst equaliser based on a saturate SOA by simulation. Successfully simulated the saturation induced non-linear effects of the equalised output burst, which affects system performance but have not been considered in previous studies in this area. These non-linear effects are also observed experimentally.
- First experimental demonstrated of a dual SOA optical burst equalisation system for burst-mode transmission in PON. Results were analysed together with the effect of optically filtering of the output signal to reduce saturation induced distortion.
- First demonstration of a XPM wavelength converter in a burst-mode access network, showing a 10Gb/s error free converted signal over a 60km backhaul without dispersion compensation. The converted signal performance is

significantly improved when compared to previous XGM wavelength converters.

- Developed and characterised a novel centralised optical processing unit (COPU) capable of consolidating multiple multi-rate CWDM PONs into a DWDM backhaul with extended reach. This distinct COPU configuration increased the input power dynamic range of the XPM wavelength converter while significantly reduced the spectral broadening non-linear effect of the burst equaliser.
- First experimental demonstration of a burst-mode wavelength converting optical access network upstream with centralised optical processing capability. The proof-of-concept system is able to consolidate wavelength, equalise burst power, regenerate and pre-chirp the output signal for long distance backhaul transmission.

The research work has resulted in the following publications listed below:

1. B. Cao, J. E. Mitchell, "Performance of Ring Access Networks in the Presence of Interferometric Noise" , in *Proceedings of the 10th International Conference on Telecommunications (ConTel)*, pp.293-297, Zagreb, Croatia, Jun. 2009.
2. B. Cao, J. E. Mitchell, "Optical Burst Equalisation in Next Generation Access Networks", *Proceedings of the London Communications Symposium (LCS)*, paper No. 43, Sep. 2009.
3. B. Cao, J. E. Mitchell, "Modelling Optical Burst Equalisation in Next Generation Access Network", *12th International Conference on Transparent Optical Networks (ICTON)*, pp. Th.A2.3, Jun. 2010

4. B. Cao, D. P. Shea, and J. E. Mitchell, "Wavelength converting optical access network for 10Gbit/s PON," *15th International Conference on Optical Network Design and Modelling (ONDM)*, pp. 1-6, Feb. 2011.

5. B. Cao, J. M. Delgado Mendinueta, J. E. Mitchell, and B. C. Thomsen, "Performance of an optical equaliser in a 10 Gbit/s wavelength converting optical access network," in *Proceedings of the 37th European Conference and Exhibition on Optical Communications (ECOC)*, Geneva, Switzerland, Sep. 2011.

6. B. Cao, J. M. Delgado Mendinueta, J. E. Mitchell, and B. C. Thomsen, "Performance of an Optical Equaliser in a 10Gbit/s Wavelength Converting Optical Access Networks", poster at *EPSRC Communications and Networking workshop in photonic communications*, Oxford, UK, Sep. 2011

7. J. M. Delgado Mendinueta, B. Cao, B. C. Thomsen, and J. E. Mitchell, "Performance of an optical equalizer in a 10 G wavelength converting optical access network," *OSA Optics Express*, Vol. 19, Issue 26, pp. B229-B234 (2011)

Chapter 2. Literature Review

Fibre-to-the-home (FTTH) has long been envisaged as an attractive solution for delivering high speed broadband services to customers. Now, the demands for Broadband Internet, three-dimensional High Definition Television (3D HDTV) and Internet Protocol (IPTV) based video-on-demand/peer-to-peer services have accelerated the deployment of optical access networks around the world. In the UK, major telecom operators and a few new technology start-up companies are planning trials [16] and deploying FTTH services in some new housing developments.

PON is a very cost effective and energy saving technology for bringing fibre access technology to homes. It uses a new point to multipoint architecture instead of today's copper point to point architecture, so that the costs of the backhaul section are shared by a large number of customers. Furthermore, since the network uses significantly smaller active local exchanges and greatly reduces the need for signal repeater equipment, the real estate and equipment saving would be a huge benefit for

operators and the energy saved from using passive architectures will also be beneficial to the environment.

However, there are still some factors that prevent the full scale deployment of PON. Largely due to the high civil engineering cost associated with investing and deploying fibres infrastructures. Also, the bandwidth of the backhaul is not fully utilised due to the current low data transmission rate implemented in these optical access networks. As a result of the capital expenditure considerations, many problems arise in access network from the need to use lower cost components with a relatively poorer figure of merit than those being used in the core networks. Due to the temperature dependent uncooled low cost lasers used in the ONUs, the access network lasers' wavelength stability is not guaranteed or not as strictly defined as would be typical in the core network, in access only a ±10nm wavelength window is defined, which is considered as a Corse WDM (CWDM) definition. Low cost OADMs are likely to have lower isolation, leading to increased interferometric noise due to crosstalk between the dropped and added wavelength. Burst mode receivers that have large dynamic range and short threshold setting times are required for 10Gb/s access networks [17]. Optical components such as SOAs are well known for their optical transparency and quick response time to input signals when compared to optical-electrical-optical (O-E-O) technologies. If processing functions such as burst power levelling could be done optically, this would reduce the burst mode receiver complexity significantly. The transparent consolidation of multiple CWDM PON segments into a DWDM long-reach backhaul could also be possible with optical wavelength conversion technologies.

The key technologies to address these issues are review in the following sections. This chapter aims to provide an introduction to the state-of-the-art PON in

section 2.1. An in-depth introduction to the current burst equalisation methods is presented in section 2.2. The possibility of optical burst equalisation is also being considered, highlighting the non-linear behaviour of the SOA when it is in high gain saturation. Finally, an overview is presented on the topic of Wavelength Converting Optical Access Network (WCOAN) for future long-reach access architecture in section 2.3.

2.1 The State-of-the-art PON

Passive optical networks are an important concept towards full optical access networks. Currently the most deployed PON technologies are the ITU-T GPON and IEEE EPON [13]. The 'tree and branch' topology of PONs contains only passive components from the local exchange to the customer's premises including passive splitters and optical fibres [18]. The resource in the local exchanges, the backhaul and the central office OLT are shared by all the customers connected to the exchange. Since all the data processing will be done at the OLT, the equipment required at the exchange site will be significantly reduced, in the way that a single setup of PON equipment can replace a large number of customer line cards in a point-to-point copper network [19]. The power requirement to supply the exchange will also be significantly reduced. An even more important property of the PON access network is that it is optically transparent from the customer's premises all the way to the OLT. Such end-to-end transparency will allow easy upgrades in the future by using higher bandwidth transceivers and adding additional wavelengths.

In 2009 and 2010, the IEEE and ITU-T have published the 10G-EPON and XG-PON [20, 21] standards, which are enhanced versions of GPON and EPON that provide 10Gb/s maximum line rates. An important feature in these new standards is

the ability to upgrade the deployed PON systems with minimal disruption to existing users. The development road map of NG-PON is illustrated in Figure 1.1.

Initially, the standardisation of XG-PON or NG-PON1 considered many possible candidates each with different architecture and service profile, among these are reach enhanced version of XG-PON and hybrid WDM/XG-PON through the use of wavelength seeding [2]. Although these technologies were deemed too forward looking for XG-PON and not selected at the time for NG-PON1, they can be considered for NG-PON2 which is the next generation of access technologies.

True WDM-PON is an attractive technology for NG-PON2 with many potential applications. The virtual point-to-point connectivity of WDM-PON allows efficient use of fibres already deployed greatly reducing the need for new fibres or the building of new fibre ducts. From the network operator's point of view [7], it is highly desirable to fully exploit and re-use the existing, investment in fibre infrastructure, so that hybrid PON that combines the TDM and WDM approaches is a promising solution for long-reach high data-rate access networks [22]. Future access technologies will also be expected to utilise high split ratios to increase the number of users, extend the transmission distance to cover a larger service area, offer higher bandwidth in order to satisfy the consumer needs and allow the room for extra services for network operators. Some of these properties were proposed and demonstrated by the long-reach optical access network [14], wavelength converting access network [13] and the European Union project PIEMAN [23]. These all aimed to combine the access and metro networks into one all-optical system to reduce the number of network elements and access/metro interfaces. The capacity can also be radically increased by using DWDM. Additionally, through the use of an extended backhaul fibre, possibly up to 100km (allows full coverage of the UK) in length

rather than the usual 20km, the physical reach is also being increased. Such new types of network can potentially lead to significant operational savings by reducing power consumptions and the footprint of the network [15].

Long-reach PON that uses wavelength converters to integrate CWDM PONs into a DWDM backhaul [13] was developed at University College London. The key objective of this work is to keep existing uncooled ONU lasers in the customer's premises to reduced cost of re-deployment. The temperature dependent wavelength drift of the ONU lasers is stabilised via a wavelength converter (WC) in the local exchange. A cooled DFB laser or wavelength tuneable laser can be used to pump the WC, therefore, each PON distribution segment is assigned a fixed wavelength for the DWDM backhaul. The advantages of this architecture include the potential to integrate both existing and newly deployed PON segments through WDM, serve a large number of users and maximise equipment sharing. In this work, the wavelength converter used was based on Cross-Gain Modulation (XGM) and the transmitter and receivers used for the performance analysis were only continuous-mode. Better wavelength conversion techniques and the incorporation of centralised optical processing [24] for a 10Gb/s burst-mode Long-reach PON can be investigated, based on this architecture concept.

Another approach to hybrid DWDM/TDM-PON uses a ring based aggregation network [25] with remote nodes (RN) linking multiple TDM access ODNs, for example, the Scalable Advanced Ring-based Passive Dense Access Network Architecture (SARDANA) project [26]. Recent field trails of this technology has demonstrate transmission over a 43km fibre ring with XG-PON line rates and reflective SOA (RSOA) ONU technology [27]. It has shown that this is a

promising solution for NG-PON. The background and impact of interferometric noise in this type of network will be introduced in detail in section 3.2 of Chapter 3.

2.2 Burst Mode Equalisation in PON

2.2.1 Burst mode Transmission

The tree topology of PON enables the PON to use a simple broadcast type downstream transmission, which is also ideal for an additional video broadcast wavelength channel. As for the upstream, burst mode Time Division Multiple Access (TDMA) is required. The ONUs at the customer's premises can only transmit at certain time slots, this result in bursts of optical signals travelling up the fibre towards the OLT receiver.

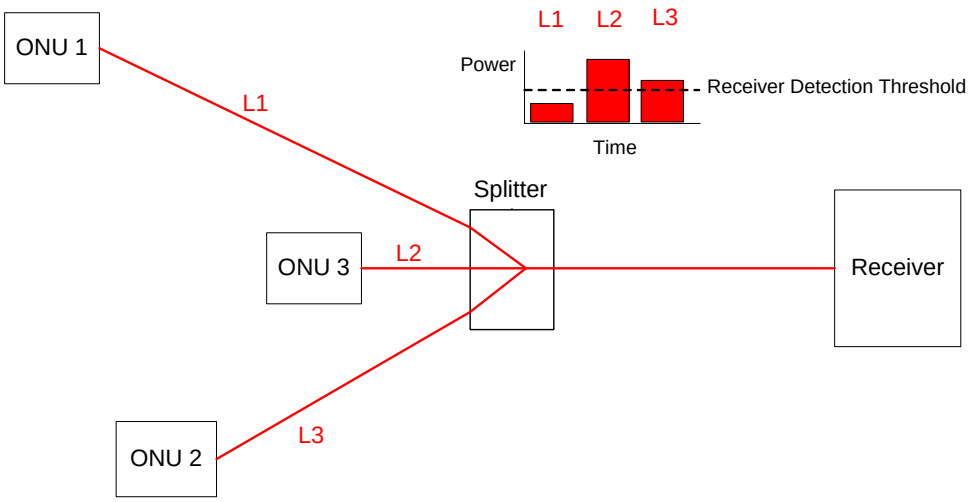

Figure 2.1 Near-far power difference arising from ONUs locates at different distances (L1, L2, L3) to the exchange/splitter

The power of the bursts may vary from burst to burst depending on the split loss and the distance between the ONU and the exchange. The longer distance the burst travelled, the weaker the power it will have when arriving at the receiver, the optical power loss is cause by the attenuation of the signal in the fibre. Standard continuous mode receivers are not designed to adapt to these power variations and phase alignment on a burst-by-burst basis in a nanosecond time scale, especially in

NG-PON where the threshold adjustment time will be even shorter due to the higher data rate. Burst mode receivers (BMR) are available for current 2.5Gb/s GPON, as NG-PON will be at 10Gb/s, the next generation of BMR working at 10Gb/s with fast response times and high dynamic range is either not yet available commercially [28] or not currently cost effective to deploy. The 10Gb/s BMR's complexity and high cost may be reduced if a burst equalisation scheme was employed at the local exchange or just before the OLT. If the power variations can be optically equalised, it will allow the standard receivers to be used, further reducing the cost of the access network. In the current generation of GPON systems, a power-levelling mechanism that allows the OLT to inform the ONU to adjust their output power exists [29]. However, since GPON is based on 64 users per OLT, the 6dB dynamic range of the current OLT controlled power adjustment mechanism will not be sufficient for the next generation access networks with both greater number of users and the much higher near-far dynamic range.

2.2.2 Burst Equalisation Techniques

In the research towards next generation access, several burst equalisation schemes has been proposed. They belong to three main categories of methods, which are electronic burst equalisation, electronic controlled optical burst equalisation and all-optical burst equalisation.

Electronic burst equalisation is usually integrated with the receiver in the OLT, they are often refer to as burst mode receivers (BMR). In conventional receivers, the receiver's input is ac-coupled, it provides high sensitivity for the receiver but the coupling capacitor's charging and discharging time prevents the received signal amplitude to vary rapidly with time. Therefore, the threshold setting of the receiver is fixed. BMR's input is dc-coupled, allowing it to have an adaptive

threshold that must adapt to the amplitude of the received signal in the scale of nanoseconds [30]. Recently, researchers [31] have demonstrated experimentally a BMR capable of operating at 10Gb/s with or without the aid of Forward Error Correction (FEC), the dynamic range achieved are 17.8dB and 22.8dB with FEC applied. The high performance BMR are very useful in future access networks, but currently they are usually expensive to manufacture due to the utilisation of fast Analogue to Digital Converter (ADC) and Digital Signal Processing (DSP) chips designed for the specific type of signal formats. The other drawback of BMR is that when the optical network is upgraded to a higher data rate, the equalisation component will need to be upgraded along with the receiver, adding a further maintenance cost to the network operators. Though the shortcomings of electronic BMRs may be overcome by increased performance and lowered cost in electronic signal processing in the future, optical equalisation may aid the performance or reduced the cost of BMR, especially in access network where lower cost components are usually preferred for earlier rollout of large scale services.

Electronic controlled optical burst equalisation was also suggested, one technique employed FPGA control electronics for tracking the power of the incoming burst and controlling the gain of the SOA [32]. Such a system is designed to be very useful in the long distance transmissions where the signals need to be regenerated, retimed and reshaped. However, for access networks which is usually less than 20km it may not be necessary since it is electronically complex. It also used RZ line coding for making the signal less susceptible to Inter Symbol Interference (ISI) due to dispersion effects, but that will not be compliant to the NRZ line coding used in current PON standards, which is easier and cheaper to generate thus keeping the ONU cost low. Another solution combines the electronic SOA gain controller

with high performance BMR achieved 7dB burst equalisation using NRZ coding [33]. The proof of concept system that clamp the gain of the SOA by monitoring the input optical power was also presented [34], this method has the benefit of controlling the gain saturation induced distortions, however, the electronic controlled attenuator has a rise and fall time of 50μs and 20μs respectively. These relatively long rise and fall time will require longer guard time and burst overhead for the power to adapt, considering the GPON upstream burst size is only 125μs [29], therefore, the total throughput of the system may be reduced. Though the above solutions are very attractive for high end core network burst switching, they will be less attractive for PON access network because of the higher cost, standard definitions, complexity and power requirements.

An all-optical approach to burst equalisation will be attractive for access. It simplifies the power equalisation system by reducing electronic controls to the minimum or none. An all-optical process will also be attractive for bit rate independent operation and the benefit of optical transparency, meaning future upgrades to the network will be simpler. They can also be placed in the exchange or split sites because of the reduced complexity and size. The equalised burst also mean that the receiver at the OLT can be a less complex, less expensive, reduced dynamic range burst mode receiver, or, even a conventional receiver can be used.

A method was proposed to use an all-optical approach for re-amplification and re-shaping the signal [35], this scheme is designed for packet switching systems in the core network and high performance all-optical processing, it uses a monolithic integrated wavelength converter, a XGM SOA, a gain saturated SOAs and a CW laser to achieve a 8dB equalisation in burst power. The scheme's idea was to use the XGM SOA to wavelength convert part of the incoming signal to an inverted-mode

signal, then apply it to the gain saturated SOA together with the input signal to keep the average input power to the SOA constant in order to suppress the gain modulation, avoiding nonlinear effects in gain saturation [35]. The study of the performance of SOA in deep saturation was carried out in [36], this paper compared the performance of the different modulation formats when SOA are used as a power booster or limiting amplifier, it concluded that the RZ-DPSK format have the least performance penalty. While RZ-DPSK modulation format can be considered in future access networks, the current cost limitations for the colourless ONU will not consider complex modulation scheme yet, direct modulated NRZ on off Keying is still the preferred format and it was standardised in GPON and XG-PON.

Burst levelling using a saturated EDFA as a limiting amplifier was proposed in [37]. However, since the gain recovery required in a 10Gb/s access network is in the nanosecond scale, the 110 to 340μs EDFA gain recovery time is not fast enough [38]. Therefore, a burst equalisation scheme based on SOA seems logical because of its simpler structure and faster gain recovery time. Recent research and proposed future access network technology roadmap [4, 39] also indicate that active components such as optical amplifiers will be placed in the exchange site of PON as reach extenders. Therefore, these active optical amplifiers will be part of the network and they can be used in all-optical burst equalisation with the minimal modification done to the network. In existing literatures, simulations were performed on the idea of using a saturated SOA as a limiting amplifier to perform bursts power equalisation [40, 41]. While the paper [40] showed a similar concept setup, the result it showed was only the gain curve and power output of the SOA, time domain and spectrum simulation results were not available which is useful for analysing the nonlinear effects at gain saturation, the experimental Extinction Ratio (ER) also did not agree

with the simulated ER performance. The second paper [41] also presented a similar concept in simulation that achieved a reduction of 16.2dB in burst power difference. It claims the ER penalty was too high for low recovery time which is less than 1.6ns, further simulations were performed using a saturated SOA recovery time of 9.6ns. In real SOAs the recovery time is in the range of 0.2ns to 0.3ns, because of the longer gain recovery time was used, the gain was assumed to be unchanged throughout the burst period, thus the rapid gain modulation by the incoming data signal within the burst was not considered, along with the nonlinear effects in the frequency domain [42] as a result of this gain modulation. Therefore, a model that considers gain modulation, the time domain and frequency domain signal characteristics at gain saturation is required to fully and correctly model the burst equalisation system.

Overall, the questions to be solved in access network burst equalisation techniques include:

1. Demonstrating a proof-of-concept system by experiment that can perform all-optical burst equalisation. A simple and cost effective solution that is suitable for future access networks is needed, to achieve burst equalisation for the ONUs' near-far power difference problem and analyse its performance in 10G-PON or similar network environment.
2. Creating a simulation model that closely matches the physical characteristics and performance of the SOA in deep saturation, so that it can be used to analyse burst equalisation using a gain saturated SOA as a limiting amplifier, the model will also need to be validated by experiment measurements or known data.

2.2.3 Using SOA as a Nonlinear Device

An SOA is a device similar to the semiconductor laser, its operation is also based on the stimulated emission of photons. In an SOA, the electrons are pumped into the active region via an external current source, most of these electrons with higher energy occupy energy states in the conduction band, leaving holes in the valence band, a condition known as population inversion. The SOA relies on population inversion in the active region to provide gain through the stimulated emission process. The stimulated emission is a mechanism that occurs when a photon with the right energy is incident on the active region, causing stimulated recombination of an electron in the conduction band with a hole in the valence band, the energy lost is emitted in the form of an identical photon. This newly emitted photon will be at the same frequency, phase and direction as the incident photon. The two identical photons together can in turn cause subsequent stimulated emission processes of more identical photons. Such a chain reaction will produce greater number of photons at the output of the amplifier than at the input, hence the gain of the amplifier.

The important factor for stimulated emission to occur on a massive scale within the active medium of the SOA is population inversion, which requires the electrons in the SOA to be electrically pumped to the conduction band. The term unsaturated gain applies when there are enough electrons with sufficient energy to undergo stimulated emission exist in the conduction band to provide amplification to a small signal. Because the pump current is limited, when the input signal is so large that there are an insufficient number of carriers in the excited state, not all the photons in the incoming signal can cause stimulated emissions, then the total gain of the SOA with a large-signal will be less than that of the small-signal case. The SOA

gain is considered in saturation because the rate of carriers to be pumped to the excited state is limiting the rate of photon emissions and therefore, limiting the gain [43].

SOAs therefore, are non-linear devices, often used for signal processing because of its gain saturation characteristics. It can also be used as a device for all-optical power equalisation, also known as the Self Gain Modulation (SGM). In this case, the higher input powers experiences less gain due to the SOA's gain saturation, the lower input powers experiences normal gain so that these different levels of power can be equalised [37].

2.2.4 Semiconductor Optical Amplifier Modelling

The modelling of gain saturated SOA is important in the analysis of burst equalisation performance of the SOA based systems. In the applications discussed in Chapter 3 of this thesis, the SOA model is required to simulate the time domain, frequency domain signal characteristics and gain saturation characteristics, have the following simulation capabilities:

Power and Gain Characteristics - It is required to simulate the SOA in the unsaturated regime and more importantly the saturated regime of operation. This will require modelling the gain and output power characteristics all the way up to the high saturated region in the SOA, to achieve this, the model will need to match the gain saturation experiment result as close as possible.

Gain saturation nonlinear effects - In addition to amplification, SOA also exhibits nonlinear effects when it is in gain saturation. The nonlinearity is the phase modulation of the signal propagating through the SOA, caused by the refractive index change as a result of the carrier density modulation [44]. The phase modulation depends on the input signal power and the amplifier gain. Since the

signal modulates its own phase through the SOA gain saturation, this phenomenon is called Self Phase Modulation (SPM) [42, 45]. The SOA model will therefore, need to simulate SPM at gain saturation.

Sample based - SOA models can be static or dynamic depending on the physical properties being modelled. A static or steady-state model [46] are usually used to model the SOA characteristics with respect to the propagation axis of the waveguide, known as the z dimension, which is the length of the active region in an SOA. The static model is useful for modelling signal independent characteristics of the SOA, such as carrier density profile with respect to active region length. When an input signal is considered, time as a second dimension will also need to be modelled. A dynamic or sample based model is used to simulate the distortions in the SOA that alter the signal bits and resulting in effects such as frequency shifts, since these effects are time dependent. The modelling of SOA in the burst equalisation scenario requires the use of a sample based model, because the time and frequency domain characteristics of the output signal are equally important to observe. A model solved using numerical techniques will be preferred over analytical techniques, since it will be easier to implement in computer based simulations and often applicable over a wide range of operating regime.

A travelling-wave SOA model based on the rate equations and differential equations a widely cited dynamic model of SOA was described by Agrawal and Olsson [42, 45] in 1989. Indeed, many dynamic models developed for SOA analysis are based on Agrawal's theory. It was pointed out by Mecozzi [47] in 1996 as being the only theory available at that time for describing the nonlinearity in gain saturated SOA under pulse condition. The power, phase change, and spectral broadening effects of a pulse propagating through the SOA were analysed by the model.

Agrawal's theory assumes the gain saturation of the SOA only depend on carrier (electron) depletion as a result of stimulated emission.

A later research paper by Mecozzi and Mork [47] reported besides carrier depletion, the gain of a SOA is also depend on the energy distribution of carriers, especially in highly excited semiconductors, the gain saturation due to intra-band dynamics is important, these factors also contribute to gain suppression. They also extended the theory of Agrawal and Olsson by including saturation caused by intraband dynamics in their model. The Mecozzi's model was further developed into a set of analytical equations in [48] to characterise both time and z dimension of the active medium. These analytical equations was then simplified in [49] and turned into a set of ordinary differential equations (ODE) that only depend on the time variable, this was done by integration of the gain over the z direction which is the device length. It made the model easier to implement with computer simulation. However, the carrier distribution along the propagation direction is not considered, therefore, the direction of propagation of the pulse will not make any difference. Agrawal's model will be used in the next chapter for simulating SPM in pulse input, both models will be investigate for their time domain simulation performance and gain saturation characteristics simulation accuracy of the SOA.

2.3 Wavelength Converting Optical Access Network (WCOAN)

The access network bandwidth required by the end user is ever increasing, currently the deployment of access solutions EPON/GPON has begun to gather pace and their successor 10GEPON and XG-PON1 are also being standardised, trailed and deployed. Wavelength Division Multiplexing (WDM), increase bit rate and extended reach architectures [13] is expected to be used in the next generation of optical access technology. The fibre efficiency can be significantly increased by

using Dense WDM (DWDM) operation, as multiple wavelengths spaces at 100 GHz (or possibly 50GHz) apart can utilise a single backhaul fibre.

In PON deployment, the laser in the ONU is a major contributor to the ONU cost. To keep the costs low, ideally the ONU laser will not be temperature controlled and therefore, the wavelength could drift over a range much greater than a DWDM channel. A direct approach to address the temperature dependent drift would be to either use tuneable lasers at the ONU with accurate wavelength locking, or seed wavelengths supplied from the central office which are then modulated at the ONU by a reflective SOA (RSOA) or reflective modulator. Such methods have been demonstrated recently in the EU project PIEMAN [15]. However, this approach would require changing the already deployed ONUs with built-in lasers to the new ones with built-in RSOA, making the transition from 10G-EPON/XG-PON to hybrid WDM-TDM PON economically and logistically more difficult for operators. Furthermore, a fraction of the upstream CW seed wavelengths is reflected back due to Rayleigh backscattering [15], which will interfere with the RSOA modulated upstream signal. The use of a dedicated second batch of access feeder fibre is necessary to eliminate the backscattering noise, but adding feeder fibres also increase the building and material cost of the access sites. From a gradual transition and services roll-out view point, a technique that is backward compatible with existing PON distribution architecture and allows the use of low cost ONUs at the customers' premises would be logistically and economically favoured. If uncooled lasers are to be used in long reach architectures, an efficient backhaul scheme is required to integrate multiple TDM-PONs into a WDM backhaul.

In the future, it is expected that the network consolidation of multiple PONs into a long reach DWDM backhaul will reduce the number of active OLT sites, with

the remaining sites serving a larger number of customers. Such consolidations will lead to longer reach requirements for the backhaul [1]. The optical backhaul distance will increase to >20km and WDM backhauls will likely be used to enable multi-services support and an open business model [50]. The combination of DWDM backhaul and a Time Division Multiplexed PON (TDM-PON) distribution section seem to be promising as it presents the advantage of long reach backhaul, while significant cost saving can be made by allowing the un-cooled, wavelength variable laser sources to be used in the customers' ONU. In standard 10G-EPON or XG-PON, the components used in both upstream and downstream direction are tolerant to wavelength drift of ±10nm without affecting the performance. The wavelength plans are 20nm CWDM bands separating the up- and down- stream. However, when DWDM backhaul wavelength plans are implemented, tight control of wavelength in the backhaul section is compulsory. This is because Arrayed Waveguides Gratings (AWG) will be used to separate and recombine the multiple wavelengths for backhaul transmission. The AWG channels act like multiple optical band-pass filters, if a signal wavelength drifting out of its assigned AWG channel due to possibly a temperature dependent wavelength source, the signal will be lost to the receiver. If the signal wavelength continues to drift, it may also interfere with the signal from adjacent channels, introducing crosstalk noise to the adjacent channel.

Previous work [13] by Dr. Darren Shea at UCL has proposed the use of all-optical wavelength converters to stack multiple TDM-PON wavelength into a DWDM backhaul for 2.5Gb/s GPON. The concept is shown in Figure 2.2 and is an precursor of the proposed solution presented in Figure 1.2.

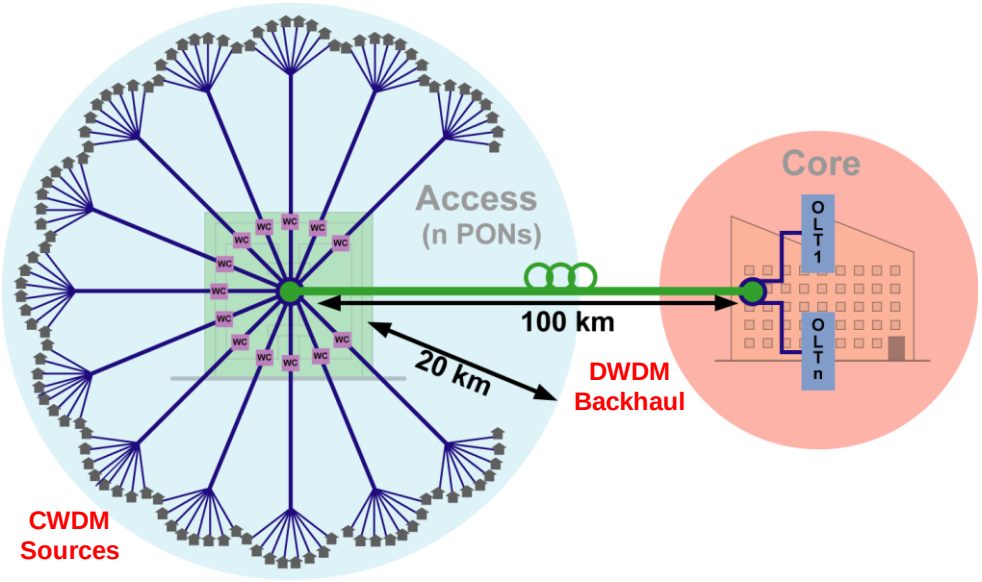

Figure 2.2 CWDM PON distribution section with DWDM backhaul to integrate multiple PON using wavelength converters [13]

The wavelength converter (WC) stabilised the CWDM wavelength from the un-cooled ONU laser source which may have ±10nm wavelength drift. The WC's seed wavelengths are also assigned so that the signals from multiple PON are transmitted through the backhaul, with possible redundant path to prevent accidental fibre cut. Several PONs can be aggregated allowing the backhaul cost to be shared by a large number of customers, increasing the backhaul efficiency and utilisation. A low cost, long-reach optical network combining both access and metro networks can be established through the use of WCs, without significantly changing the standard PON architecture and existing metro backhauls [13].

In the PON distribution section, the signal from the ONU will have to travel through passive splitters to reach the WC at the exchange site. Each 2 way split have an insertion loss of at least 3dB, for example, a 32 way split is 2^5 splits, it will have a loss of 3dB x 5 = 15dB. As a result of the loss in the splitter and the distribution fibre, the signal power reaching the exchange site is very low, thus optical amplifications are required to overcome the signal power loss in the longer reach backhaul.

2.3.1 Optoelectronic Wavelength Conversion

The simplest implementation of wavelength conversion is through the use of optoelectronics. The signal is first received, then electronically processed and finally, re-transmitted. Optoelectronic wavelength conversion is very tolerant to input signal characteristics and can be wavelength independent, because the receiver will turn the optical signal into electrical signals, then the electronic amplification and regeneration of the signals are well established, at least for single change signal data rate transmission up to 2.5Gb/s [51]. However, in the PON upstream, 10Gb/s burst mode transmission is employed, this posed a significant challenge to the optoelectronic wavelength conversion, since the cost of OEO increases rapidly due to the use of burst mode receiver and high bandwidth components. The input signal power dynamic range of optoelectronic wavelength conversion depends on the receiver dynamic range inside the optical-electronic-optical (OEO) device, but as the dynamic range increases, the cost and complexity of the device will also increase. The re-transmission part of the OEO device usually consists of a laser and an external modulator. Since there is no optical transparency between the input and output, no optical filtering is required to cut off the input wavelength. This also rule out the possibility of simultaneous conversion of multiple data rate signals, unless complicated electronics or very fast digital signal processing (DSP) techniques are used to process the high and low data rate signals separately, but doing so will increase the cost rapidly as well.

2.3.2 All-Optical Processing and Wavelength Conversion

All-optical processing of the input signal does not require a receiver or an OEO unit, instead, a non-linear optical element such as SOA is used. The non-linear optical element is transparent to optical signals, it performs optical manipulation of

the signal using optical techniques which do not require electronic receivers. This reduction in detection and processing electronics reduces the cost of wavelength conversion and regeneration. An ideal node would provide all-optical processing, including wavelength conversion which is able to map the wavelengths from multiple CWDM (20nm channel) ONUs onto a set of stabilised DWDM (100GHz channel or possibly 50GHz) ITU grid wavelengths for transmission over the backhaul fibre, which may consist of dual fibres. This approach reuses current core fibres and may or may not include amplification in the backhaul.

All-optical processing methods have been proposed for and used in core networks. A burst mode capable, 3R regeneration system was studied in [52]. The system used four cascaded SOA-MZI switches to achieve error-free reception when the input bursts have 9dB power variation. This study was based on optical packet switching networks, where the wavelength is fixed, therefore, the wavelength drift of the input signal was not considered. It used RZ modulation format that is not suitable for PON because it does not comply with the standards of PON which uses NRZ format. The 3R required 4 stages of SOA-MZI and thus 4 SOA-MZI devices were used, hence the system is expensive and too complicated for a simple and low cost exchange site processing unit required in WCOAN. In the case of a wavelength converter in the access network it is planned to analyse the performance of a single SOA-MZI device since the re-timing, decision and de-multiplexing stages in packet switching [52] are not necessary in the exchange site processing unit.

A study demonstrated the multi-wavelength conversion of 10Gb/s NRZ and RZ signals using SOA-MZI device for wavelength conversion [53] showed that the wavelength dependency power penalty of this device was as low as 1.4dB, for eight wavelength ranging from 1552.52 to 1558.98 nm. This study was demonstrated the

conversion of 10Gb/s NRZ continuous mode signals in a metro network setup, using only one SOA-MZI device. Instead of analysing the input signal wavelength drift, it analysed the performance of modulating the signal on to multiple CW seeding wavelengths to achieve multi wavelength multicast. Therefore, the wavelength dependency study was only carried out for the probe wavelength, though it would be beneficial to also analyse the performance penalty due to the input signal wavelength drift. The input signal to the WC in PON will be the signal from the ONUs in the customer's premises, which are optical bursts.

Several all-optical wavelength conversion technologies were reviewed in [51], including coherent and in-coherent techniques. The coherent techniques such as four wave mixing (FWM) and difference frequency generation (DFG) preserves the phase information but do not provide regeneration of the signal. In PON, current 10Gb/s system have not yet used coherent modulation and detection in commercially installed architectures. The signal considered in the scope of this thesis is only intensity modulated, therefore, the preservation of phase information is not a strict requirement for the systems describe here. In addition, the output wavelength of the coherent converted signal depends strongly on the difference between the pump and input wavelength, an ONU wavelength drift could result in converted output signal wavelength drift, which is not desired in a PON WDM-backhaul that needs strict wavelength control. FWM is also inherently polarisation dependent [51], which make it undesirable in PON as the ONU polarisation cannot be controlled.

Incoherent techniques such as cross gain modulation (XGM) and cross phase modulation (XPM) do not preserve the phase information, but they are more efficient because of SOA gain and regeneration capabilities. The output signal wavelength for XGM and XPM depends only on the probe wavelength, therefore, stabilisation of the

input signal wavelength is possible. The polarisation dependency of the WC depends on the SOA used [51], if the SOAs are polarisation independent then the input signal polarisation will not affect the conversion performance. The XGM SOA and the XPM SOA-MZI can provide R and 2R regeneration of the input signal respectively. Since the ONU signal gone through multiple splitters are weak, the regenerative capabilities of the in-coherent techniques are favoured in PON because of it provides power amplification of the ONU signal to allow for optical power loss in the >20km backhaul fibre. XGM produces digitally inverted output optical signal while XPM can produce either inverted or non-inverted output signal. A detailed experimental performance comparison between XGM and XPM techniques will be presented in Section 5.3.

2.4 Summary

In this chapter, the interferometric noise generation in ring based access network was introduced, classifications and performance impact of the in-band crosstalk noise was describe in existing literature. The wavelength tolerance and its effect on the performance is an un-explored area of interest, especially for the ring access networks which small wavelength drift is expected due to the use of lower cost components. The performance in the presence of interferometric noise is also related to the receiver bandwidth. The performance analysis will be reported in Chapter 3.

The burst mode transmission in PON and the resulting near-far power difference problem was introduced. Several techniques has been proposed to achieve burst equalisation, an all-optical burst equalisation based on using the SOA in high saturation mode is the most attractive and cost effective solution for future access networks. However, the nonlinear properties of a SOA in deep saturation need to be

modelled properly to aid the design of such power equalisation system. A dynamic model is selected and will be tested in the Chapter 4.

A proof of concept wavelength conversion and all-optical processing system was also introduced. It can be used to consolidate multiple existing PON ODN architectures into a long-reach wavelength division multiplexing backhaul. The detailed characterisation and performance measurement of this proposed system will be presented in Chapter 5.

Chapter 3. Interferometric Noise in Ring Based Access Networks

3.1 Introduction

A number of researchers have suggested central distribution ring networks as an architecture for future hybrid WDM and time division multiplexing (TDM) access network. Initiatives utilising such ring network include the SARDANA project [26] and the SUCCESS project [11]. In these projects, tree TDM networks are linked via remote nodes (RN) sited on a ring network which is terminated by a central office (CO) node. The ring network utilises WDM so that each wavelength can be dropped to serve different TDM tree networks, as illustrated in Figure 3.1 A Ring access network outline containing a central office site serving three RNs. In a ring access networks, the Remote Nodes (RN) that aggregate multiple PONs with the central office contains Optical Add Drop Multiplexers (OADM). Although heavily attenuated, some of the dropped wavelength can still pass through the OADM due to filter leakage in low cost network components. If the difference between the added

wavelength and the leaked dropped wavelength falls within the receiver bandwidth, then interferometric beat noise will arise at the receiver, affecting the signal quality received by the subsequent RN on the ring.

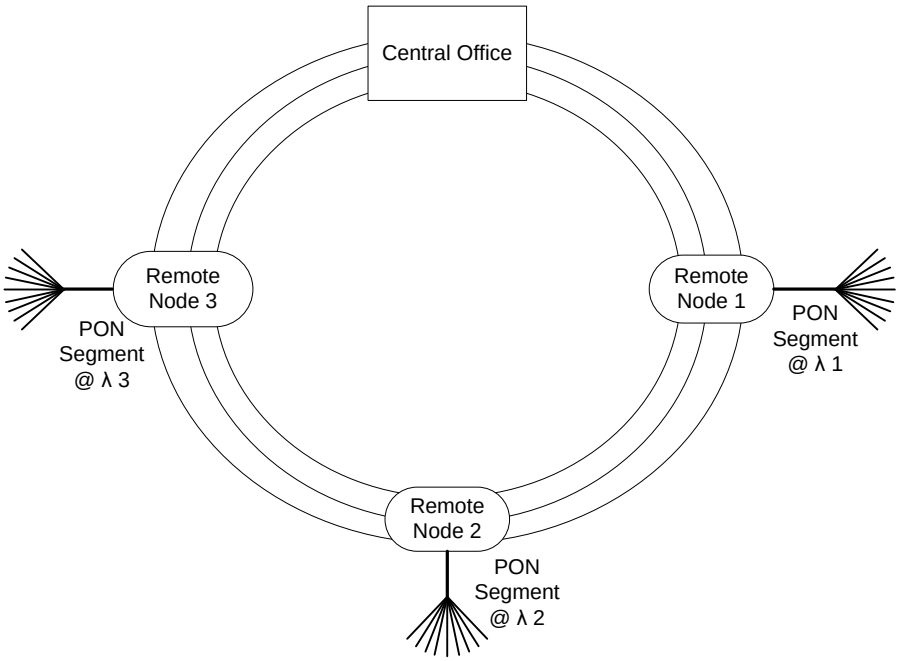

Figure 3.1 A Ring access network outline containing a central office site serving three RNs

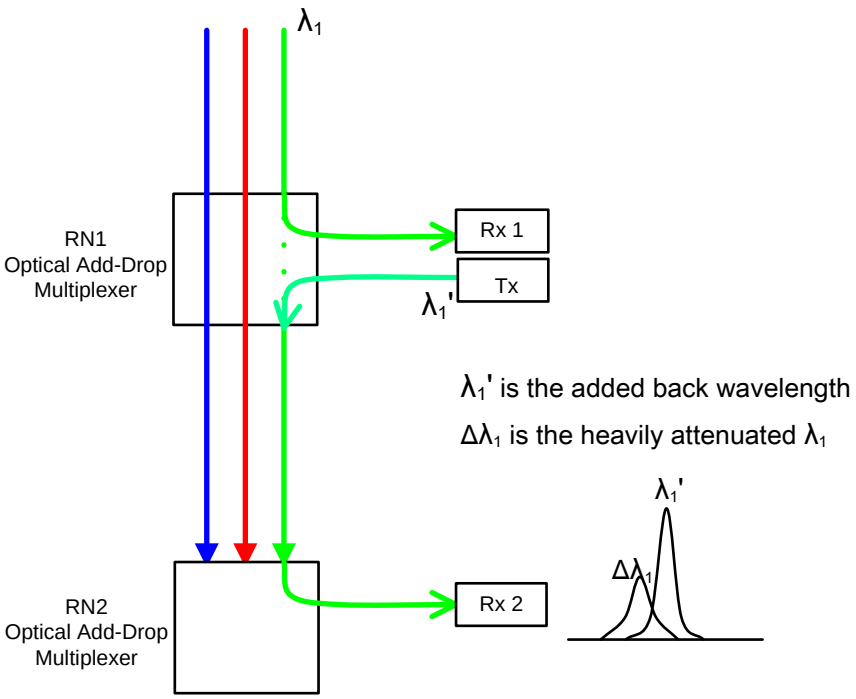

Figure 3.2 Interferometric noise generation in Ring Access Network due to filter leakage

Traditionally, core WDM networks have very good wavelength stability, but in access networks some tolerance in wavelength is expected due to the desire to reduce the cost of components. A section of a ring network containing two Remote Nodes (RN) is shown in Figure 3.2. The two RNs will contain OADMs that are responsible for dropping one wavelength (for example λ_1) and letting the other wavelengths continue on the ring. Although heavily attenuated, some of λ_1 can still pass through the RN due to filter leakage. If the added wavelength, λ_1', is the same or almost aligned to the dropped wavelength λ_1, then interferometric beat noise will arise within the receiver bandwidth [54], resulting in in-band crosstalk thus affecting the signal quality received by RN2.

This chapter aims to evaluate the tolerance to wavelength drift in the presence of interferometric crosstalk. This will include an experimental demonstration of the relationship between the BER performance and the electrical filter characteristics for various levels of filter leakage. Understanding the acceptable performance limits of filter leakage may allow the use of low cost optical component in the OADM. This provides the motivation for analysing the relationship between the interferer power (generated by leakage of the dropped wavelength) and the wavelength variation between the added and leaked signals. In this chapter, we first describe in section 3.2 the nature of Interferometric Noise (IN) and how IN could be presence and become an issue in a ring access network and then in section 3.3 the experimental setup and results showing the BER performance characteristics are presented, demonstrating the impact of such interferometric noise. It is also shown how the BER characteristics change with the choice of electrical filtering. Section 3.4 presents simulations to further investigate the relationship between BER

performance and the 3dB filter bandwidth and filter roll-off, with the results obtained from the experiment analysed and conclusions presented in section 3.5.

3.2 Background and Theory

3.2.1 Classifications of Interferometric Crosstalk

The interference of two monochromatic waves can be used to analyse crosstalk in an optical communication system. If the signal instantaneous power $P_d(t)$ is interfered by a crosstalk signal with instantaneous power $P_x(t)$, the resulting photo current at the photo detector will contain the data and the crosstalk signals, along with the interferometric beat term which depends on the relative phase difference and polarisation vectors of the signal and crosstalk $\vec{\rho}_d$ and $\vec{\rho}_x$

$$I \propto P_d(t) + P_x(t) + 2\sqrt{P_d P_x}\cos\{\Delta\omega\tau + \Delta\phi(\tau))\}\vec{\rho}_d \cdot \vec{\rho}_x \qquad (2.1)$$

The classification presented in [55] listed several types of crosstalk, which were characterised by the "relative phase" $\Delta\omega\tau + \Delta\phi(\tau)$ of the co-sinusoidal terms in equation 2.1.

In the single source case, the data and the crosstalk signals originate from possibly the same laser source with the same frequency ω_o, the coherence time τ_c and phase noise $\phi(\tau)$, the crosstalk signal then goes through a different path and is delayed by τ relative to the data signal. The relative phase between the two signals will be $\omega_o\tau + \phi(\tau) - \phi(\tau - \tau_c)$.

Coherent crosstalk occurs when the delay experienced by the crosstalk τ is much smaller than τ_c, near the $\tau = 0$ coherence limit, it is characterised by the absence of phase noise [56]. If the delay is constant, the relative phase value depends on $\omega_o\tau$, and then the interferometric term may be determined.

Homodyne Incoherent Beat Noise Crosstalk occurs as the delay τ becomes much larger than τ_c, the resulting interference is at the incoherent limit. The phase noise in the source is converted to intensity noise on detection [57]. This type of beat noise is also called Phase Induced Intensity Noise (PIIN). If a 1mW continuous wave (CW) distributed feedback (DFB) laser source was to be used, this incoherent region can be reached by an interferer delay path length of more than 10m [54].

The single source case was not considered in the OADM of ring based access network, because the leaked interferer signal and the data signal will be coming from different sources. In the separate source case, the data and the crosstalk signals originate from two different laser sources and they may be at different frequencies $\omega_d \; and \; \omega_x$. The relative phase in this case will be $(\omega_d - \omega_x)t + \phi_d(t) - \phi_x(t)$.

Incoherent noise-free crosstalk occurs when the beat frequency is outside the receiver bandwidth. Therefore, the beat noise will be removed by electronic filtering at the detector and only the additive crosstalk components remain. This type of crosstalk is also known as Out-of-band crosstalk [54].

Heterodyne Incoherent Beat Noise Crosstalk will occur as the beat frequency of the two sources fall partially or totally within the detector bandwidth, the random variance of phase noise may also affect the received signal, together they can generate interferometric noise, reducing the BER. In a ring access network remote node, this type of crosstalk is most likely to occur.

For the crosstalk types above, apart from the Incoherent noise-free crosstalk, the beat noise components all fall within the receiver bandwidth and are categorised as In-band Crosstalk. Partially coherent crosstalk is also possible but difficult to

analyse as it lies between the two extremes of coherent and incoherent crosstalk [54, 55].

3.2.2 Performance Impact of In-band Crosstalk

The interferometric beat noise is generated mainly due to imperfections in the network components such as add-drop multiplexers. Optical filters are widely used in multi-wavelength network components such as add-drop multiplexers, wavelength router and optical cross connects. However, they do not provide perfect isolation of the unwanted signal, allowing leakage component of the unwanted signal being added to the selected signal. If the leakage component of the unwanted signal (interferer) is at the same wavelength as selected signal's wavelength or if the frequency difference of the two signals is within the receiver bandwidth, as discussed earlier in section 3.2.1, the beating of the selected signal and the leakage signal on a square-law, envelope photo detector inevitably produces interferometric noise. This beat noise component can cause significant performance degradation [58], inducing large BER floors.

The performance degradation has been reported for a single interferer at the same wavelength as the data signal. The interferer beat noise crosstalk was analysed as homodyne incoherent beat noise crosstalk (also known as phase induced intensity noise [59]). Homodyne means the interferer signal originated from the same source as the data signal and is an attenuated and delayed version of the data signal with the same wavelength. The single interferer investigation provided insight into the characteristics of interferometric noise. It showed the relationship between power penalty and crosstalk power levels exhibits an asymptotic behaviour [60], as a small decrease in total crosstalk power yield better BER performances and lower power penalty.

Later publications extend the single interferer analysis to multiple interferes [55] and unequally powered interferers [54], using a large number of techniques ranging from Gaussian approximations to full system simulation as summarised in [54]. All the above performance studies are very useful for core WDM network where the wavelength of the signal is controlled. These analysis generally assumed the signal and interferer are of the same wavelength or come from the same sources, crosstalk between different source data are considered to be incoherent noise-free as the beating term is outside the receiver bandwidth [61]. The reason for this consideration is due to the fact that when the wavelengths in the WDM networks are precisely controlled, the wavelength for each channel can be maintained so that they will not interfere with each other. However, in the ring based access networks, the data and the interferer signals may come from separate un-cooled laser source at various powers because of the lower component cost considerations. The signals in access can also be generated from a tuneable laser, or a wavelength converted source. Therefore, some level of wavelength drift is expected in access networks due to heating up of the un-cooled laser or transmitters performance differences between the equipment throughout the access network. The strictly defined wavelength assumption used in previous core WDM network performance analysis will no longer valid in ring access networks. From the classification of interferometric noise earlier, it was known that the wavelength drift, phase noise, and power differences of the signals coming from separate sources will degrade the performance of the network if they produce significant in-band crosstalk. To my best knowledge, the analysis of wavelength tolerance and the relationship between BER performance and electrical filter characteristics as a result of the wavelength drift have not been studied, it will also be very useful to account for the various levels of filter leakage.

Therefore, the study of wavelength tolerance and its effect on the performance of future access network will be important, because it may allow the use of low cost optical components in future access network that satisfy the necessary performance requirement.

3.2.3 The Relationship of IN with Receiver Bandwidth

The beat noise contribution to the overall performance degradation dominates when its contribution is much larger than the additive crosstalk noise [54]. When the data and crosstalk signal are at different wavelength, this beat noise component can fall in-band or out-of-band depending on the wavelength differences. Therefore, as the beat noise term dominates, only the in-band crosstalk will impact the performance strongly when it falls inside the receiver bandwidth. Figure 3.3 presented a simulation setup which generates the result in Figure 3.4, showing the detuning of the interferer wavelength at 0.01nm steps away from the data source which is at a fixed wavelength.

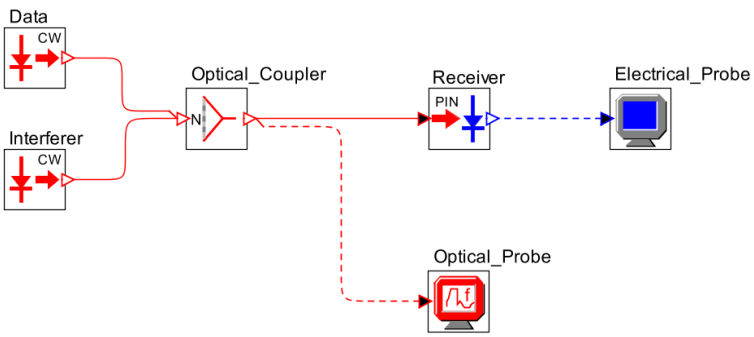

Figure 3.3 Simulation setup with two laser source and the photodetector

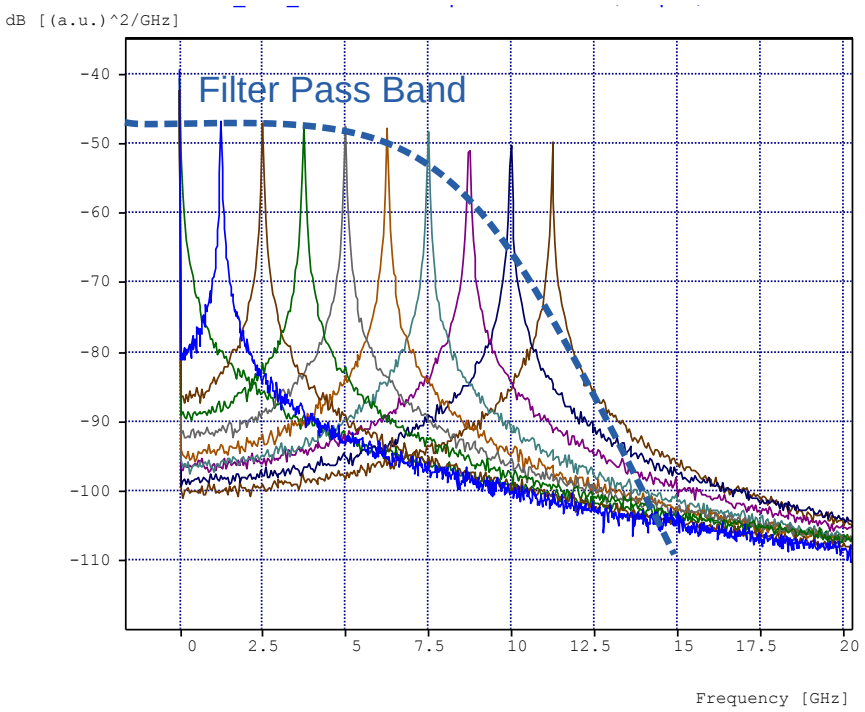

Figure 3.4 The overlapped receiver electrical spectrum as the interferer is detuned away from the data signal at 0.01nm steps.

From the result above it is noticed, as detuning of the interferer wavelength increased, the beat noise component gradually moved out of the electrical receiver bandwidth, assuming the bandwidth of the receiver is at 10GHz. The performance characteristics with respect to electrical bandwidth was briefly analysed in a paper [62] published after the work in chapter 3 was done. Their analysis focused on the data and crosstalk signal which are at the same wavelength coming from the same source, while our work focused on the performance characteristic when the data and interferer signal are from different sources and when they are very close in wavelength (at less than 0.08nm or 10GHz apart, which makes the beat noise fall within the Rx bandwidth). This wavelength difference exists in access network, but not in core networks where wavelength are strictly define. The main finding of the paper is the performance penalty was significantly increased, when the signal is filtered by a large number of optical filters in multiple optical cross connects. It was because the narrow optical filter bandwidth was below 15GHz and the increase in

filter detuning in cascaded filters causes ISI, which lead to eye closure at the receiver. In access networks, the add-drop multiplexer and optical cross connect number will be very small and therefore, not likely to cause a performance decrease. The impact of ISI caused by electrical filtering will be a more important observation for access networks. As expected, narrow electrical filtering bandwidth in the receiver will start to cause eye closure at around 6GHz and less. The results in [62] also showed the performance is good (i.e. high ER, large eye opening) and remained so at a filter bandwidth of 6.5 GHz and above. Because the study was also done with data rate at 10Gb/s, this result offers a good reference for the electrical filtering characteristics in later experiments. However, the study didn't consider the case when the beat noise is partially in-band or nearly out-of-band, for example, a 0.08nm detuning of the interferer wavelengths may cause the beat noise frequency component to situate at almost 10GHz. In that case, a narrower receiver electrical bandwidth that is less than 10GHz will make previously in-band beat noise component out-of-band, and the wavelength detuning causes performance change. Therefore, the performance at wider electrical bandwidth may be worsen as a result of the partially in-band beat noise. In Chapter 3 the performance and electrical filtering characteristics at the detuned interferer wavelength will also be investigated.

3.2.4 The Generation of Interferometric Noise

We considered two signals are present in the fibre, namely, the desired data signal and the crosstalk signal's electric fields are given by $E_d(t)$ and $E_x(t)$ respectively. The total electric field of the two signals at the photodetector is given by equation 3.1. The data signal is denoted by subscripts d and x denotes the crosstalk signal.

$$E_{\mathrm{tot}}(t) = E_{\mathrm{d}}(t) + E_{\mathrm{x}}(t) \tag{3.1}$$

Here we consider the single interferer signal case with both the desired data and the interferer modulated using On Off keying (OOK), with the electro-magnetic field of an optical signal with power P emanating from a DFB laser given by:

$$E(t) = \vec{\rho}\sqrt{P}\exp j[\omega t + \phi(t)] \tag{3.2}$$

Where $\vec{\rho}$ is the polarisation state, P is the signal power, ω is the optical frequency in radians and $\phi(t)$ the optical phase.

When one wavelength is drop and then added inside an OADM, we substituting the electrical field of equations 3.2 into equation 3.1 resulting to the following,

$$\begin{aligned} E_{\mathrm{tot}}(\mathrm{t}) = \vec{\rho}_{\mathrm{d}}\sqrt{P_{\mathrm{d}} m_{\mathrm{d}}(t)}\exp j[\omega_{\mathrm{d}} t + \phi_{\mathrm{d}}(t)] \\ + \vec{\rho}_{\mathrm{x}}\sqrt{\alpha P_{\mathrm{x}} m_{\mathrm{x}}(t)}\exp j[\omega_{\mathrm{x}} t + \phi_{\mathrm{x}}(t)]) \end{aligned} \tag{3.3}$$

Here α defines the relative power P_x/P_d of the cross-talk term, and $m(t)$ expresses the binary symbols forming the on-off keyed message where $m(t) \in \{r, 1\}\,(0 \le r < 1)$ and r is the extinction ratio factor [54]. When a perfect extinction of the signal occurs at the binary 0 level, $r = 0$.

In optical square-law, envelope photo detection, the photocurrent i(t) is proportional to the squared magnitude of the electro-magnetic field. At the Receiver, using a normalised responsivity of $\Re = \frac{ne}{hv} = 1$, the instantaneous optical power is:

$$\begin{aligned} i(t) = \Re|E_{tot}|^2 = |E_{tot}|^2 = \\ P_d m_d(t) + P_x m_x(t) + \\ 2\sqrt{P_d P_x m_x(t) m_d(t)}\cos[(\omega_d - \omega_x)\mathrm{t} + \phi_d(t) - \phi_x(t)] \end{aligned} \tag{3.4}$$

From equation 3.4, there are three components representing the detected photocurrent, there is the desired data, the additive crosstalk and interferometric

noise [54]. The phase noise is generated for $\phi_d(t)$ and $\phi_x(t)$, based on Wiener Levy random process [63]. The interferometric noise is mainly a oscillating cosine term around the "1" power level, with the frequency of $\omega_d - \omega_x$, while the phase noise is usually very small compared to the interferometric noise, because the phase noise variance depends on the linewidth of the laser source, which is typically in the range of 1MHz to 10MHz for commercial, low cost DFB lasers. The bit-by-bit interferometric noise for a 7.5GHz Δf (frequency separation between the interferer and data signal) and assuming only "1" to "1" level crosstalk interaction is plotted in Figure 3.5. The interferometric noise itself has an arc-sine distribution as shown in Figure 3.6

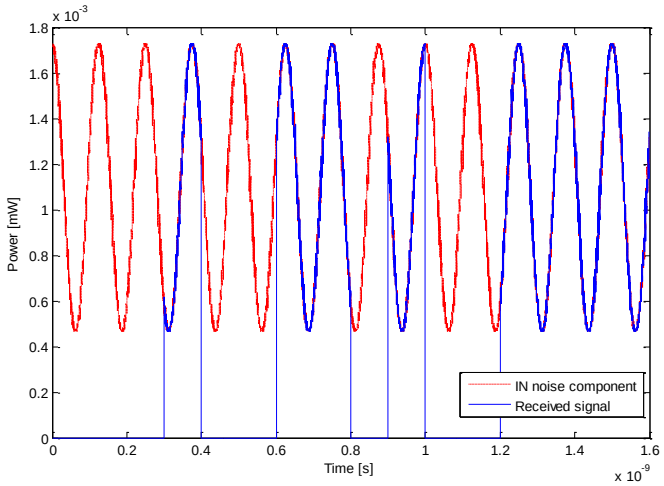

Figure 3.5 Bit-by-bit level view of the received signal with a separate interferometric noise component shown in red

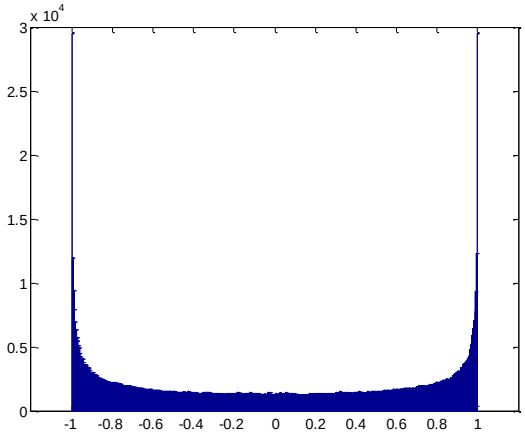

Figure 3.6 Arc-sine distribution of the interferometric noise

The interferometric noise term is dependent upon the wavelength difference $\omega_{\mathrm{d}} - \omega_{\mathrm{x}}$ between the two signals. This term is also dependent upon the phase difference $\phi_d(t) - \phi_x(t)$ which demonstrates that the interferometric beat noise contribution is much larger than the classical crosstalk, and therefore, the interferometric noise is often the dominant noise [64] if it falls within the receiver bandwidth. From equation 3.3 we know that the beat noise is also polarisation dependent because of the $\vec{\rho}_{\boldsymbol{d}}\vec{\rho}_{\boldsymbol{x}}$ term. It has previously been demonstrated that in a system with random polarisations, the system is more likely to perform in the worst case, because the probability density distribution has shown that the probability is at its highest when the polarisation vectors are aligned [65]. Since it is useful to test for the worst case scenario in order to find out the limit of the systems, the polarisation vectors $\vec{\rho}_{\boldsymbol{d}}$ and $\vec{\rho}_{\boldsymbol{x}}$ were set to be aligned in the following analysis.

The classification described in section 3.2.1 lists several types of interferometric noises. The specific type we discuss hereafter belongs to the heterodyne incoherent beat noise crosstalk. It will occur if the beat frequencies of the two sources fall partially or totally within the receiver's bandwidth. This type of crosstalk is also termed in-band crosstalk [54], which can be found in a ring access network because the dropped and injected wavelengths have almost the same wavelength or possibly drift to the same wavelength due to un-cooled lower cost sources.

3.2.5 The Effect of Electrical Filtering on Interferometric Noise

The worst case interference will occur when the desired data signal and in-band crosstalk are at exactly the same wavelengths as electrical filtering will not remove any of the interfering signal. However, as the wavelength of the interferer is detuned away from the wavelength of the desired signal, the beat frequency, which is

the frequency difference between the signal and interferer, will increase placing the beating term on a carrier frequency away from the baseband data. The beat noise component will become attenuated as it moves near the filter band edge, eventually becoming totally out of band and heavily attenuated, and can no longer having significant effect on the system performance. Therefore, the characteristics of the electronic filtering used will have a significant effect on the out-of-band or near-out-of-band beat noise component.

In the experiment we investigated how the choice of the filter can change the BER performance. Figure 3.7 shows the frequency response measurement of a Nortel 10GHz PIN Receiver and its response when combined with a Picosecond Pulse Labs 7.5GHz 4th Order Bessel-Thompson electrical filter. In section 3.3 we will demonstrate the impact that this difference in frequency response had on performance due to the Interferometric noise.

From the measured results, we determined that the Nortel 10GHz PIN receiver has a -3dB cut-off point at 11GHz and its roll-off characteristic is 36dB/decade. The Picosecond 5458 was chosen for our experiment because its response near the 3dB cut-off is lower than the 4269 filter, it also had a slightly steeper roll-off. The combination of the PIN Receiver and the filter had a -3dB cut-off at 6GHz and the roll-off is estimated at 22dB/decade. The lower cut-off characteristic of the filter will be able to attenuate the in-band crosstalk noise close to and above the cut-off frequency, effectively making the receiver bandwidth smaller. Hence, as the interferer signal frequency is detuned further away from the data signal, the beat frequency, which is dependent upon $\omega_d - \omega_x$, will increase, causing the frequency of the beat term to increase. A filter with a lower cut-off frequency will therefore, attenuated the beat noise at lower frequencies, as the interferer

frequency is detuned from the data signal frequency, with the possibility of improving the BER performance.

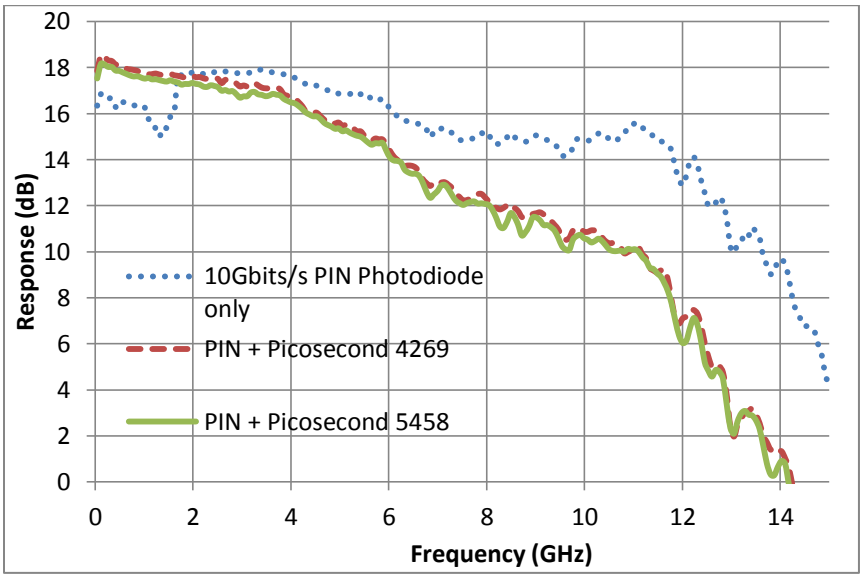

Figure 3.7 Filter combined with receiver response measurements, compared with receiver response measurement

3.3 Experiment Setup

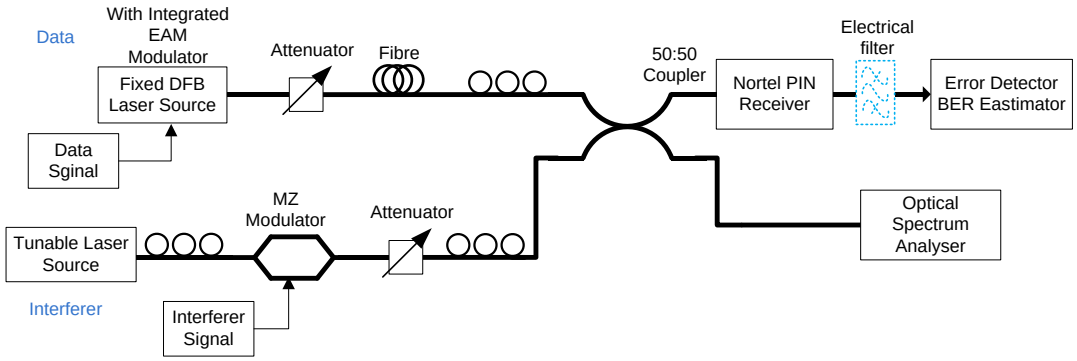

Figure 3.8 Experiment configuration showing the mixing of the desired data signal and the interference signal into a PIN photodiode receiver. Note that the filters were added between the PIN receiver and the Error Detector

The experimental setup is shown in Figure 3.8. The data signal was generated from a fixed wavelength laser at 1551.012 nm. This continuous wave (CW) optical signal was modulated by an integrated Electro-absorption Modulator (EAM) in the same package as the laser. An electrical Pseudo Random Bit Sequence (PRBS) signal generated by the Anritsu Programmable Pulse Generator (PPG) was modulated on-to the CW optical carrier. The modulated signal then went through an

attenuator and 4km of single mode fibre (SMF), this introduces 20 μs delay to the signal which is much longer than the 1 μs coherence time in typical DFB lasers. Since this distance is much greater than the laser coherence length of 200 meters [66], the SMF used only in the data signal path can de-correlate the desired data signal with respect to the interferer.

Since the interference is polarisation dependent, in order to test for the worst case performance limit, the data and interferer polarisation vectors need to be aligned so that the beat noise causes most errors in the receiver signal. Hence, the data signal was passed through a polarisation controller at this stage. The signal then went into a 50:50 four port combiner/splitter. One of the output ports is monitored by an optical spectrum analyser (OSA) while the other output is fed into a Nortel 10Gb/s PIN receiver which is connected to the Anritsu Error Detector (ED) via electrical cables. The attenuator was adjusted to 10.4 dB so that a back-to-back baseline BER of 10^{-9} was obtained. The OSA has a limited resolution of 0.01nm, to check that the data and interfering signals are aligned at 1551.012nm, an electrical spectrum analyser (ESA) was used to check the received signal beat frequency, the lowest beat frequency peak was found when the tuneable laser was set to 1551.012nm, therefore, it is considered that this wavelength is where the two modulated sources aligned.

The interfering optical signal was created by externally modulating a wavelength tuneable laser source. The external Mach-Zehnder (MZ) modulator is polarisation dependent therefore, this tuneable CW wavelength was passed through a polarisation controller for polarisation alignment. The inverse PRBS input from the Anritsu PPG was modulated on to the optical carrier and its wavelength initially tuned to match the fixed laser source. This modulate optical signal then went through another attenuator and a polarisation controller to the second input of the 50:50 four

port combiner/splitter. The attenuators were used to control the power of the data signal and the interferer signal.

This experiment measured the BER performance characteristics with only the PIN Receiver. The interferer attenuation was changed from -40dB to -18dB in steps of 2dB. The wavelength of the interferer laser source was adjusted in 0.01nm (1.25GHz) steps to 1551.092nm to record the effect when the crosstalk signal is moving away from the data signal. Measurements taken from those points allowed us to see the BER performance affected by the crosstalk noise at different interference power levels as well as the change in beat frequency.

Then the experiment was repeated with the 7.5GHz electrical filter described above connected between the PIN receiver and the Anritsu ED. The data signal was attenuated 9.7dB again to obtain a 10^{-9} back to back reference BER. Measurements were taken by changing the attenuation value in steps of 2dB starting from -40dB to -18dB.

3.3.1 Experiment Results

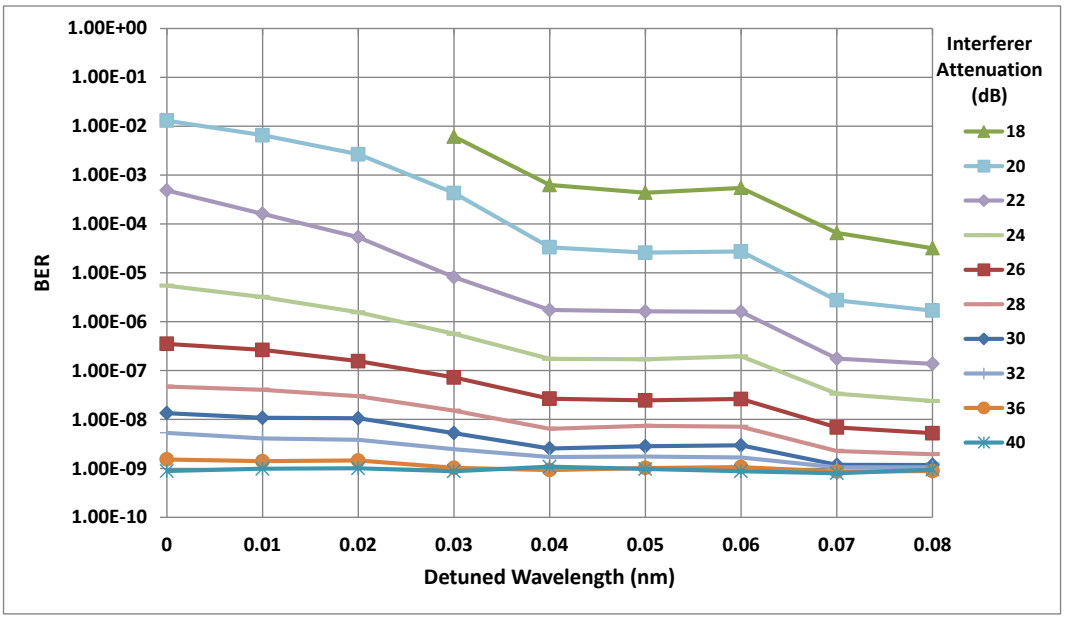

Figure 3.9 BER performance characteristics with the Nortel PIN receiver only and no external filter connected

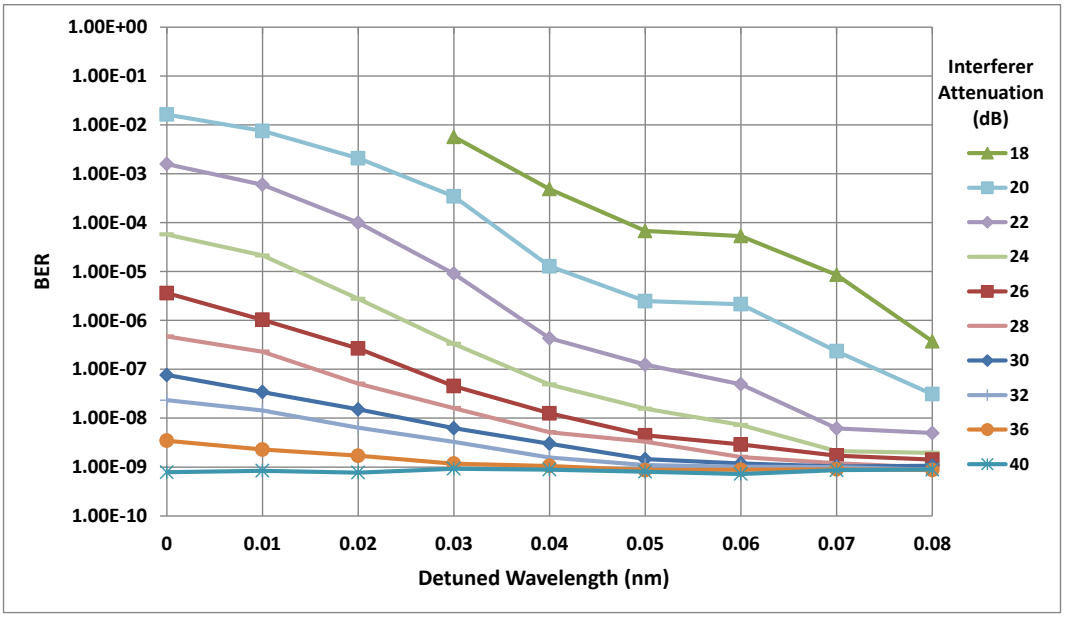

Figure 3.10 BER performance characteristics with the Nortel PIN receiver combined with 7.5GHz external electrical filter

The experimental results in Figure 3.9 and Figure 3.10 showed the BER performance characteristics against different detuned wavelengths at several interferer attenuation levels. When the interferer signal was attenuated by -32dB or more, the BER of both systems did not show BER performance changes of more than 1 order of magnitude, for the detuned wavelengths up to 0.08nm (10GHz). When the interferer was experiencing less attenuation, the BER changes are more significant due to the stronger influence from the interferer signal causing more noise and errors. For interfere attenuation of -18dB the ED was unable to synchronise to the pattern at detuning of less than 0.03nm, therefore, the BER measurement was not available at those points. At -20dB to -24dB interferer attenuation, each -2dB change in attenuation represented 1 order of magnitude increase in the BER performance. The BER performance was improved by 4 orders of magnitude as detuning the interferer wavelength from 0 to 0.08nm. At the same interference levels and through the use of a7.5GHz bandwidth electrical filter after the receiver, the improved by 5 orders of magnitude as the interferer wavelength is detuned from 0 to 0.08nm.

Comparing with the case without the filter, the filtered signals have better performances beyond 0.05nm detuning. At 0.08nm detuning, their BER performance is on average 1 order of magnitude better than the receiver only case which contained a filter with 10GHz bandwidth. For interferer signals attenuated by more than 24dB, the BER performance enhancement by filtering was less effective, since the interferometric noise was also weaker.

Figure 3.9 and Figure 3.10 can also be plotted in the classical crosstalk representations, as in Figure 3.11 and Figure 3.12.

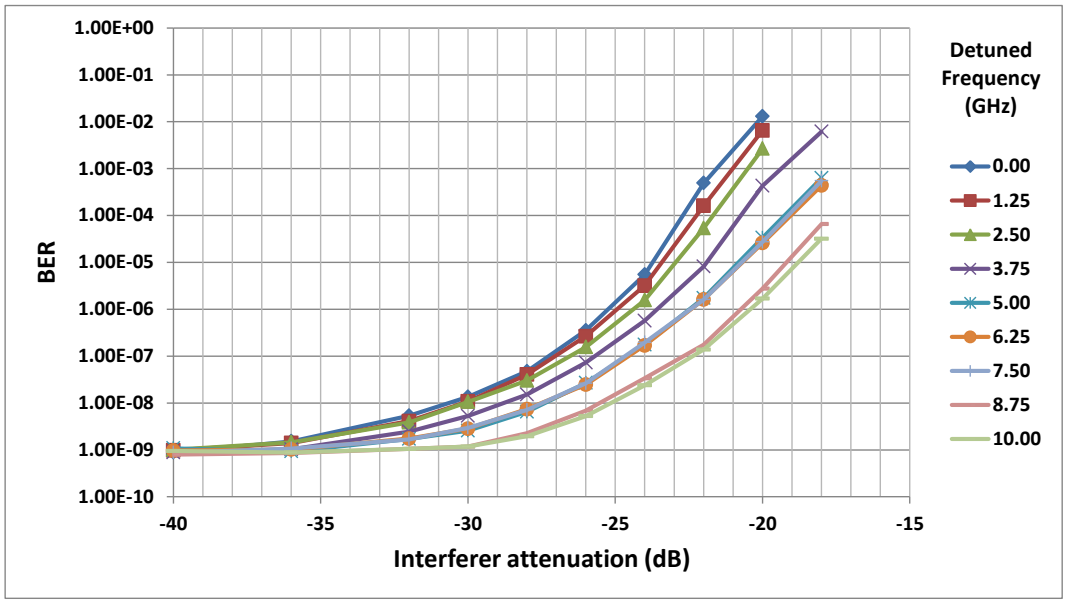

Figure 3.11 BER performance verses interferer attenuation levels, Nortel PIN Rx only

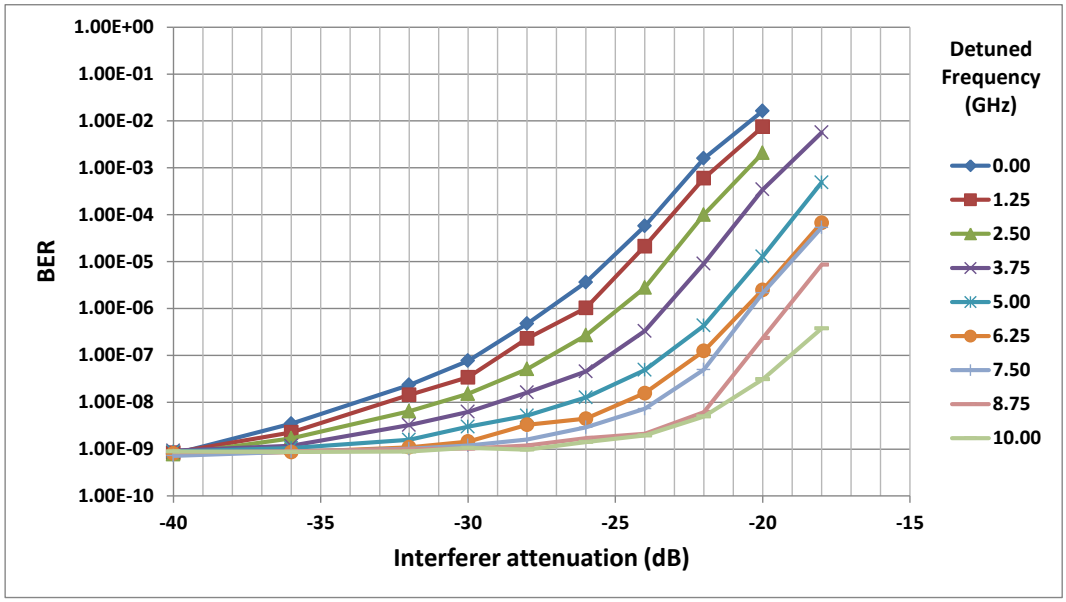

Figure 3.12 BER performance verses interferer attenuation levels, Nortel PIN Rx with 7.5GHz electrical filter

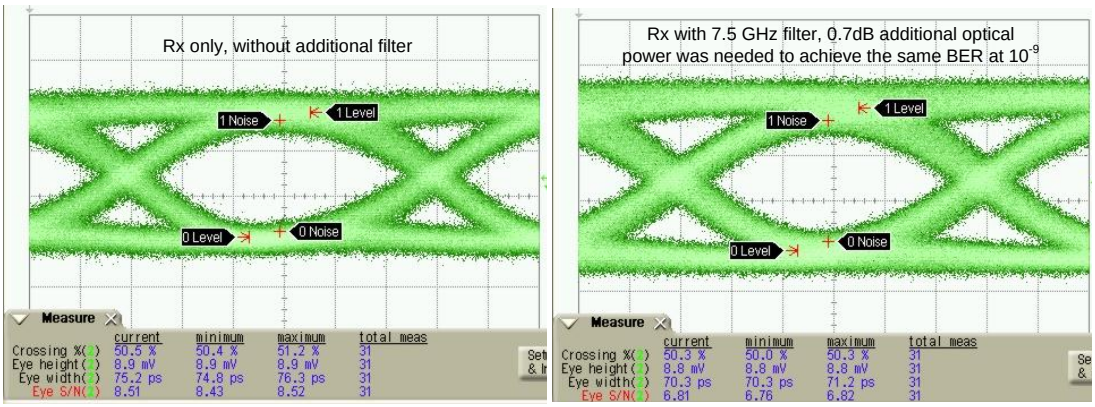

Figure 3.13 Eyes of the received data signal at 10^{-9} BER, left: No filter applied, right: 7.5GHz filter with 0.7dB more optical power than the left eye

The effect of the electrical filter is clearly visible when comparing the two results. Detuning the interferer away from the data frequency has moved the curves downward, representing better BER performances. On the other hand, the BER performance for detuned frequencies 0GHz, 1.25GHz and 2.50GHz in the case with the additional filter is not as good as the case without it. Since a 0.7dB increase in data signal power was needed to compensate for the extra 7.5GHz passive filter in order to achieve the same BER floor of 10^{-9}. This passive filter attenuated the RF output by 1dB, also because of the narrower bandwidth of the 7.5GHz filter, the

received SNR decreased by as much as 2.7dB as result of reduced eye height and eye width along with some phase distortions. Increasing the optical power compensated for the eye height reduction, but the eye width reduction and phase distortions after the filter were not compensated. As can be seen from Figure 3.13, even at the same BER, the SNR of the receiver only case is 1.7 higher than the compensated eye when the 7.5GHz filter is applied. When the interferer is very close to the data signal frequency, the BER performance of the case with the 7.5GHz filter will be more sensitive to interferometric noise, as it already has a lower SNR. Therefore, when the interferer is within 3.75GHz from the data signal frequency, the BER performance is not as good as the case with only the receiver. The additional filter does not have a significant effect on the interferometric noise in the region where the beat frequency is <3.75GHz because the filter cut-off frequency is at 6GHz, so as soon as the interferer is detuned by more than 5GHz, an improved BER performance can be seen with the narrower bandwidth filter applied, even for an relatively lower data signal SNR.

3.4 Simulation

3.4.1 Model of the experiment

To enable an extended investigated analysis of the impact of filtering simulations were performed in OptSim. This platform was chosen for this simulation requiring physical layer modelling as it considers both electrical and optical effects, and it also allows customised filter to be imported so that comparisons between the ideal and actual electrical filtering effects are possible. The filter response of the PIN receiver and 7.5GHz electrical filter response were imported into OptSim, since the electrical filters in OptSim do not have identical responses to these physical filters, to allow validation against the experimental results.

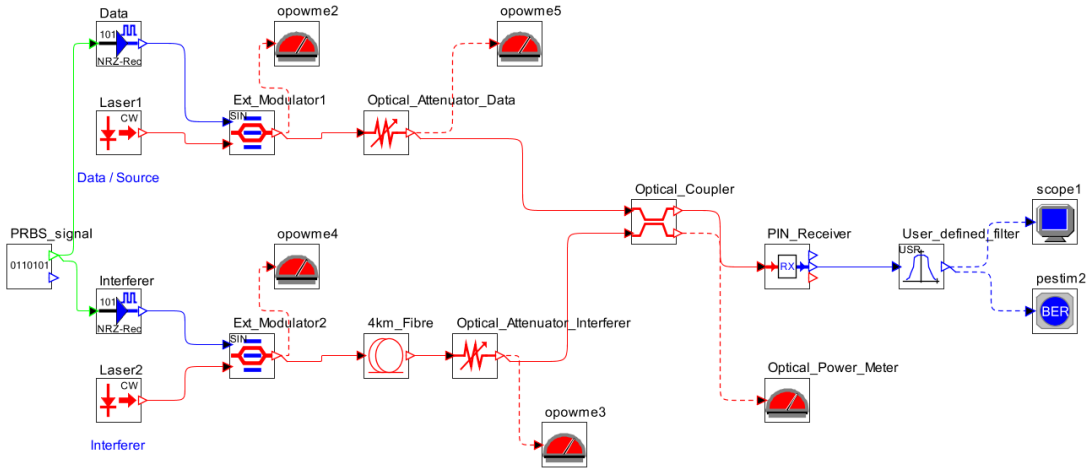

Figure 3.14 Simulation schematic mirroring the experimental setup

In OptSim, a sample mode simulation with an identical schematic to the experiment setup in Figure 3.8 was constructed, as shown in Figure 3.14. The polarisation controllers were not represented in the simulation, this is because in OptSim the optical signal's polarisation can be set to "single polarisation", therefore, the polarisation is assumed to be always aligned. This setting gives the worst case performance when simulating interferometric noise, which served the same purpose as the polarisation controllers used in the experiment. The signal bit streams are generated by a PRBS logical source and then it is converter to an electrical signal by a laser driver module. The external laser modulator then modulates this electrical signal on to a CW signal generated by a laser with linewidth at 1 MHz, which is the same as the datasheet specified DFB laser linewidth used in the experiment. The modulator has a realistic ER of 10.3dB to match those measured during the experiment. In this simulation, a Pseudo Random Bit Sequence (PRBS) electrical signal is generated for both the source and interferer, except the interferer signal was passed through a fibre module in OptSim that is 4km longer than the source signal to decorrelate the bit streams. These two de-correlated optical signals were then passed through a 50:50 dual input and dual output optical coupler and fall on to the PIN receiver.

The wavelength of the interferer laser could be adjusted at each simulation run to simulate the effect of the wavelength of the crosstalk signal moving away from the data signal. The interferer laser source was turned off initially to allow a reference BER of 1×10^{-9} to be obtained from the data signal. The power of the interferer signal was controlled by an attenuator while the data signal attenuation was held at the value used to obtain the reference BER.

The data signal's laser wavelength was set to 1551.012 nm. This value is the same as the fixed wavelength laser source used in the later experiment. The crosstalk laser wavelength was also set to 1551.012 nm to simulate the heterodyne incoherent beat noise crosstalk condition, this wavelength was then changed each run at 0.01 nm step with a total of 8 steps to 1551.092 nm so that wavelength detuning of up to 0.08nm can be simulated. The interferer attenuation was changed at the same steps as the experiment.

Similar to the experiments, the simulation was carried out for two conditions. The first condition is when only the internal 11GHz bandwidth post detection filter is present between PIN receiver and the ED; the second condition is when the Receiver and its internal 11GHz bandwidth filter is combined with a 7.5GHz low-pass filter. The filter responses are made by importing the frequency responses of the PIN receiver and the combine frequency response of the PIN receiver with the Picosecond 7.5GHz filter into OptSim's customised filter. The frequency responses were measured on a Lightwave Component Analyser (LCA) and then imported into OptSim.

3.4.2 Simulation Results

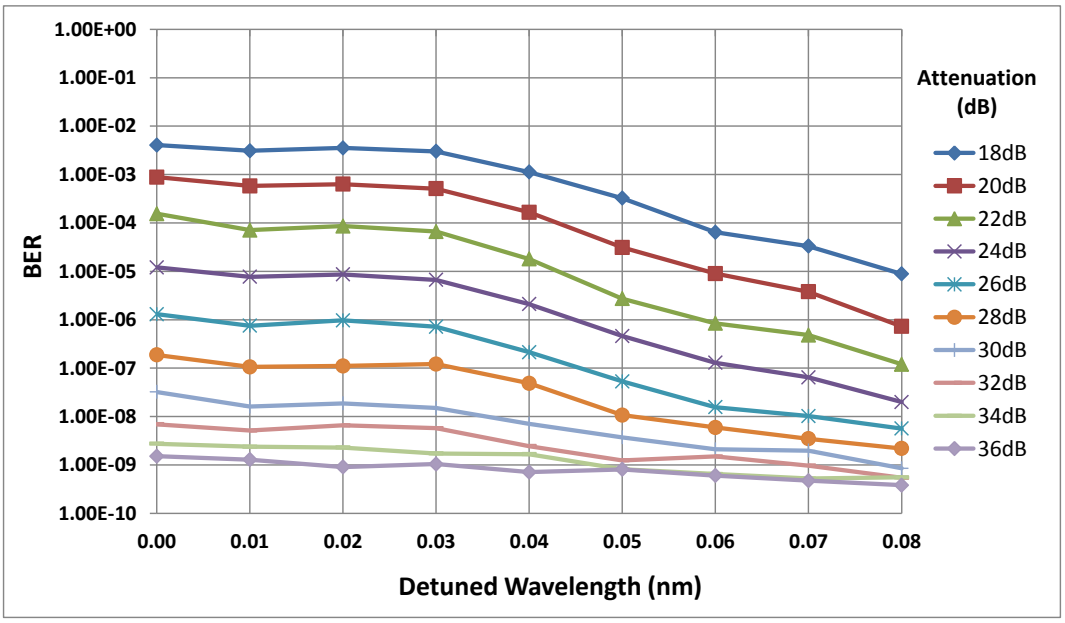

Figure 3.15 BER performance simulated characteristics with PIN receiver only and no external filter applied

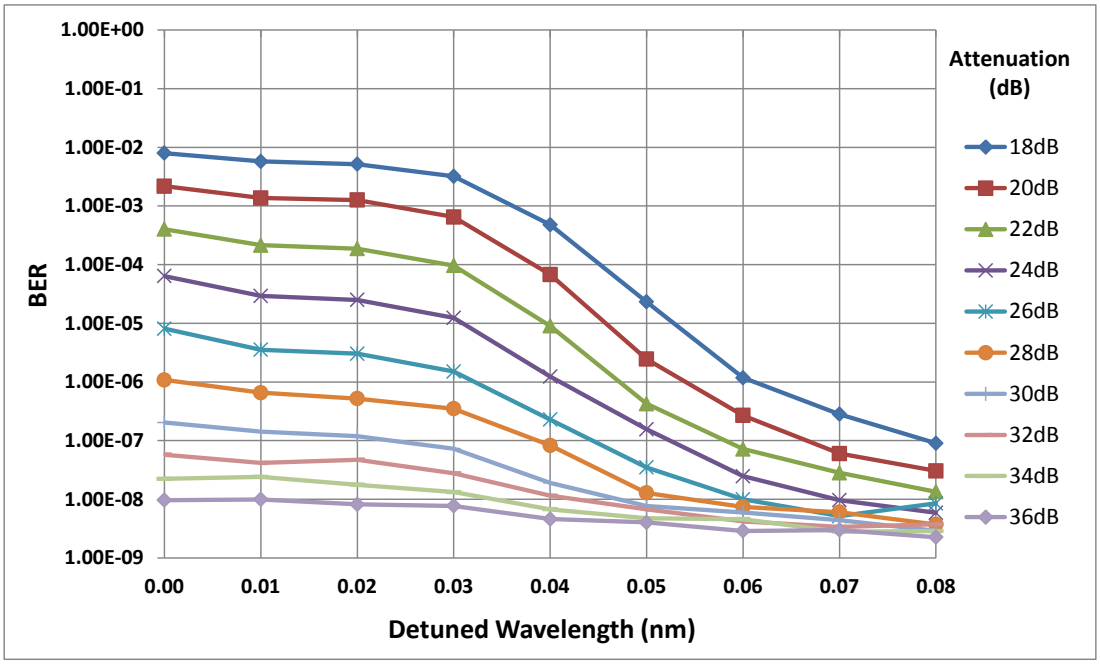

Figure 3.16 BER performance simulated characteristics with PIN receiver combined with customised filter using the measured filter response from the 7.5GHz filter used in the experiment

These simulation results show similar trends to the experimental data. A detailed comparison of the simulation results with the experiment results will be presented in the next section.

The simulation results can also be represented in the classical crosstalk plot, as in Figure 3.17 and Figure 3.19.

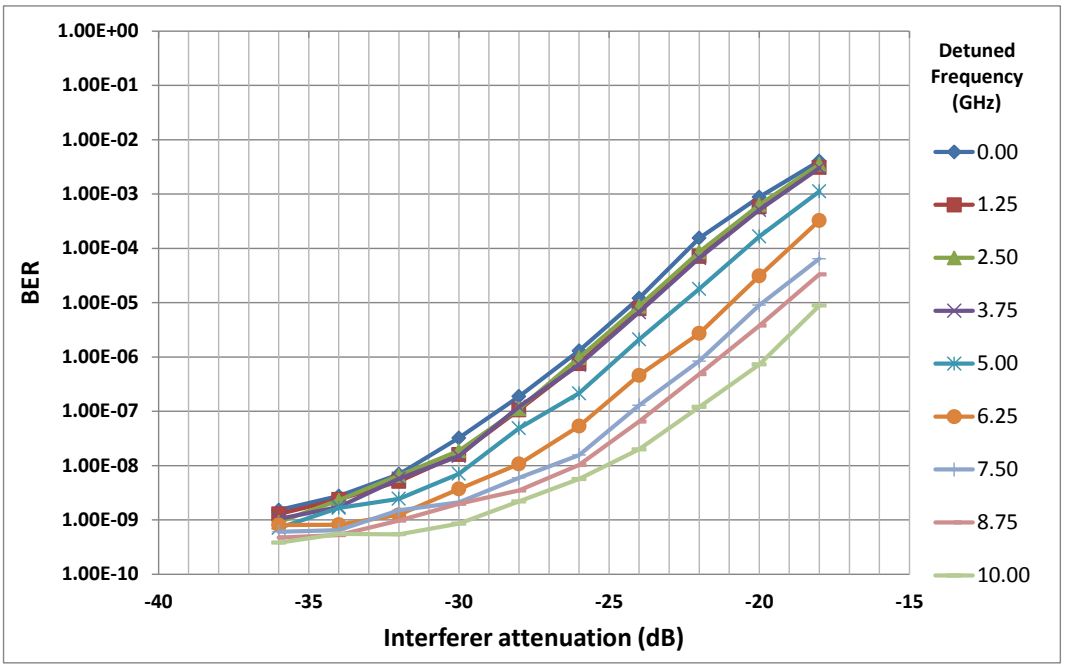

Figure 3.17 Simulated BER performance verses interferer attenuation levels for Rx only case

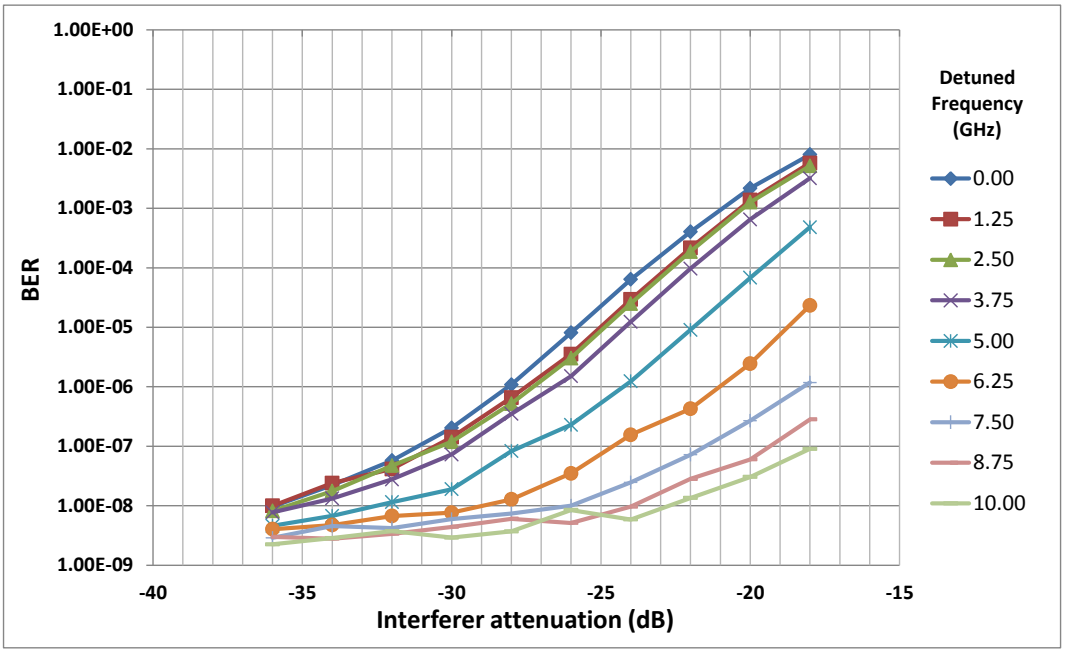

Figure 3.18 Simulated BER performance verses interferer attenuation levels for the PIN Rx + 7.5GHz filter case

3.5 Analysis of Experiment and Simulation Results

The simulation results will need to be validated by the experiment so that the simulated system can be used in the varying filter bandwidth analysis. Since there are many sets of results to compare, in order to make the presentation clear, only the results at the -20dB interferer attenuation level were compared. Among all the fully measured experiment and simulation results, this set of result was chosen because it represents the strongest effect of the interferer which lead to the largest change in BER, as the wavelength of the interferer was being detuned away from the source wavelength.

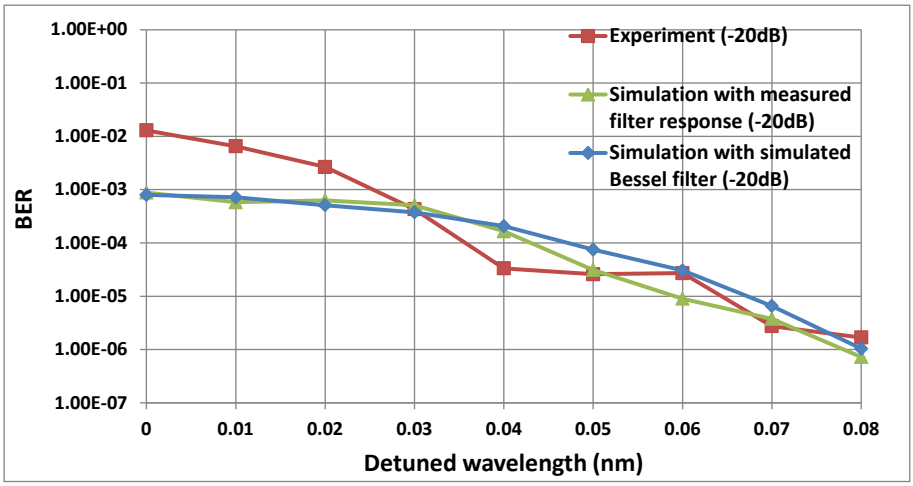

Figure 3.19 Comparing simulation and experiment results at -20dB interferer attenuations with PIN Rx only

Both the simulated BER and the measured BER from the experiment at -20dB interferer attenuation level is shown in Figure 3.19, they follow the same trend of increased BER performance as the interferer moves away from the source, and the resulting points are very similar for detuned wavelengths 0.03nm and 0.08nm, the differences increased to 1 order of magnitude when no detuning was performed, i.e. when the frequency separation between the interferer and the source is <3.75GHz. This difference could arise from the BER estimator in the simulation which calculates the BER from the Q-factor of the received simulated eye. The

simulated system estimates the BER instead of counting the actual error in contrast to the ED in the experimental setup, to reduce memory requirement and simulation time.

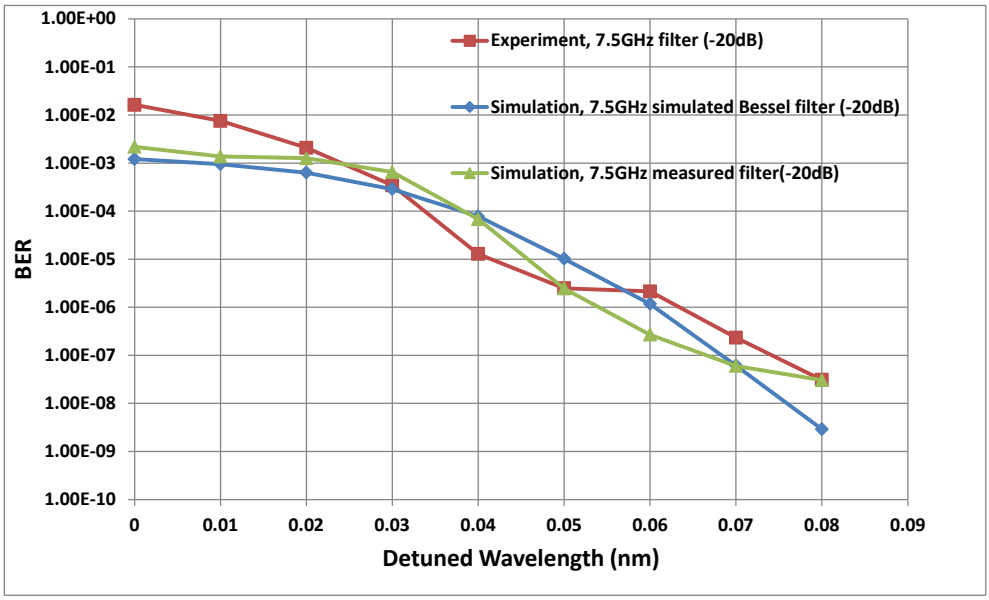

Figure 3.20 Comparing simulation and experiment results at -20dB interferer attenuations with PIN Rx + 7.5 GHz filter

Similar observations were found in Figure 3.20 where an additional 7.5GHz filter is used in combination with the receiver, with the largest difference between the experimental results and the simulated results being one order of magnitude. In the two simulation results, the BER of the imported filter response and the simulated response of the 4^{th} Order Bessel filter differed by less than 1 order of magnitude.

Looking at the classical crosstalk representations, comparisons between the simulation and experiment results also show the accuracy of the simulation in estimating the BER performance from the received signal eye, the comparisons are shown in Figure 3.21 and Figure 3.22.

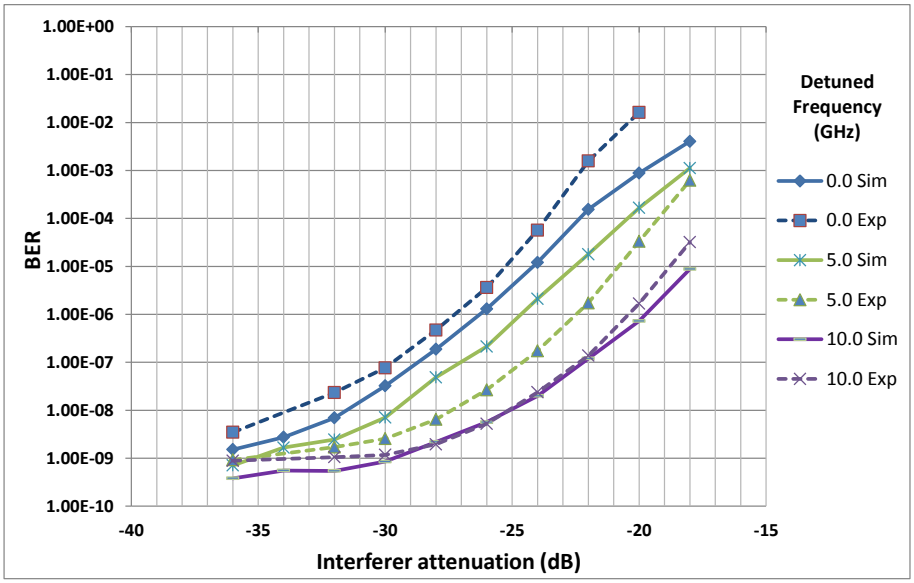

Figure 3.21 Comparing simulation and experiment results at 0,5,10 GHz frequency separation, Rx only case, "Sim" indicates Simulation result and "Exp" indicates Experiment result

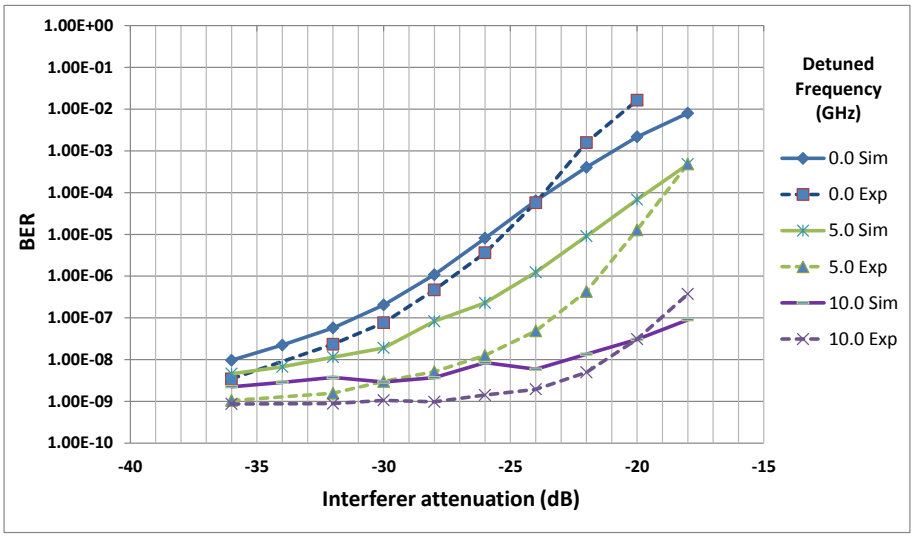

Figure 3.22 Comparing simulation and experiment results at 0,5,10 GHz frequency separation, Rx + 7.5GHz filter case, "Sim" indicates Simulation result and "Exp" indicates Experiment result

In both cases, detuned frequencies of 0, 5 and 10 GHz were selected for comparison to keep the result clear. For the receiver only case, the two sets of results matches closely at 0GHz and 10GHz frequency separation, where the BER difference is less than half an order of magnitude, at 5GHz frequency separation, the results has a larger BER difference that is 1 order of magnitude, at -22dB to -26dB interferer attenuation levels. For the case of receiver and filter combined, the two sets of result did not match as well, large differences between the simulated and

experiment results also occurs at 5GHz frequency separation (or 0.04nm detuned interferer wavelength), with the largest difference being 1.5 order of magnitude apart. This difference is again due to the fact that the simulation estimated the BER using the Q-factor, the optimum decision threshold of the BER estimator was also determined by assuming the arc-sine (another description is "two pronged") distributed interferometric noise as a Gaussian distributed noise. The biggest difference occurs at half way through the detuning which is 5GHz, could be due to the fact that this area is there a Gaussian approximation would give a large error in decision threshold and thus Q-factor and BER estimation error. It is known that using a narrower filter bandwidth can revert the arc-sine distributed noise to a Gaussian-like shape [67], the following analysis presents how the noise term changes as a result of detuning the interferer and it was carried out using the 4th order Bessel-Thompson filter.

3.5.1 The Effects of Receiver Electrical Filter Bandwidths

This section aims to investigate the effect of electrical filter on the interferometric noise, at the presence of a frequency detuned interferer. In the experiment, a fixed bandwidth 4th order Bessel-Thompson filter was. In this section, we discuss how alternative filter bandwidth can affect the BER performance. The general Bessel-Thompson filter has the following transfer function:

$$H(y) = \frac{B_0}{\sum_{k=0}^{n} B_k \, y^k} \tag{3.5}$$

Where *B* is the filter coefficient used for designing analogue filters [68] and n is the order of the filter, which at 4th order, becomes:

$$H(y) = \frac{105}{105 + 105y + 45y^2 + 10y^3 + y^4} \tag{3.6}$$

where $y = j\Omega = j\omega\tau_0$ is the normalised frequency variable and τ_0 is the asymptotic group delay constant.

Below are plots of the filter characteristics when the filter cut-off frequency is at 10GHz.

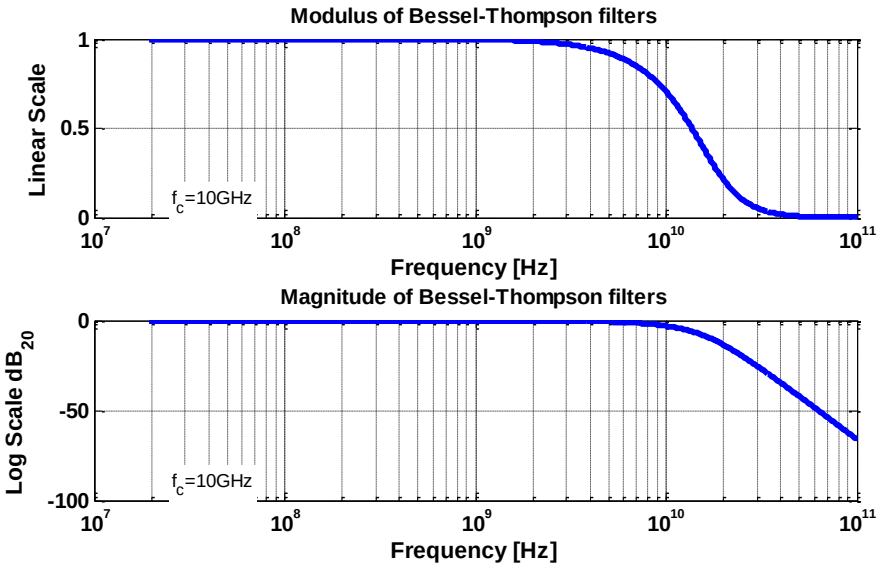

Figure 3.23 Modulus and Magnitude of the BT filter used in the numerical evaluation

The ideal 4th order Bessel-Thompson filter has a nearly flat gain up to the cut-off frequency. The impulse function was obtain by performing an inverse fast Fourier transform (IFFT) of the frequency domain filter response as the 4th order Bessel-Thompson filter impulse function does not have a simple time domain representation. The analysis here has been done using numerical methods with the noise term created in Matlab using equation 3.4. The filtered signal is obtained by convolving the interferometric noise with the filter impulse function, this process is simplified by multiplying the signal and filter response in the frequency domain and then transform the product back to the time domain using IFFT.

The filtered interferometric noise component of the signal using the 4th Order Bessel-Thompson filter is shown below. Frequency separations between the data and

the interferer of 10, 7.5 and 5 GHz are shown in Figure 3.24, Figure 3.25 and Figure 3.26 respectively.

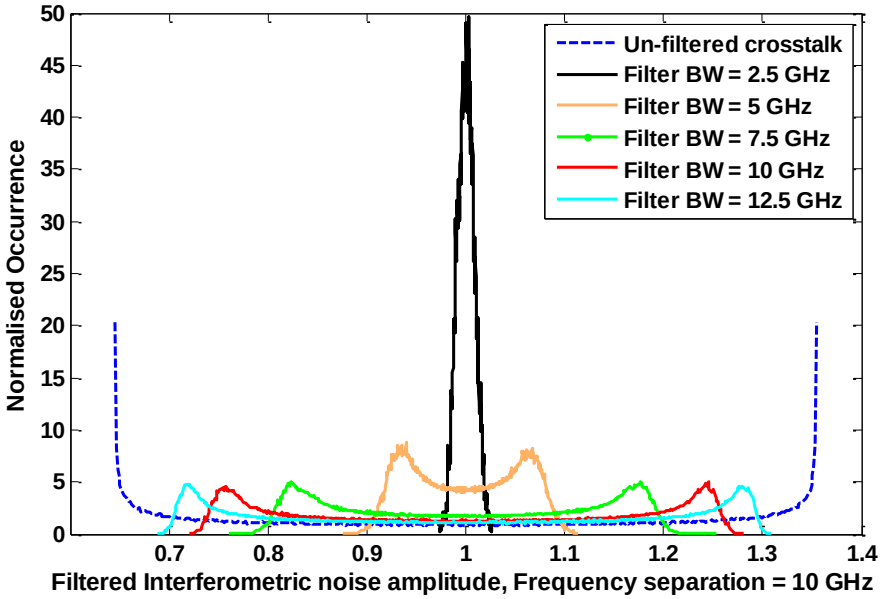

Figure 3.24 Normalised occurrence of the filtered noise term, when the signal-crosstalk separation is at 10GHz, Interferer power is 15dB below the data signal

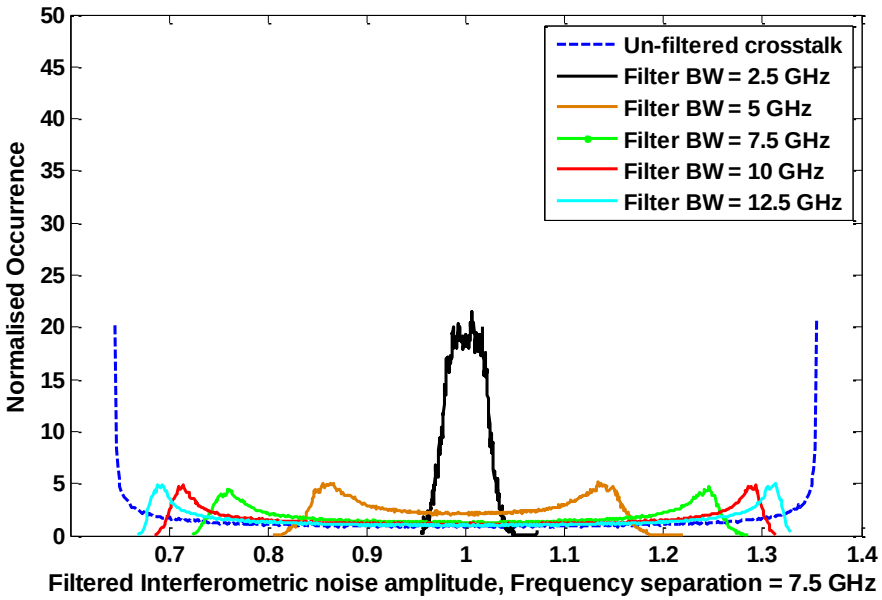

Figure 3.25 Normalised occurrence of the filtered noise term, when the signal-crosstalk separation is at 7.5GHz, Interferer power is 15dB below the data signal

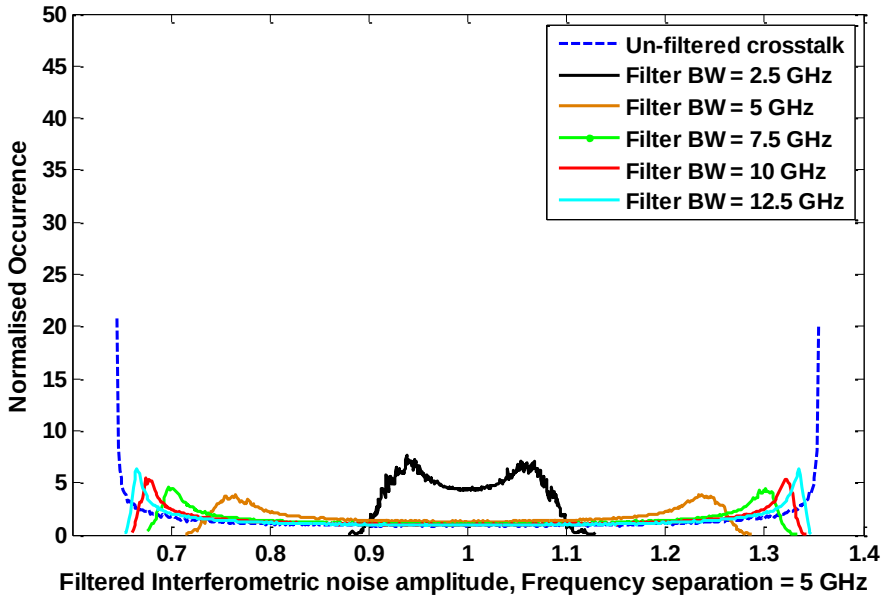

Figure 3.26 Normalised occurrence of the filtered noise term, when the signal-crosstalk separation is at 5GHz, Interferer power is 15dB below the data signal

From Figure 3.24 through to Figure 3.26 it can be seen clearly that as the signal and interferer moves further apart, the filtering becomes more effective at reducing the interferometric noise's width. If the width of the interferometric noise is large it may cross over the detection threshold and cause error during detection, thus decreasing the BER performance.

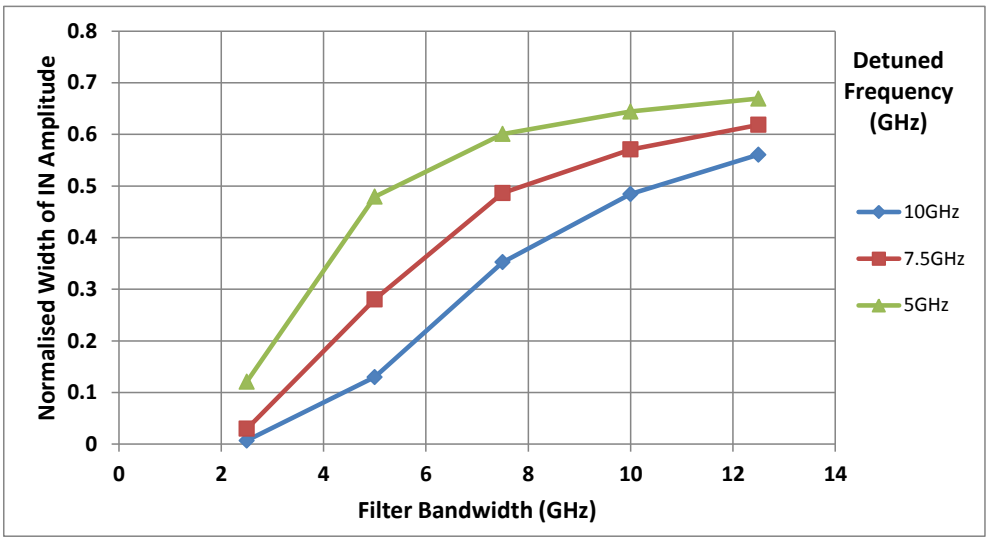

Figure 3.27 Summarising the results in Figure 3.24, Figure 3.25 and Figure 3.26

The results are summarised in Figure 3.27, it was seen that with a large frequency separation of 10GHz, the narrowing of the filter bandwidth from 12.5GHz

to 7.5GHz filter bandwidth is able to reduce the amplitude width of the noise component by about 0.2 unit of normalised noise amplitude. While narrowing to a 5GHz filter bandwidth the width can be reduced by 0.4 unit, this represent the high occurrence peak of the interferometric noise having moved away from the detection threshold by 0.1 and 0.2 units respectively. As the frequency separation between the data and interferer reduced to 7.5GHz then 5GHz, the bandwidth of the filter becomes less effective. At 5GHz filter bandwidths, the noise width reduction is only 0.3 and 0.2 units for 7.5 and 5 GHz frequency separations, respectively. This explains why in both the experiment and the simulation results the BER performance could be up to 5 orders of magnitude better as the interferer is detuned by 0.08nm (10GHz) away from the data signal frequency, especially for high interferer powers levels. The filter bandwidth of 2.5GHz are also included for reference, but it will be unlikely that using this filtering bandwidth will improve the BER performance, on the contrary, if the filter bandwidth is too low e.g. when less than 5GHz, the receiver and filter may removing parts of desired data signal along with the interferometric noise, causing inter symbol interference (ISI), because the high frequency components were filtered and this cause the received eye width to reduce as a result.

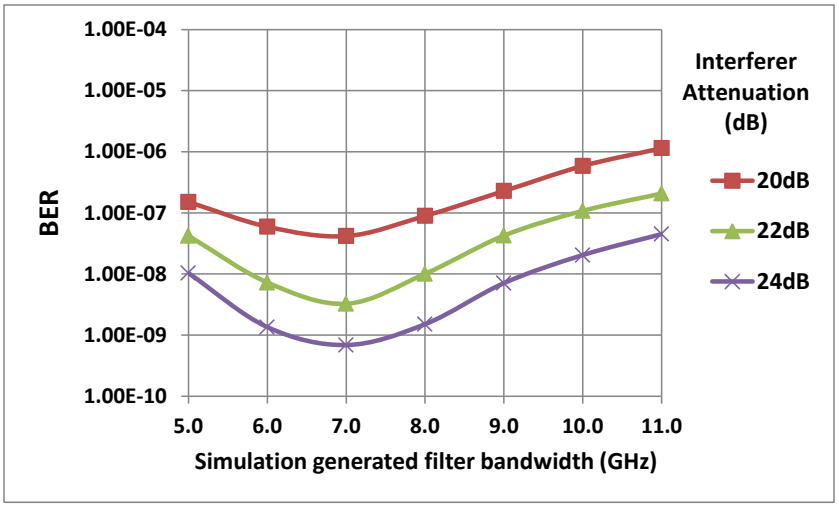

Figure 3.28 Simulated BER performance for a range of ideal Bessel filter bandwidths, data and interferer at 10GHz frequency separation

The BER performance of the simulated system with filter bandwidth ranging from 5 to 11 GHz is shown in Figure 3.28, here the data and interferer frequency separation is 0.08nm (10GHz). For a filter bandwidth of 7GHz, the received signal have the best BER performance, at higher bandwidth the received signal performance is interferometric noise limited, and at lower than 7GHz bandwidth, the BER performance start to decrease due to ISI. When the bandwidth of the filter is higher than the receiver's internal filter bandwidth, the system performance is determined by the smallest filter bandwidth, in this case the receiver's bandwidth.

3.6 Conclusions

In this chapter, we have investigated and the relationship between the BER performance and the electrical filter characteristics for various levels of interferer power, in the condition when interferometric noise is present. The less strictly defined wavelength unique to access networks was taken into account for the first time. The experiment results demonstrated that, for > 0.04 nm (5 GHz) interferer detuning, by adding a 7.5GHz bandwidth electronic filter after the 10Gb/s PIN receiver, the received BER performance is better than using a receiver alone (11GHz internal filter bandwidth). A simulation of the experimental system was also constructed in order to analyse a full range of filter bandwidths. The simulation system was validated by comparing to the experiment results, same trends were observed and the largest difference between the simulated and measured BER performance is less than 1.5 orders of magnitude apart.

An analytical model was also developed to evaluate the impact of receiver filter bandwidth on IN, the frequency separation between the interferer and data caused by not strictly defined wavelength was taken into account. In conclusion, the BER performance characteristics will change with the choice of electrical filtering in

the receiver. It was found that using a narrower filter at 70% of the receiver bandwidth can reduce the interferometric noise amplitude while not causing significant ISI. The effectiveness of the filtering increases with the frequency separation of the data and the interferer, resulting in performance gain of the received data signal.

Chapter 4. Optical Burst Equalisation in Next Generation Access Network

A number of deployed and proposed PONs utilise burst mode Time Division Multiple Access (TDMA) to make efficient use of the bandwidth available in the upstream direction. As bursts are transmitted through optical fibres with varying distance for each ONU link, there will be un-even optical burst power loss between the ONU and the OLT. Therefore, bursts arriving at the receiver will have different optical powers, as illustrated in Figure 4.1. A burst travelling through the shortest, lowest loss part of the distribution network will have relatively high power at the exchange site, usually called a “loud” burst; the low power burst which travelled longer distances or experience more split loss is often called the “soft” burst. The power ratio between the two bursts is called the loud/soft burst power ratio [69], when express in dB and from the receiver’s perspective it is called the dynamic range.

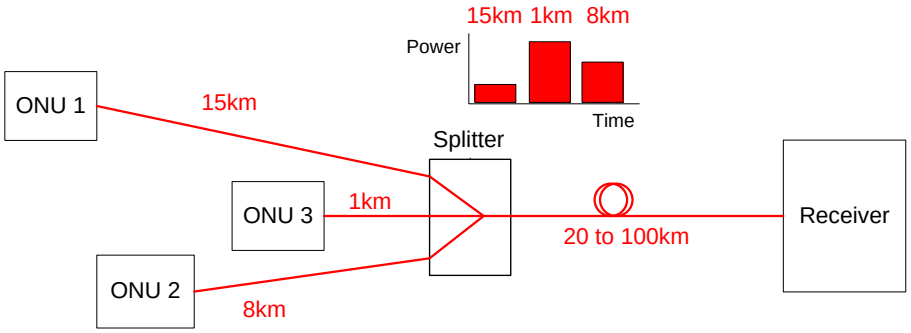

Figure 4.1 PON upstream with ONU located at uneven distance resulting in burst power difference

In the current GPON and EPON standards the transmission distance may be up to 20km, however, distances of 60km or even 100km have been proposed for the next generation access [39]. Therefore, the dynamic range or differential path loss due to burst-burst power variations may exceed the network specified, for example 15dB requirement in the GPON standard. Standard continuous mode receivers are not designed to adapt to these power variations or achieve phase alignment on a burst-by-burst basis in a nanosecond time scale. This will be especially critical in Next Generation PONs (NG-PONs) where the threshold adjustment time will be even shorter due to the higher data rate. Burst mode receivers (BMR) are available for current 2.5Gb/s GPON, and although they are beginning to emerge for NG-PON, the 10Gb/s BMR's complexity and high cost may be reduced if a burst equalisation scheme was employed at the local exchange or just before the OLT.

In a backhaul amplified PON network, the optical amplification can usually be achieved by using EDFAs or SOAs. Since the power level of the OLT transmitter is constant and the EDFA have a high gain and low noise figure, this makes EDFA ideal for broadcast type downstream transmission. In the upstream direction, the data is transmitted from several ONUs in a series of bursts to the OLT, in order to avoid noise funnelling, the ONUs need to be gated, which mean it is only switched on for 125μs at each burst of data. Both the "loud" and "soft" burst will appear in the upstream, this on-going optical power change requires the intermediate site upstream

optical amplifier to have a fast gain recovery time in order to maintain a near constant intra-burst power levels. If the gain recovery time is too long and the intra-burst power difference is too large, then the preamble used by the receiver to initially set the decision threshold will not be the optimum threshold for the data payload. As mention in section 2.2.2, EDFAs have a relatively long gain recovery time at 110 to 340μs which is too slow compared to the 125μs burst duration in current PON requirements. In this aspect, the SOAs have many advantages for the upstream burst-mode operation, including high gain and fast gain recovery time at typically 280ps [70]. Recent research and proposed future access network technology [4, 14] also indicate that SOAs or EDFAs will be placed in PONs as reach extenders. As these active optical amplifiers are already part of the network, they could be used for all-optical burst equalisation with minimal modification to the network and could potentially allow standard receiver components to be used, further reducing the cost of the access network.

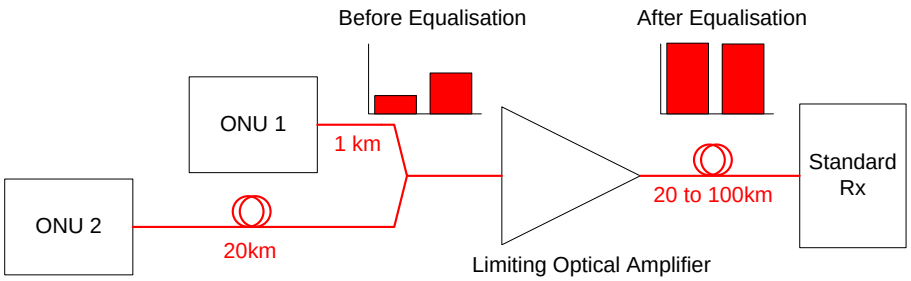

Figure 4.2 PON upstream with burst equalisation using an optical limiting amplifier

The gain saturation effect of the Semiconductor Optical Amplifier (SOA) enables it to act as an optical limiting amplifier, reducing the difference in burst amplitudes and allowing the bursts to have similar detection thresholds at the receiver as shown in Figure 4.2. The advantage over electronic burst mode receiver is that the need for rapidly variable threshold detection and adjustment is removed, possibly allowing much cheaper burst mode receiver or even standard receivers to be

used. This chapter reports on the investigation of this concept of using the SOA as a limiting amplifier to achieve power equalisation of optical bursts by both simulation and experiment. We also suggest that appropriate optical filtering may to be implemented to minimise the effect of spectral broadening of the equalised signal as a result of the SOA saturation.

In this chapter, section 4.1 explains the SOA characteristics and the reason that saturation of the SOA can cause non-linear effects in the amplified signal. Section 4.2 describes the modelling of pulse travelling through the saturated SOA, it also explains the chirp and spectral characteristics. Section 4.3 applies the model to bursts of binary data, the burst are at different power. An extension of the model was also applied and they are compared in terms of their accuracy to simulate the output signal in the time domain and the saturation characteristics of the SOA. The shortcomings of the models used are explained and future adjustment to the model is also suggested. Section 4.4 explains the saturation induced spectral broadening and a solution to reduce the non-linear effect by optical filtering. Section 4.5 describes and analyse the results of the experiment that was set up to test the burst levelling using saturated SOAs and the use of optical filtering to reduce the non-linear effects caused by saturation.

4.1 SOA Characteristics

4.1.1 Non-linear Gain Saturation of the SOA

The amplification operation of SOA is based on the population inversion of electrons and the stimulated emission process in the SOA active region. This stimulated emission is optically confined to the active region due to the refractive index difference which exists between the active region and the cladding p-type and n-type regions. The fraction of the energy confined within the active region is known

as the optical confinement factor Γ [71]. As described in section 2.2.3, the population inversion is maintained by electrically pumping the SOA. When the input signal power is high, the rate of pumping is insufficient to keep a large number of electrons in the excited state. The SOA is considered in saturation because the rate pumping is limiting the rate of photon emissions and therefore, limiting the gain. The following experimental characterisations measured the non-linear gain saturation of the SOAs used in this work.

Two optical amplifier models were available, one designed as a pre-amplifier and one as a booster amplifier. The saturation characteristics of the pre-amplifier SOAs (Kamelian OPA-20NC-FA) used in the experiment were measured with an EDFA amplified CW laser input to drive the SOA into saturation. The input verses output power and the gain saturation characteristics are presented in Figure 4.3. The booster amplifier (Kamelian OPB-15NC-FA) characteristic is shown in Figure 4.4.

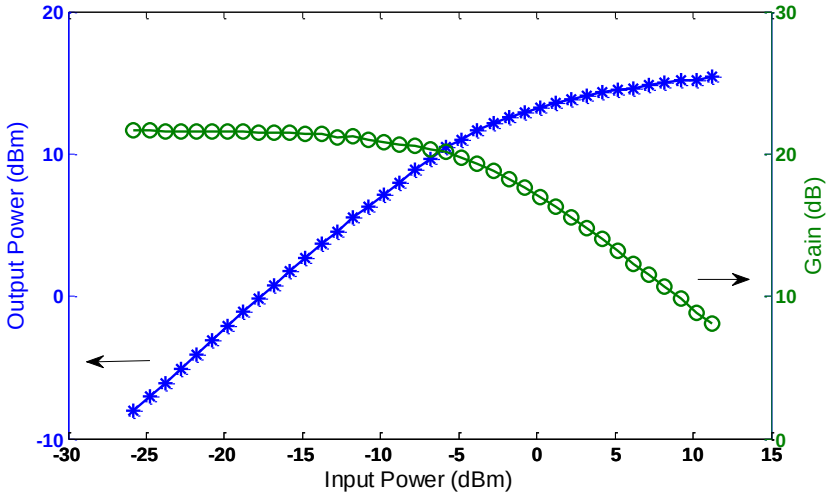

Figure 4.3 Pre-amp SOA input/output power and static gain saturation characteristic

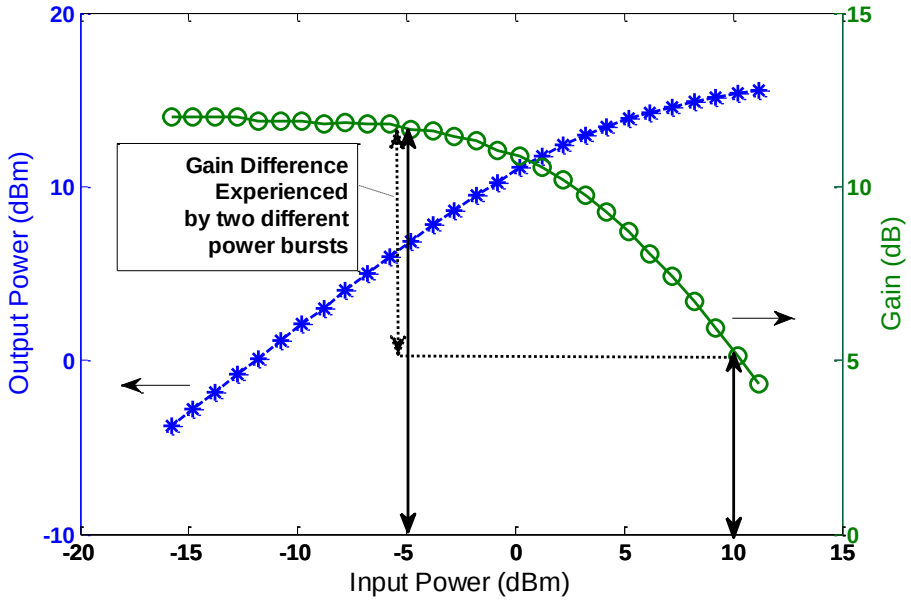

Figure 4.4 Booster SOA input/output power and static gain saturation characteristics

We will now consider the gain performance of the SOA when the signal power originated from the ONU was transmitted through the distribution network and power splitters based on the above characteristics. The received power at the local exchange is typically below -15dBm due to splitter and optical path loss. A pre-amplifier (pre-amp) operating in the linear region was needed to provide sufficient gain to saturate the booster SOA which functions like a limiting amplifier. Figure 4.3 showed that the pre-amp when operating at -15dBm or below has a 21.7dB linear unsaturated gain, which can provide up to 6dBm input power to the booster SOA which is inside its saturation region. In Figure 4.4 the dotted arrows highlight that an input signal of power -5dBm will experience a gain of 11.8dB while an input signal at 10dBm power will experience only 5dB gain, therefore, reducing the power difference between the two signals from 15dB to 8.2dB at the output of this SOA. In terms of bursts, the "soft" burst will experience more gain than the "loud" burst, thus the burst could be equalised.

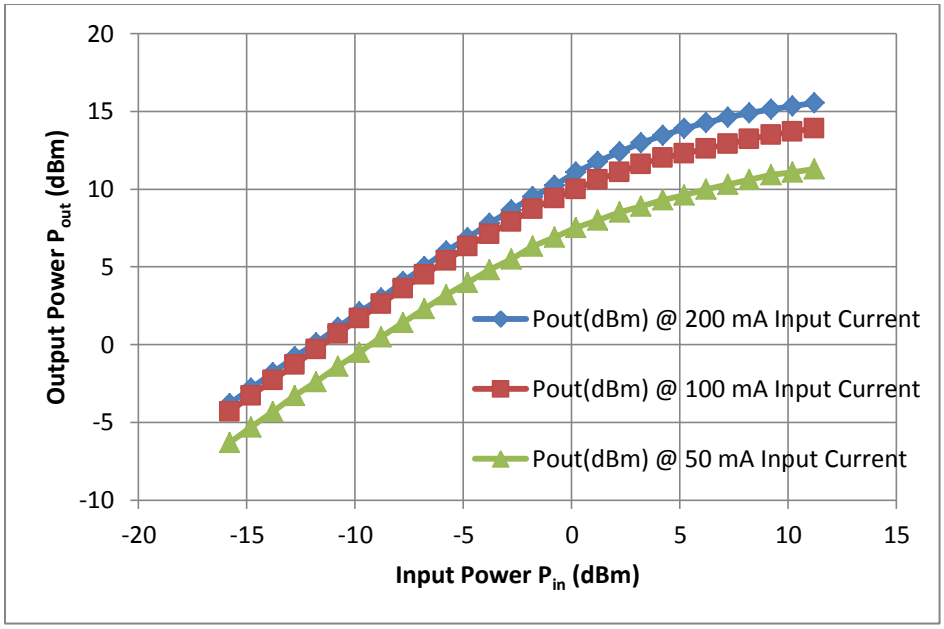

Figure 4.5 Booster SOA output power saturation characteristics at different SOA bias current

The pre-amp has a fibre to fibre maximum or unsaturated gain of 21.7dB and the booster has a maximum gain of about 12dB, while they both have a saturation output power $P_{o,sat}$ at around 12.5dBm, which is defined as the amplifier output signal power when the amplifier gain has fallen by 3dB from its small-signal gain maximum[72]. The output power in deep saturation can reach as high as 15.5dBm in this static characterisation with a CW input. From Figure 4.5 it can be seen that the maximum saturation power depends non-linearly on the bias current, this characteristic can be explained by the number of electrons pumped into the device and the electron depletion as a result of gain saturation. Higher input bias current results in higher output power for the same input power, which effectively increases the saturated output power and the gain at high saturation. This is because an increase in bias current directly increased the number of electrons being pumped into the SOA and the electron depletion rate will therefore, be balanced out by the pumping which makes it harder for the SOA to saturate. It is also observed that the unsaturated gain does not change linearly with bias current, when the bias current is above a certain threshold, in this case 70mA, the increase in unsaturated gain is very

small compared to the increase in bias current. This is because in the unsaturated region, above the threshold bias current the electron density becomes sufficient for stimulated recombination and the unsaturated gain has reached its maximum. In the following experiments a 200mA bias current was used for both SOAs, because it is the typical operating bias current for this SOA which provides high gain and fast gain recovery. The gain recovery time decreases with increasing bias current and the length of the SOA active region, it is usually 200ps for commercially available SOAs [36].

Modulated optical signals contain the energies carried by the binary "0s" and binary "1s". For a semiconductor laser with an external modulator the energy emitted in the binary 0 bit period is non-zero, with the value depending on the design and drive of the modulator. The Extinction Ratio (ER) is defined as the ratio between the power associated with the "1s", P_1, and the power associated with the "0s", P_0.

$$Extinction\ Ratio\ (dB) = 10 \cdot \log_{10}\left(\frac{P_1}{P_0}\right)$$

The SOAs amplifies both the energies of the "1s" and the energies of the "0"s. The addition of amplified spontaneous emission (ASE) noise as a result of using the SOA effectively reduces the ER, therefore, keeping the ER high while amplifying/levelling the signals is desirable but will be difficult, because there are also saturation induced distortions that occur at gain saturation due to the carrier density modulation, which also reduces the ER and hence impact the performance of the equalised signal.

4.1.2 Saturation Induced Phase Modulation in the SOA

The normal use of SOA is for amplifying modulated continuous optical signals, if the signal power is high then gain saturation will occur and this will not be

a major problem if the SOA gain dynamic is a slow process. The gain dynamics of an SOA is determined by the carrier recombination lifetime, which is typically hundreds of picoseconds. With a 10Gb/s modulated signal at the input to the SOA, the gain dynamics of the SOA used in NG-PON will be very fast as the pulse width is only 100ps which is in the same order as the carrier recombination lifetime. Furthermore, for the purpose of signal power levelling or equalisation, the booster SOA will be operating in saturation mode, hence a SOA model that considers the fast gain dynamics is needed for the performance analysis of the burst equalisation system.

Considering a SOA operating in deep saturation, as the signal power increases the electrons in the active region become depleted resulting in a decrease in amplifier gain. A fast changing modulated signal will cause fast depletion and injection of electrons into the SOA active region, which changes the refractive index as a result of the Kramers–Kronig Relations [72]. Therefore, operating the SOA under deep saturation will equalise the signal power but it can also cause unwanted distortions in the equalised signal due to the carrier density modulation in the SOA active region. The distortions in the equalised signal may damage performance, they will need to be taken into account when simulating and modelling the optical burst equalisation system. The refractive index change in an SOA active region may be understood through the complex refractive index $n(t) = n'(t) + jn''(t)$, where the real component n' is the real part of the refractive index representing phase modulation, and the imaginary component n'' indicates the gain modulation within the active region [44]. The parameter relating these two components is the linewidth enhancement factor (also known as the chirp parameter) α, [44].

$$\alpha = \frac{\Delta n'}{\Delta n''} = \frac{\begin{array}{c}Rate\ of\ change\ of\ the\ refractive\ index \\ with\ carrier\ concentration\end{array}}{\begin{array}{c}Rate\ of\ change\ of\ the\ gain \\ with\ the\ carrier\ concentration\end{array}}$$

Considering an electromagnetic wave propagating in the z-direction through the SOA, it can be described using the equation:

$$E(t,z) = E_o \cdot \exp[-j(\omega t - \beta z)] \tag{4.1}$$

where

E_o is the field constant,

$\beta = 2\pi/\lambda_m = (\omega/c)n$ is the propagation constant relating to the refractive index,

n is the refractive index,

$\lambda_m = \lambda/n$ is the local wavelength in the propagation medium,

λ is the free-space propagation wavelength, and $\omega = 2\pi f$ is the angular frequency.

When an input signal travels through an SOA it will cause carrier density modulation, which changes the propagation constant β via refractive index modulation, therefore, the phase of the propagating signal is modulated by the β parameter and by the change in refractive index.

When the gain of the active region is saturated by an incoming pulse, it does not recover instantly. The leading edge of the input pulse will experience the full gain while the trailing edge experiences less gain as the gain saturates during the pulse. The phase change in this process is characterised by Agrawal's equation [42] :

$$\frac{\partial \phi}{\partial z} = -\frac{1}{2}\alpha g(z,t) \tag{4.2}$$

where

ϕ is the phase,

α is the linewidth enhancement factor or chirp parameter and,

g is the time dependent gain of the active region.

Since the incoming pulse modulates its own phase at gain saturation, this phenomenon is also called Self Phase Modulation (SPM).

4.2 Simulating Self Phase Modulation with a Single Pulse

A dynamic model that considers the SPM effects is the SOA model required in this work. The first part of this study is based on Agrawal's model [42]. The model is a dynamic description of the signal in the SOA, taking into account the temporal characteristics of the carrier lifetime. It was first written in Matlab code based on the following theory and equations and will later be used in OptSim as a CCM (Custom Component for Matlab).

$$\frac{dh}{dt} = \frac{g_o L - h}{\tau_c} - \frac{P_{in}}{E_{sat}}[\exp(h) - 1] \tag{4.3}$$

where

h is the natural logged gain, i.e. $\ln[G(\tau)]$, of the SOA active region,

$g_o L$ is the small signal gain,

τ_c is the carrier lifetime,

P_{in} is the input pulse instantaneous power,

E_{sat} is the saturation energy and,

note here that $G_o = \exp(g_o L)$ is the unsaturated amplifier gain [42].

The output pulse shape can then be obtained from this equation:

$$P_{\text{out}}(\tau) = P_{\text{in}}(\tau)\exp[h(\tau)] \tag{4.4}$$

where P_{out} is the instantaneous output pulse power. The term $h(\tau)$ is the gain of this theoretical SOA and is solved from Equation 4.1 using the Runge-Kutta 4$^{\text{th}}$ Order numerical integration methods.

The frequency chirp is also given in [42], based on the phase change described earlier.

$$\Delta\nu = -\frac{1}{2\pi}\frac{d\varphi}{d\tau} = -\frac{\alpha}{4\pi}\frac{dh}{d\tau} = -\frac{\alpha}{4\pi}\frac{P_{in}}{E_{sat}}[G(\tau) - 1] \qquad (4.5)$$

A Matlab simulation of a travelling pulse was created by using Equations 4.1 to 4.3, the results generated and shown in Figure 4.6 through to Figure 4.8 was validated by comparing with the results given by the paper [42]. This validation process was important because it can reveal errors in the programming and it can confirm that the time domain and frequency domain signal behaviours are identical to the known results before moving on to using the model for further simulations.

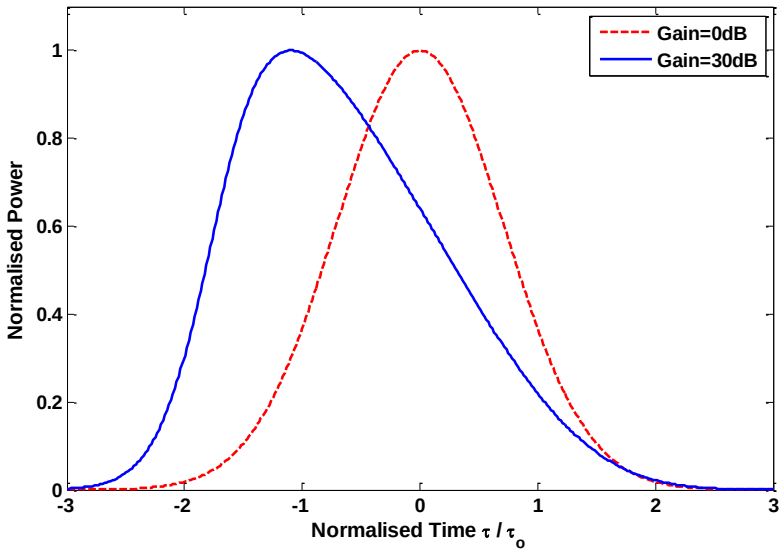

Figure 4.6 Time domain signal frequency shifted

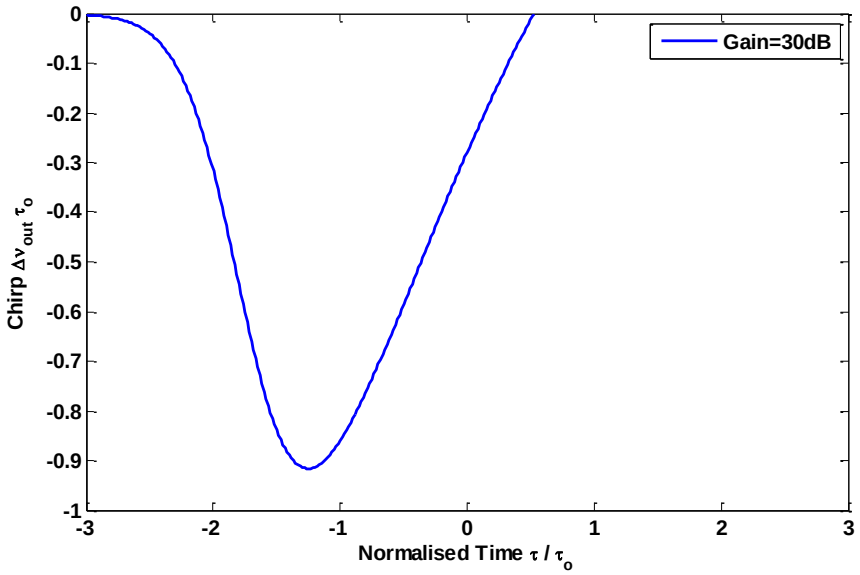

Figure 4.7 Chirp of the Gaussian pulse

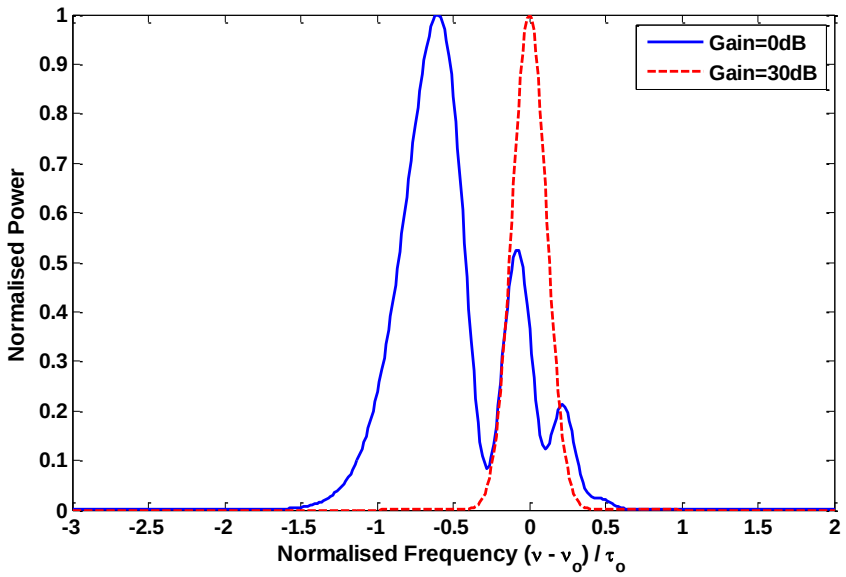

Figure 4.8 Power Spectra of the shifted signal

The model was successfully validated because all three simulation results are identical to the ones presented in Agrawal's paper [42] for a Gaussian pulse input, with a linewidth enhancement factor of 5. As well as validating the model, these results also provide easy to understand details of the SPM and chirping of the input pulse. A shift of the pulse towards the lower frequency side was observed as the amplifier gain increases to 30dB. The leading edge of the pulse has a higher gradient

than the trailing edge of the pulse, because the leading edge experienced more gain thus higher magnitude of phase shift than the trailing edge. The chirp shape in Figure 4.7 corresponds to the frequency shift in Figure 4.6, the power spectra in Figure 4.8 also showed a shift towards the low frequency side which resulted in spectral broadening of the pulse. It is expected that with a large number of pulses, the chirp effect on a signal pulse is re-produced on every bit of the actual signal that travel through the amplifier under saturation, which cause significant overall spectral broadening in the received signal spectrum.

4.3 Simulating the Equalisation of Bursts

The RSoft OptSim package was used to perform system simulation of optical networks. OptSim is designed for simulating and analysing signal propagation and performance of optical systems, it contains a large amount of built-in components such as lasers, modulators and measurement probes. This allows fast prototyping of an optical system, it also considers logical and electrical signals, so that the input signal can be adjusted to suit the need of the system. The physical layer burst structure was deduced from the GPON standard's upstream frame structure [29] and applied using 10Gb/s data rate, as the burst structure information in the NG-PON standard was not available at the time of this work. It is also expected that NG-PON will have a similar physical layer burst structure based on the timing definitions used in GPON. The frame length is fixed at 125μs, if a single burst occupied one frame, the burst will be 125μs long (1.25×10^6 bits at 10Gb/s). At the beginning of each burst, the physical layer overhead is a mandatory 192 bits. That includes 64 bits for the guard time, 108 bits for the preamble (101010…10) and 20 bits for the delimiter (ten 1s and ten 0s). To reduce the simulation time, the payload of the burst is reduced to 500 bits, because the receiver relies on the overhead section to determine power

threshold of the incoming burst, the preservation of the overhead time is important while the payload section will only extend the simulation time.

When the desired component with the required characteristics are not available in OptSim, the software package also supports the importing of a special customised component, whose behaviour during the simulation is described by an external Matlab script, called the Custom Component for Matlab (CCM). Such a component executes an external routine in Matlab to perform the custom transfer function on the signal from OptSim. Agrawal's SOA model [42] that was written in Matlab code was modified so that it becomes a transfer function routine in the simulation. The Gaussian pulse input was adapted to accommodate a stream of data array passed down from any previous OptSim component. The output of the CCM no longer generated a result set in Matlab, instead a stream of data array containing the complex electro-magnetic field information represented optical signal was pass onto any next component in OptSim. The CCM was managed in a transparent way in the simulation with optical input and output signals, therefore, it behaves like a black box optical component in the system simulation. The component also had an externally adjustable gain variable. Instead of using a Gaussian pulse, a random sequenced binary signal was used at the input to modulate the laser in the simulation.

Also a burst generator unit was written as a Matlab component that generates bursts of equal power level with the two outputs of the generator feed alternating burst with set guard time, preamble and delimiter to the external modulator. Lasers with 0dBm power were modulated with the bursts, while the attenuators have losses of 10dB and 5dB respectively, so that the bursts entering the SOAs are at 5dBs apart. The preamp SOA had a 26dB gain and the booster had a 16dB gain. The system schematic in OptSim is shown in Figure 4.9.

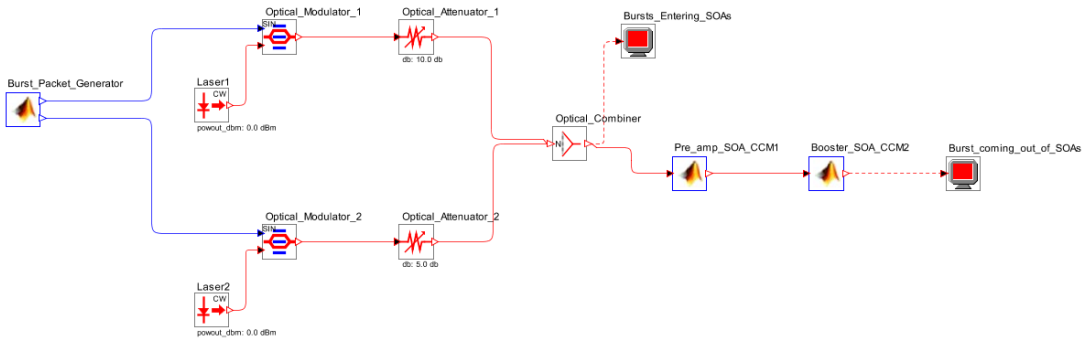

Figure 4.9 Burst Equalisation Simulation using Customised MATLAB Component (CCM)

The initial OptSim results using the Agrawal's SOA model were not ideal, as there are gain spikes occurring at the beginning of each burst and the gain does not seem to recover afterwards, causing a larger than expected gain distortion that is almost one third of the burst amplitude. The reason is that the initial model used a fixed-step solver to solve *h* in differential equation 4.3, where the accuracy of the solution is proportional to the step size of the solver [73]. At the beginning of each burst, the sudden rise of the optical power created a large error in the gain which caused the high spike at the beginning of the bursts.

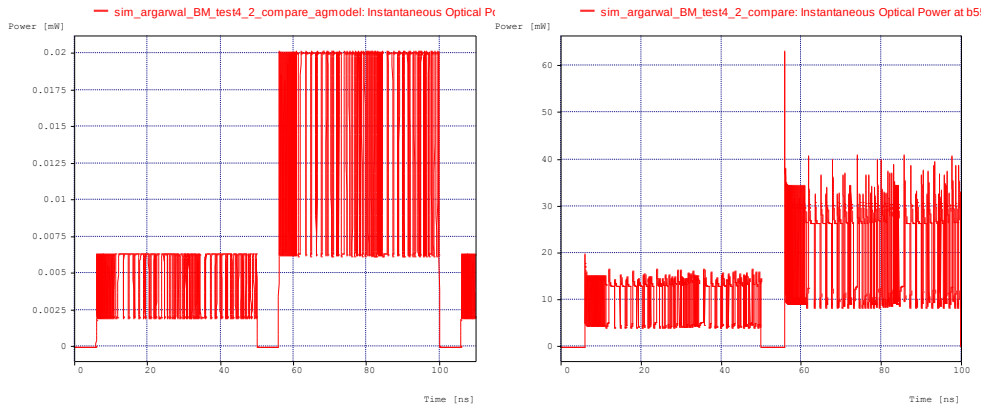

Figure 4.10 Input bursts (left), Gain spike in time domain simulated SOA output (right)

Although a 0.75 bandwidth filtering of the input electrical signal was used to smooth the edges of the pulses in the input bursts, the gain spike still remained significant. The result is shown in Figure 4.10. A variable step size is required so that when the system state is changing rapidly the step size is reduced to provide

better accuracy. This variable step solver is provided in Matlab's tool box and it is also based on Runge-Kutta 4th order numerical solver used for this simulation.

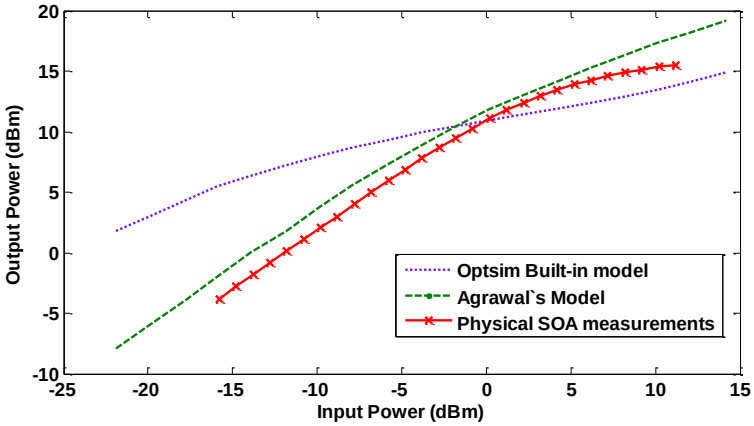

Figure 4.11 Agrawal's model, SOA gain saturation characteristics compared with the physical SOA measurements

Although Agrawal's model predicts the temporal effects on the signal well and fits the experiment result better than the built-in model in OptSim, it did not equalise the burst well. This can be explained by the simulated power saturation characteristics seen in Figure 4.11. At high input power, the physical SOA output power saturates; the curve representing the physical SOA in Figure 4.11 started to saturate at around 15.5dBm output power, as the input power equals the output power. However, the output power in the simulation result did not saturate and kept increasing. This suggests that the effects that cause gain compression at high saturation are not correctly modelled. The unsaturated output power in the simulation results was also constantly higher than the physical SOA measurements as well. Therefore, in an attempt to model the high saturation regime characteristics of the SOA, a more recent model developed by Mecozzi et al. [49] based on the extension of Agrawal's theory was tested, as it included the dependency of SOA gain on the energy distribution of carriers which was neglected in Agrawal's model [47]. The hypothesis was that since these considerations contribute to gain suppression at high

saturation, the model based on Mecozzi's theory may result in a better simulated SOA gain saturation characteristics.

As described in the literature review, this model was proposed in [48] as an extension to Agrawal's SOA model. Then a computer simulator was presented in [49], which characterised the input to output response using three sets of differential equations to describe a combination of interband (between the conduction and valence band) and intraband effects (energy distribution of electrons in the conduction band). These changes all contribute to the overall complex gain across the active waveguide, which are related to three different physical processes: one interband effect, the Carrier Density Depletion (equation 4.7) which is similar to Agrawal's equation 4.3 and the two ultrafast nonlinear intraband processes (Spectral Hole Burning and Carrier Heating), as described by equations 4.8 to 4.9. The input signal at a specific wavelength causes stimulated emissions only between specific energy levels in the SOA active region material, at high input power this burns a hole in the conduction band since the electrons at that specific level are depleted [74], this is called Spectral Hole burning (SHB). This temporarily changes the carrier density until the hole is filled by carrier re-distribution after a time τ_1 which is the spectral hole burning time. Carrier heating is the effect for changing the carrier distribution temperature to reach the lattice temperature of the semiconductor material, the resulting increase in temperature decreases the gain [72]. Two mechanisms can induced the heating, they are free carrier absorption which moves carriers to higher energy levels in the band and carrier-carrier scattering which allows carriers with high temperatures to share their energy with the rest of the distribution. Therefore, the overall gain profile is a sum of all three transfer functions relating to both the interband and intraband effects [49] as in equation 4.6. The following Ordinary

Differential Equations (ODE) were taken from [49], they were implemented in the SOA model with a variable step solver in Matlab.

$$G(t) = \exp[g_m(t)] = \exp(h_N + h_{SHB} + h_{CH}) \tag{4.6}$$

$$\frac{dh_N}{dt} = -\frac{h_N}{\tau_S} - \frac{1}{P_S\tau_S}[G(t) - 1]P_{in}(t) + \frac{g_O}{\tau_S} \tag{4.7}$$

$$\frac{dh_{SHB}}{dt} = -\frac{h_{SHB}}{\tau_1} - \frac{\varepsilon_{SHB}}{\tau_1}[G(t) - 1]P_{in}(t) - \frac{dh_N}{dt} - \frac{dh_{CH}}{dt} \tag{4.8}$$

$$\frac{dh_{CH}}{dt} = -\frac{h_{CH}}{\tau_h} - \frac{\varepsilon_{CH}}{\tau_h}[G(t) - 1]P_{in}(t) \tag{4.9}$$

Where

G(t) is the time dependent overall gain in the active region of the SOA;

$g_m(t)$ is the natural log of the overall gain;

g_O is the natural log of the small signal gain $G_O, G_O = \exp(g_O)$;

h_N, h_{SHB}, h_{CH} are the contribution of carrier depletion, SHB and carrier heating to the overall gain respectively;

$\varepsilon_{SHB}, \varepsilon_{CH}$ are the gain compression coefficient for SHB and carrier heating respectively;

τ_S is the total spontaneous lifetime;

τ_1 is the spectral hole burning time;

τ_h is the carrier heating time;

P_S is the saturation power;

$P_{in}(t)$ is the instantaneous input power.

Once the input power and the values of these parameters are given, the ODEs can be solved using the numerical solver in Matlab. The three contributions to the overall gain are added together to give the natural log of the overall gain profile

$g_m(t)$, which can be used to calculate the output field and the overall phase change using the equations below, again from [49].

$$\emptyset(t) = -\frac{1}{2}\alpha_N(h_N - g_O) - \frac{1}{2}\alpha_T h_{CH} \tag{4.10}$$

$$E_{\text{out}}(t) = E_{\text{in}}(t) \cdot \exp(\frac{1}{2}g_m + \text{j}\emptyset) \tag{4.11}$$

where

$\emptyset$ is the phase of the output field,

$\alpha_N$and α_T are the linewidth enhancement factor relating to carrier depletion and carrier heating and,

$\frac{1}{2}g_m$ is the natural log of the amplitude gain.

Both Agrawal's and Mecozzi's theory [42, 48] assumed the SOA is an ideal amplifier with zero internal loss, however, the waveguide internal loss will need to be included for the SOA to simulate a real device. The internal loss can be simulated by considering the SOA as a device divided into M segments of length Δz, then inserting linear attenuators between the segments. Each segment will have a small signal gain that is $G_O^{1/M}$, followed by an attenuator of loss $A = \exp(-\alpha_{int}\Delta z)$, assuming $\alpha_{int} = 4000\text{m}^{-1}$, z = 500μm. It was found that M=3 is sufficient to accurately characterise the device [49]. The time domain result using the same input as before and the new model including intraband effects, variable step size and waveguide internal loss is shown in Figure 4.12.

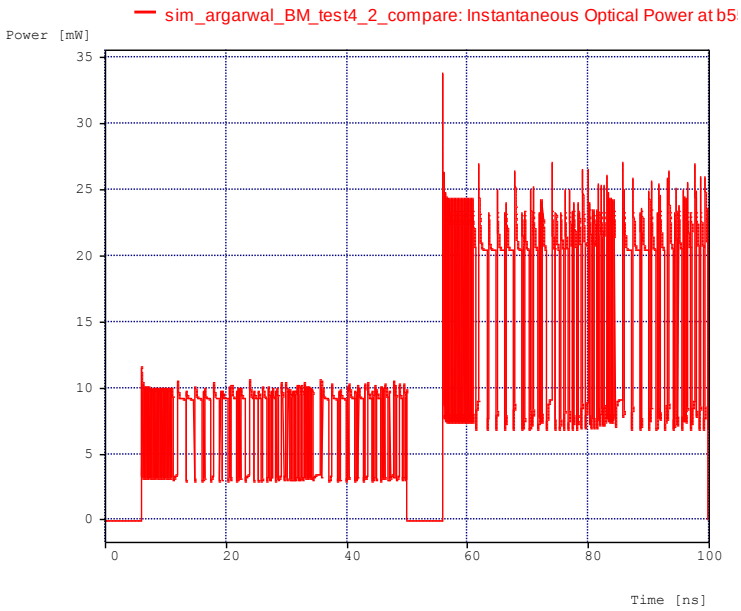

Figure 4.12 Burst at the output of the Mecozzi's model, showing reduced spike.

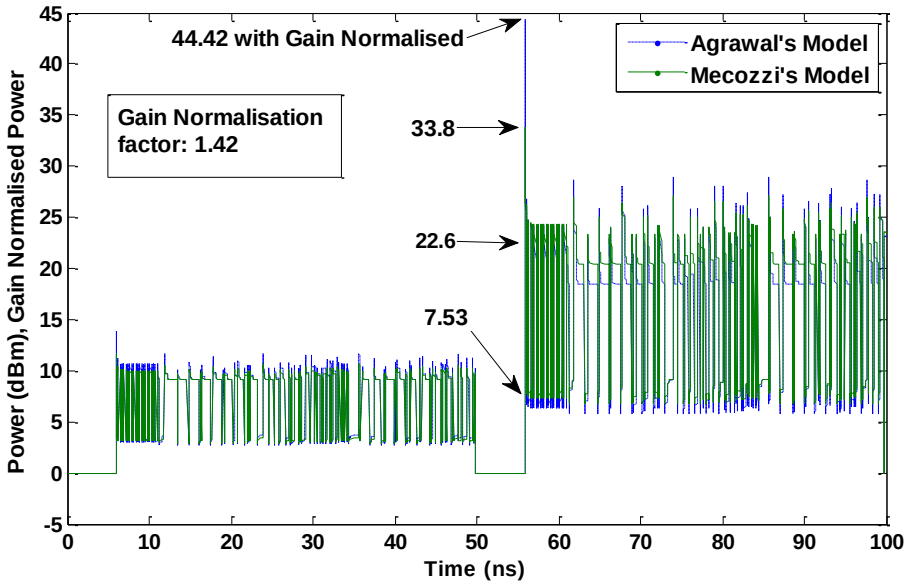

Figure 4.13 Comparing the spikes in the bursts of the two models, with Gain Normalised Agrawal's model result.

In the result of the simulation using Mecozzi's model the spike power is reduced from 63.1dBm in Figure 4.10 to 33.8dBm in Figure 4.12, since the gain was also reduced due to the introduction of waveguide internal losses. Figure 4.13 is presented to show the reduction in the spike power without the influence of the reduction in gain. The gain normalisation factor is calculated as the power ratio between the two results. The result using Agrawal's model is then normalised by this

factor so that it is comparable to the result using Mecozzi's model. This shows that using the variable step solver as well as considering the intraband effects can improved the accuracy of the simulation result especially when rapid changes occur in the signal.

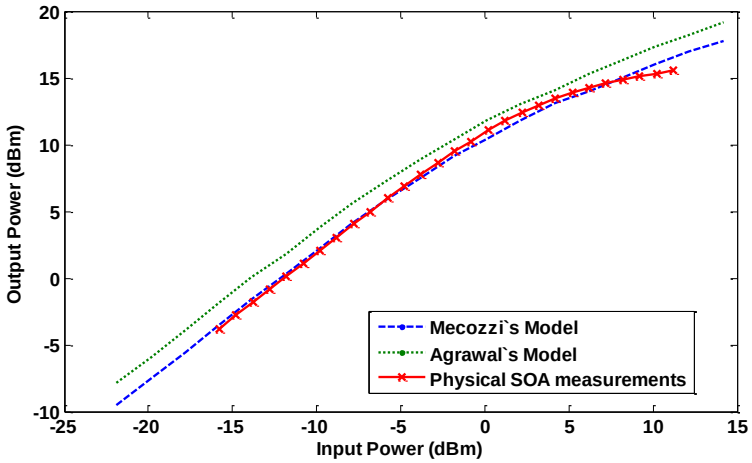

Figure 4.14 Gain saturation characteristics of the two models compared with experiment result

The simulation result of Mecozzi's model is almost identical to the physical SOA measurement between -15dBm to 0dBm input power. Therefore, in the unsaturated regime, the model re-produced the physical SOA results. The lowered output power of Mecozzi's model compare to Agrawal's model is due to the included waveguide internal loss. However, by using the new model the output power saturation characteristics did not improve at the high input power, which should have been the high saturation region of the SOA, at input powers above 0dBm.

The input and output power saturation characteristics of both SOA model were measured and compared with the experimental booster SOA measurements in Figure 4.14. The Mecozzi's model showed similar trend to the physical SOA up to about 5dBm input power. We expect the curve to flatten at 15dBm output power as the SOA saturates then increase linearly again as the SOA will become transparent, but the Mecozzi's model saturates at about 10dBm output power then start increasing

linearly. The saturation region of the Mecozzi's model was too short compared to the physical device, therefore, we will have to use lower input powers in our simulation, so that we do not exceed the 5dBm input power to maintain validity of the model.

Although the SOA model is still not simulating the SOA characteristics precisely, it is already capable of simulating the time-domain nonlinear effects of a saturated SOA, this is important because these effects were not considered by previous literature analysing similar methods of burst equalisation. The successful simulation of these nonlinear effects will also provide the basis for the spectrum analysis of the output signal from the saturated SOA, which will aid the subsequent recover and detection of the original signal. Improvements can be made to the model so that at the high saturation regime, the theoretical simulation matches the experimental result more precisely.

4.3.1 Shortcomings and Adjustments to the SOA Model

The SOA models used above assumed a constant carrier lifetime at 200ps. This assumption is valid for ultra-short pulse interactions (at less than 50ps pulse width [75]) and the small-signal regime of SOA operation, i.e. when the SOA is operating far from saturation, which is not the case here. In the case of pulse width more than 50ps and less than 100ps, which is the main consideration for 10 Gb/s access network, the saturation induced gain compression dominates. Therefore, the response of the amplifier is mainly determined by the effective carrier lifetime, which is carrier density dependent [75]. The effective carrier lifetime is governed by two terms: the spontaneous emission rate and the stimulated emission rate.

To correctly model the experimental gain saturation characteristics, a carrier density dependent carrier lifetime is required to replace the constant carrier lifetime

parameter in the equations 4.7. The effective carrier density is given by equation 4.12 in [75].

$$\frac{1}{\tau_{eff}} = \frac{\partial R(N)}{\partial N} + \frac{\partial g(N) P}{\partial N \, P_{sat} \alpha_o \tau} \tag{4.12}$$

Where

τ_{eff} is the effective carrier lifetime;

N is the carrier density;

τ is the constant carrier lifetime;

$R(N)$ is the rate of recombination;

$g(N)$ represents the material gain;

α_o is the differential gain, which is $\partial g(N)/\partial N$.

In a bulk SOA model, the differential carrier lifetime is simplified to equation 4.13, note that for spontaneous recombination, $\tau_{eff} = \tau$.

$$\frac{1}{\tau_{eff}} = \frac{1 + P/P_{sat}}{\tau} \tag{4.13}$$

Therefore, when P the input power of the signal is low, P/P_{sat} will be very small and can be neglected, so that the effective lifetime is the same as the constant carrier lifetime. When the input power is high, the term P/P_{sat} is larger than one, making the effective lifetime shorter, thus changing the gain at high input power.

The modification to the model was implemented in the simulation and the result was compared with the experiment measurement of an SOA as shown in Figure 4.15.

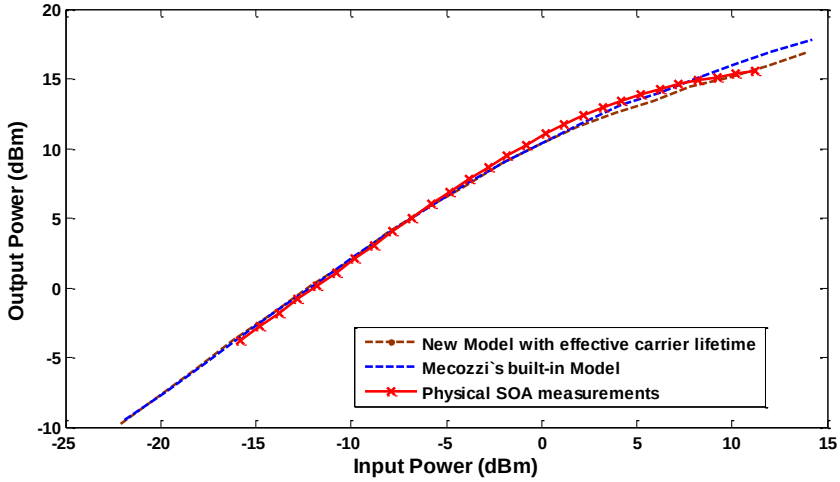

Figure 4.15 Saturation characteristics of the models (New model has the effective carrier life time implemented) compared with experiment results

The simulation results of both models are almost identical to the physical SOA measurement between -15dBm to 0dBm input power. Therefore, at the unsaturated regime, both models re-produced the physical SOA results. At high input power, when the SOA reaches saturation, the carrier lifetime adjusted model's gain is saturating sooner than both Mecozzi's model and the SOA device. The lower gain saturation power of an SOA can limit the output power of the high powered burst and amplify the low powered burst to achieve equalisation. The equalisation using gain saturation is more clearly visible in the time domain result of the system simulation.

4.3.2 Burst Equalisation Simulation Results

Using the simulation system configuration shown in Figure 4.9, and implementing the carrier lifetime adjusted model, the time domain signals before and after the equaliser is shown in Figure 4.16. The 5dB burst power level difference were almost equalised and the effect of gain modulation at the leading edge of each pulse can also be seen.

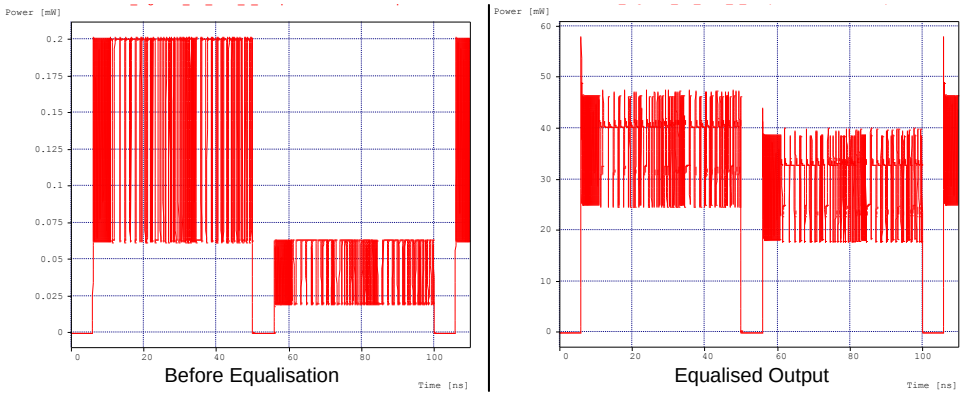

Figure 4.16 (left) The input signal to the limiting amplifier and (right) the output signal showing amplified and equalised bursts.

Frequency chirping is produced when the phase modulation occurs together with the signal distortion at saturation due to refractive index changes. The signal frequency spectrum will be broadened by the chirped component of the signal. The simulation reflects this as the spectrum of the input and equalised signals are compared in Figure 4.17, the optical frequency shift is clearly visible after equalisation by a saturated SOA. The broadening of spectrum is discussed further in section 4.4.

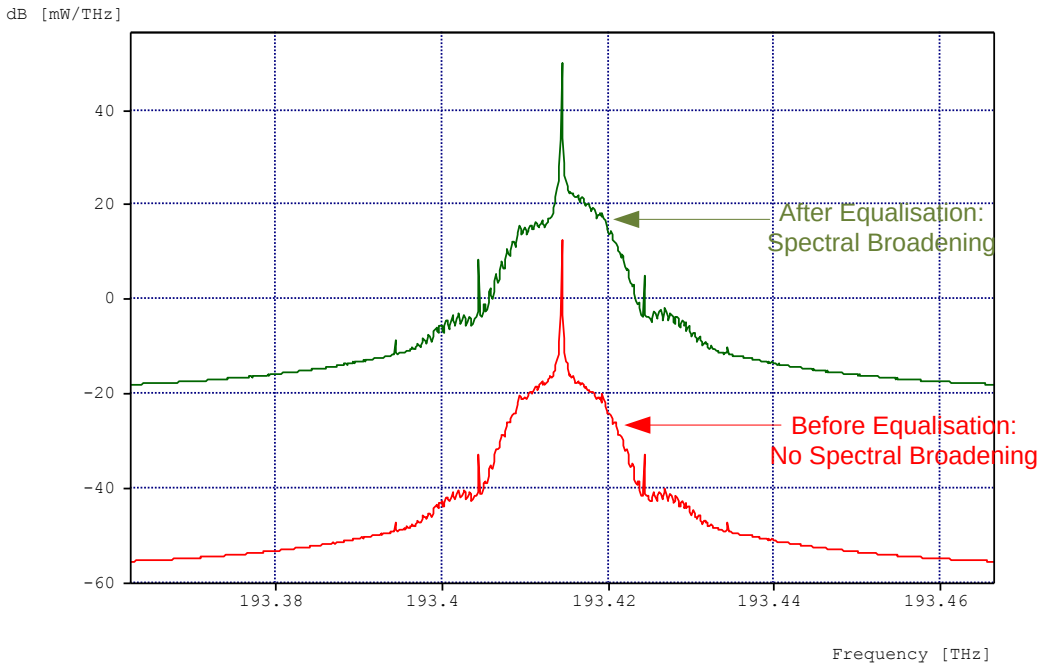

Figure 4.17 Spectrums of the simulated input (green) and equalised output signal (red)

4.4 Spectral Broadening and Optical Filtering

4.4.1 The Mechanism of Spectral Broadening

When an intense optical signal is input to an SOA, the stimulated emission process will cause the electron density in the conduction band and the signal gain to decrease, the depletion and recovery of electrons are not instant, therefore, the amplified optical signal at the output is distorted. During this modulation of the electron density and gain, the refractive index of the SOA active region is modulated at the same instance, therefore, frequency chirping occurs together with the signal distortion in the time domain. The signal frequency spectrum will be broadened by the chirped component of the signal in which the chirped signal will be frequency shifted with respect to the un-chirped component of the signal. As a result of the co-existence of chirp and signal distortion, suppressing the broadening in the frequency domain is expected to reduce the signal distortion in the time domain as well. The effect of filtering was observed in [76] when an input of continuous signal at 7Gb/s is passed through a single SOA. It showed the BER performance of the unfiltered output signal has degraded while for the filtered signal there was no degradation. Instead of avoiding the nonlinear spectral broadening by avoiding gain saturation, it is possible to reduce the signal distortion after the burst is levelled to further simplify the equalisation system.

4.4.2 Simulated Performance Result with Optical Filtering

The SPM induced by gain saturation will lead to spectral broadening of the pulse [42]. The use of narrow optical filtering to reduce the waveform distortion induced by saturated SOA in optical switching was reported in [77]. It suggest that by using an optical band pass filter, nonlinear patterning effects of ultra-short 2ps pulses can be reduced from 2.5dB to 1.1 dB by detuning a 1nm optical band pass

filter towards the side of spectrum that is opposite to the red-shifted chirped components. In the context of burst equalisation system, the performance based on the extinction ratio and BER changes by the applied filter need to be analysed.

Using the simulation model in section 4.3, the BER performance of the equalised bursts were assessed, an optical filter was also implemented in the simulation to show the differences in performance changed by optical filtering. The result is shown in Figure 4.18.

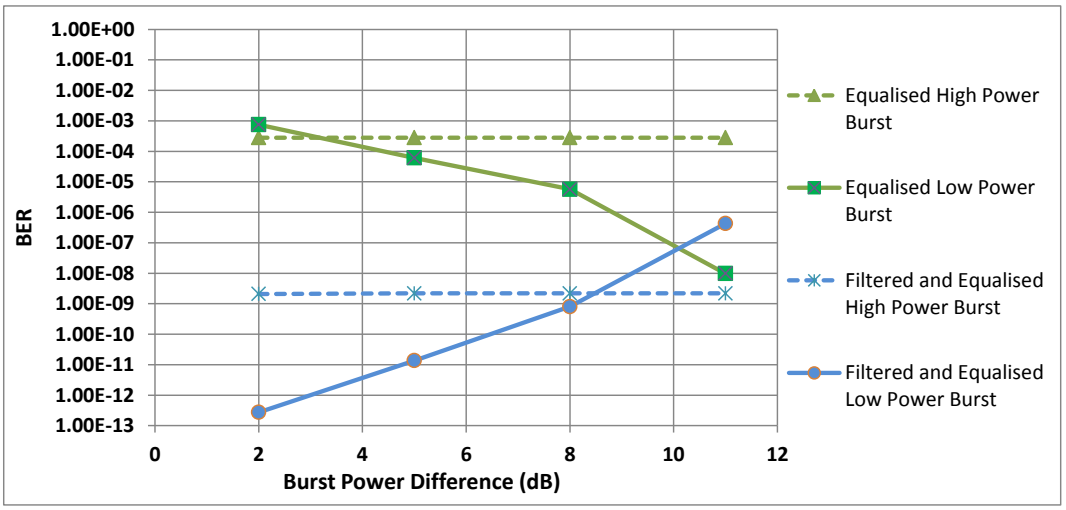

Figure 4.18 Simulation estimated BER comparison between, equalised and filtered burst signal

The "loud" burst power were kept constant, the burst power differences is made by reducing the power of the "soft" burst. As the power differences between the two bursts increased, i.e. as soft burst weakens, the BER performance of the soft burst gets better due to the less saturation induced distortion it had experienced. The equalised high power burst is not error free but have a BER of 5×10^{-4}, this is because the higher burst power saturates the SOA and experiences saturation induced time and frequency domain distortions as well as ASE noise. After the signal passed through a narrow optical filter, with a cut-off frequency at 25GHz from the centre signal wavelength (50GHz DWDM AWG), the loud bursts BER performance is 5 orders of magnitude better the unfiltered case. The soft burst were

initially free of error when its power is 2dB below the loud burst, when this low power burst was getting too weak for detection, i.e. at 11dB below the loud burst, its BER became 1×10^{-6}.

4.5 Burst levelling Experiments

Experimental demonstration of this optical equalisation system with filtering was also created. In order to find a filter with a 1nm bandwidth that also has a sharp cut-off, several optical band-pass filters were measured and the selected filter characteristic is shown in Figure 4.19.

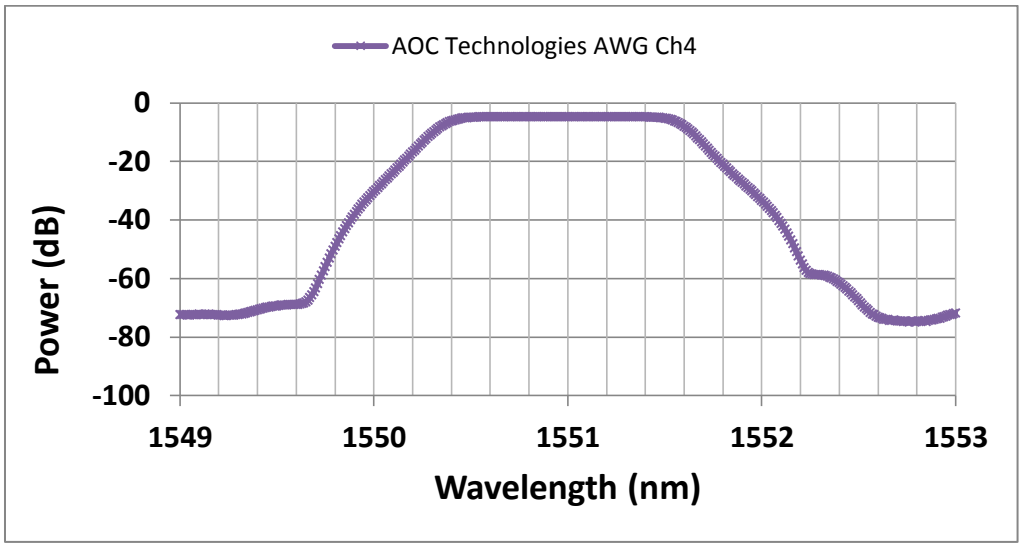

Figure 4.19 Optical filter characteristics

Although a tuneable filter would be ideal in this case, the ones available do not have a sharp enough cut-off. Therefore, arrayed waveguide (AWG) acting as an optical filter that had a suitable sharp cut-off as well as within the wavelength range of the filtering operation will be used in the experiment followed, for studying the performance changes at near the filter cut-off wavelengths.

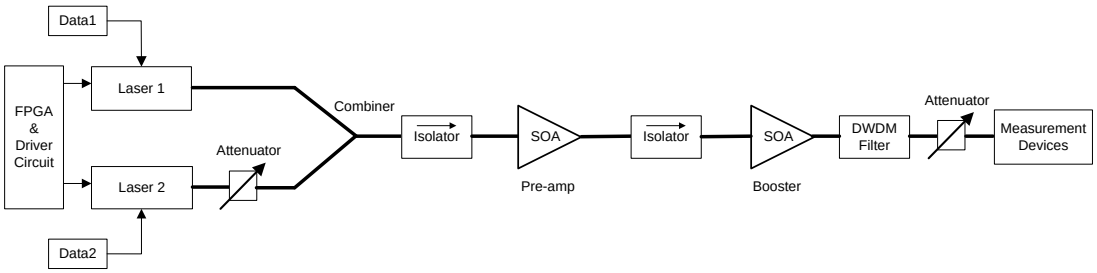

Figure 4.20 Burst equalisation experiment configuration block diagram

The burst levelling experiment configuration is shown in Figure 4.20. Two lasers were gated by two outputs from a Field-programmable gate array (FPGA) to simulate the burst from ONUs. Each packet is 125μs long, modulated by a data signal from a 10Gb/s Pseudo random bit sequence (PRBS) generator, with a 500ns guard time between the two bursts used to prevent overlapping. A 5dB optical attenuator was placed after one of the laser output to simulate the optical path loss of a distant ONU, thus providing the power difference between the two ONUs. The two signals merged at the splitter/combiner just like they would in a real PON. The isolator before each SOA was there to prevent noise from the SOA travelling back to the laser. As described in theory, an optical filter was used to remove the chirped component from the received signal. In a real network the filter can be custom made or picked therefore, it would have been optimised for the network condition. A 10dB attenuator was placed before the Digital Communications Analyser (DCA), because the power from the output of the SOA was too high for its photodetector.

The combined effect of chirp in the SOA and fibre dispersion resulted in spectrum broadening as shown in Figure 4.21. The broadening is a shift in frequency of the chirped component of the signal away from the centre peak frequency which is the un-chirped component of the signal. As demonstrated via simulation in section 4.4, it is expected that through the use of optical filter with a cut-off near the chirped

component, the distortions situated at the broadened part of the spectrum can be reduced.

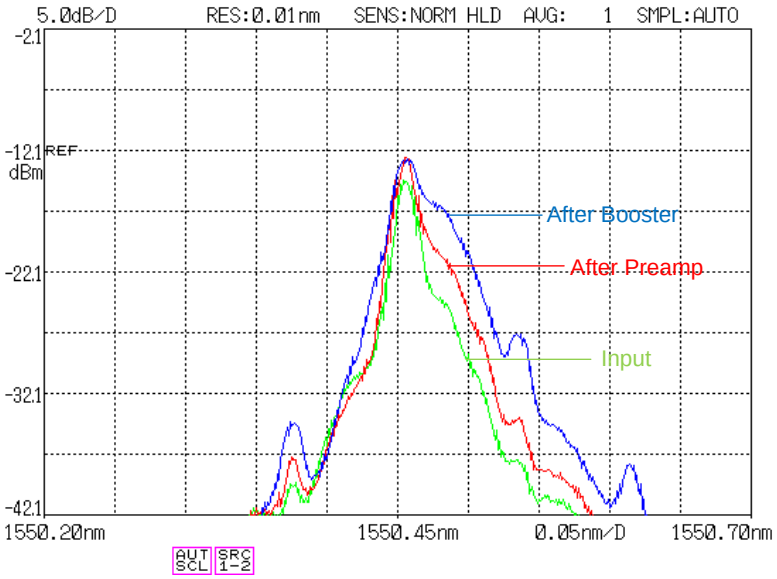

Figure 4.21 Signal Spectrum at the cascaded SOA input, after the preamp SOA and after booster SOA amplification showing spectral broadening at SOA gain saturation

The aim of the experimental system is also to level the bursts and reduce the non-linear distortions in the signal, together with the reduction of wideband ASE noise due to filtering, this approach is also expected to increases the output signal's extinction ratio. Since the AWG filter's pass-band wavelength is fixed, the source laser is tuned instead to observe the performance change near the filter's pass band edge. Changing the laser diodes' control temperature within a reasonable range (25℃ ±15℃) is equivalent to tuning the wavelength. A tuning table was kept for the relationship between the temperatures and the laser wavelengths. It is found that the wavelength of the laser changed linearly with temperature in this range, the temperature is therefore, translated into wavelength for the ease of analysis and understanding. The wavelength of the laser was also tuned to measure the optical spectrum, ER and BER near the cut-off of the optical filter, in the aim to find out how the performance of the system is changed by the applied optical filtering.

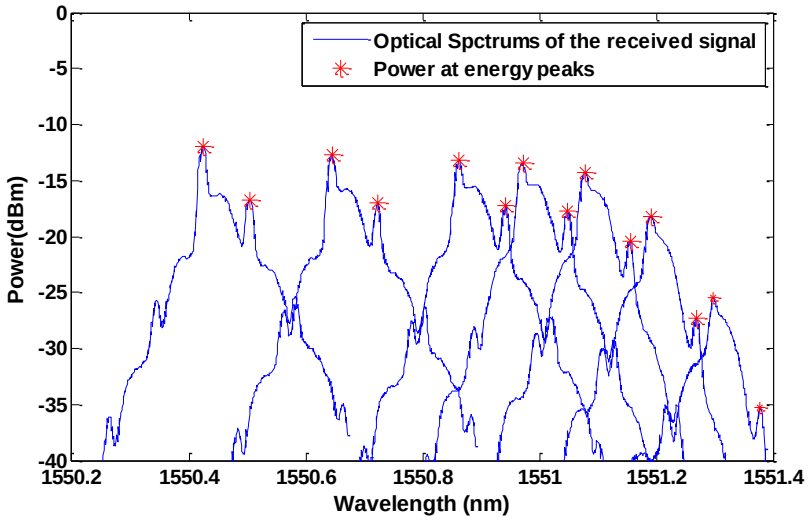

Figure 4.22 Power Spectrums of the amplified signal, the peak and the second highest peak were used as a reference for the chirp and un-chirped components respectively

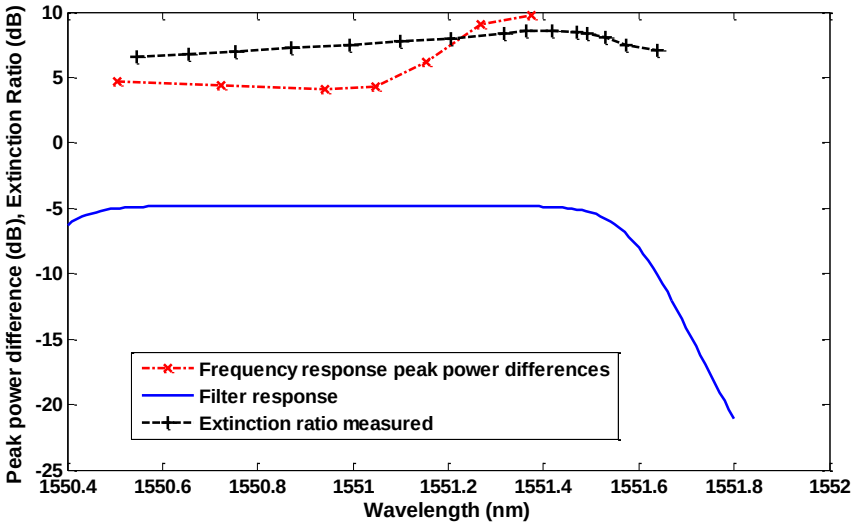

Figure 4.23 Comparison of filter response with ER and peak power differences as wavelength of the signal is detuned to near the filter edge

The results in Figure 4.22 are spectrums of the output optical signal measured by a spectrum analyser as the wavelength of the laser is tuned towards the optical filter edge. The difference in peak power between the energies of the un-chirped component reference peak and the energies of the chirped-side reference peak is increasing towards the filter edge. The plot of these data is shown in Figure 4.23, it compares the measured peak power differences and output signal extinction ratio with the measured filter response.

From Figure 4.23, it can be seen that the ER increased by 2dB near the edge of the filter at about 1551.5nm, representing lower noise floor and reduced the signal distortions at the chirped signal frequency. The ER then decreases because the un-chirped signal frequency components have moved into the filter cut-off frequency. The frequency peak power difference is plotted as a dash curve with X marks in Figure 4.23, it is showing a significant increase in peak power difference near the filter edge, representing the weakening of the broadened part of the signal frequency response. The BER performance was also measured, it showed in Figure 4.24, where the BER performance reached 10^{-9} near the filter edge at about 1551.5nm. This is the same wavelength where the ER has shown the 2dB increase. The performance decreased again sharply to 10^{-2} at 1551.7nm once the filter started to suppress the un-chirped main signal.

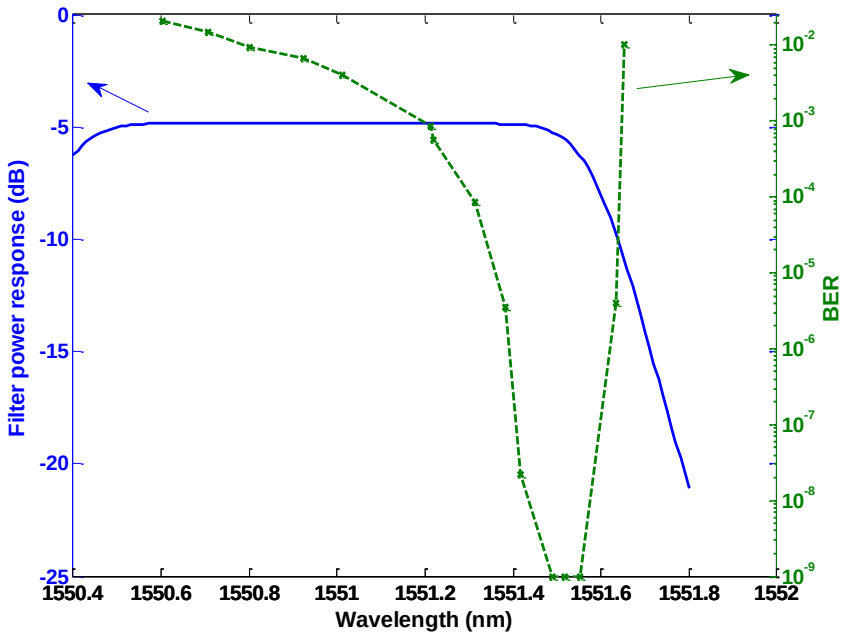

Figure 4.24 BER performance at ONU wavelengths near the filter edge

4.5.1 Power Balancing the SOAs and Extinction Ratio Performance

In the previous experiment, no optical attenuator was placed between the pre-amp and booster SOAs to limit the power going into the booster SOA. The pre-

amp output power should be just sufficient to saturate the booster SOA for burst equalisation to occur. If that power is too high, it may cause un-necessary signal distortion by operating the booster SOA further into the saturation region. Aside from the distortion of the binary "1" of the signal pulse, high ASE noise and elevated "0" floor also occurs at very high saturation, a near worst case example is shown in Figure 4.25.

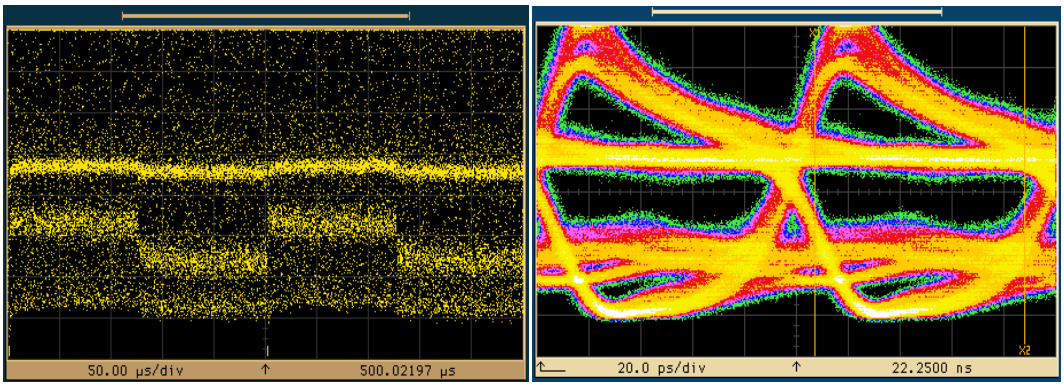

Figure 4.25 Equalised bursts and the eye diagram of one burst with elevated "0" floor and reduced extinction ratio

The elevated "0" will have significant impact on the ER, which it is a ratio between the power associated with the binary "1" and the power associated with binary "0". The two bursts at the input to the preamp SOA had high ERs at 12.87dB (high power burst, laser 1) and 11.5dB (low power burst, laser 2). After the two amplification stage, their unfiltered ERs were 4.43 and 6.36 dB for the high power burst and the low power burst respectively. The lower power burst coming from laser 2 experience more amplification in the linear unsaturated gain region, therefore, its ER was higher than burst from laser 1. In the following result in Figure 4.26, the lower ER of the high power burst from laser 1 was measured, indicating the heavier saturation induced distortion it experienced.

An attenuator was place between the preamp and the booster SOA for the purpose of reducing the signal power entering the booster SOA. The ER of laser 1 was measured with wavelength tuning and the optical filter applied. The optical filter

removed some excess wide band ASE noise, therefore, the filtered signal ER at 6.5dB was 2.1dB higher than the unfiltered case of 4.43dB, with 0dB attenuation.

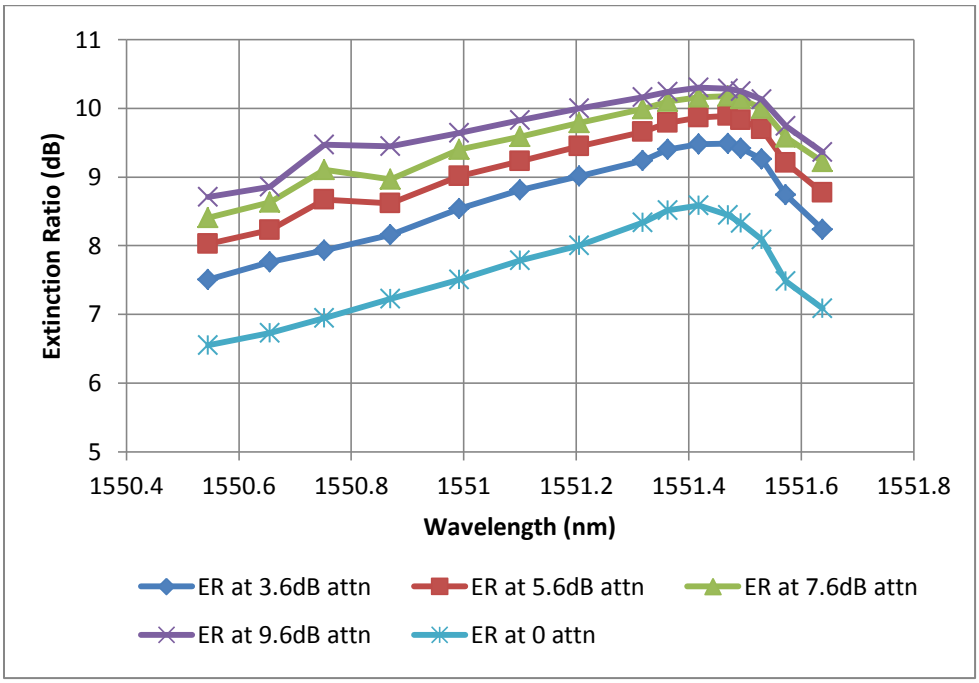

Figure 4.26 Extinction Ratio at different losses when the attenuator is placed between preamp and booster SOA

Similar ER increases that were observed as the results shown in Figure 4.23, as the wavelength was tuned from the centre of the filter pass band to the filter band edge. The ERs measured at various levels of power balancing attenuation is shown in Figure 4.26. Lowering the signal power by 3.6dB after the preamp SOA have increased the ER by 1dB. However, the ER increase became less significant at < 0.5dB, if the signal power is attenuated by 5.6dB or higher. Care must be taken not to attenuate the signal power too much as this will lead the SOA to operate out of the saturation region.

4.6 Conclusions

The near-far power difference problem of the upstream PON burst-mode transmission results in fluctuating burst-by-burst power being received at the OLT. An all-optical solution, including the use of a saturated SOA as a limiting amplifier

to level the burst power was studied. Sample based dynamic SOA models that can be used with OptSim were developed. In contrast to previous work in this area, our studies considered not just the saturation induced non-linear gain but also the saturation induced frequency distortions in the SOA. Two mathematical theories of the saturated SOA were implemented as MATLAB coded blocks in OptSim. The comparisons of simulation results show that Mecozzi's model implemented using a variable step size solver and added internal loss gave better time domain results, represented by the much reduced gain spikes. At deep saturation, it was suggested that using an effective carrier lifetime instead of a constant lifetime can give more precise results at deeply saturated SOA. This parameter is important for accurately simulating the time and frequency domain effects due to gain saturation. Burst equalisation simulation results also showed that by using narrow (25GHz) optical filtering, the BER performance as a result of the saturation induced distortion may be increased by more than 5 orders of magnitude.

The idea of using SOA as a limiting amplifier was experimentally demonstrated and shown to level the bursts that had a 5dB input power difference. This burst power dynamic range translates to about 25km of fibre distance between two ONUs assuming a 0.2dB/km loss SSMF. The dynamic range of the system at 5dB is still not high enough if long-reach access network is considered, systems that provide more dynamic range, as well as additional features such as wavelength conversion, is studies in Chapter 5. The method that uses sharp optical filter to reduce the effect of spectral broadening caused by the non-linear effect in SOA was suggested and tested, it showed 2dB increase in extinction ratio and 4 orders of magnitude increase in BER performance near the filter edge. The power balancing within the all-optical burst equaliser was also investigated, by using an attenuation of

3.6dB placed between the two SOAs, the equalised loud burst ER is 1dB higher, subsequent 2dB increases in attenuation increase the ER by 0.5dB or less. The key is to set the attenuation value as low as possible to avoid unnecessary saturation induced distortions and ASE noise, while the loud burst must be allowed to saturate booster SOA for burst equalisation to occur.

Chapter 5. Centralised Optical Processing in a Long-reach Wavelength Converting Optical Access Network

5.1 Introduction

Wavelength division multiplexing (WDM) is widely acknowledged as a key technology in the next generation of optical access networks, which will offer higher line-rates, increased numbers of users, and extended reach, as well as being the most energy efficient next generation access architecture [1, 4]. Thus, the evolution from Gigabit Passive Optical Network (GPON) to Next Generation PONs (NG-PONs) requires the integration of WDM in the already deployed GPON infrastructure. Centralised optical processing may be placed at the intermediate exchange site in a Wavelength Converting Optical Access Network (WCOAN) [13], allowing uncooled, colourless transmitters to be used at the customer's premises so that the access

network is scalable and economically affordable to deploy. This exchange node will provide all-optical signal processing as suggested in section 2.3.2, including wavelength conversion and possibly signal regeneration, to consolidate the multiple wavelength-drifting burst-mode data streams from each PON segment and convert them to a set of fixed WDM wavelength channels for transmission over the backhaul fibre.

In order to achieve the requirements for integrating CWDM PONs into a single wavelength efficient WDM access backhaul, this chapter conducts a characterisation and performance analysis of incorporating a SOA-MZI optical regenerator as a Cross Phase Modulation (XPM) wavelength converter (WC) into a PON with a DWDM backhaul. The all-optical processing functions of the SOA-MZI and the proposed Centralised Optical Processing Unit (COPU) will be studied. An experimental demonstrator of the wavelength conversion upstream system will be built based on the proposed access network described in section 5.2. Then the BER and transmission distance performance of the Cross Gain Modulation (XGM) and XPM WC at 10Gb/s operation is compared in section 5.3, showing that the XPM WC is more suitable for 10Gb/s PON. The SOA-MZI device is characterised in section 5.4, the phase shifter voltage characteristic is shown enabling us to find the operating point and lower loss input output ports of the SOA-MZI. Different operating modes of the device are compared based on chirp and dispersion dependent performance in long-reach application. The probe power range is also characterised. The input power dynamic range (defined as the maximum range of input power range that result in an error free BER) and wavelength drift tolerance of the experiment system will also be measured and analysed in section 5.5. The need to perform burst equalisation, wavelength conversion, input power dynamic range

enhancement and signal regeneration eventually lead to the proposition of a combination of devices which is the COPU, it will be experimentally studied in section 5.6. Burst mode conversion performance is also studied and the dynamic range of the COPU in burst mode was determined. The digital burst mode receiver used in this experiment was developed by José Manuel Delgado Mendinueta [78], whom also collaborated with us on the burst mode experiment. The BER performances for the processed optical bursts at 0, 22, 40, 62km backhaul transmission distance transmission distance was also presented.

5.2 Integrating PON with DWDM backhaul

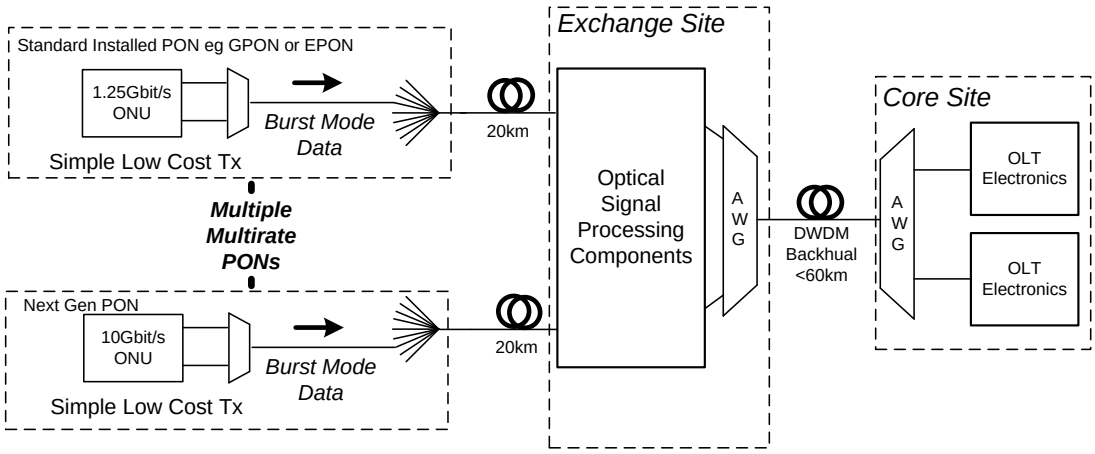

Figure 5.1 Long-reach PON with centralised optical signal processing

Expanding the WCOAN architecture shown in Figure 1.2 in detail, the integrated TDM-PON with DWDM backhaul access network upstream is shown in Figure 5.1 where the network can be thought of as two sections: A passive feeder network and an exchange site with backhaul transmission.

The first is a distributed fibre access network connecting each customer to the local exchange. This is constructed in an identical fashion to traditional PONs with distributed passive optical power splitters. The main issues in this section are the high loss associated with the power splitting arrangement, the unlevelled optical

burst power due to distance ranging and transmitted power tolerance of the ONUs, and the wavelength drift of the ONUs laser sources because of temperature variation for low cost, uncooled lasers used there. For every factor of 2 increase in the number of customers served, >3dB loss is added to the loss budget. For a split factor of 256 a loss of ~28dB with component tolerance is seen while at a split of 32 this is 18dB. This, coupled with the demand for low cost/low power transmitters in the ONU provided to the customer, means that the power available at the exchange site will be restricted. Uncooled DFB lasers have a frequency variation with temperature of ~10GHz/K which is determined by the device expansion and the refractive index change [79]. The acceptable temperature variation requirement will depend on the location of the ONU (outside or in the customer premises), with the worst case, outdoor scenario requiring operation over a temperature range of -20°C to 70°C. This requirement means that any WDM channel spacing would be limited to at least 1THz.

Long-reach WDM access networks typically use active optical amplification at the exchange sites to enhance transmission distance. At the exchange site, shown in Figure 5.1, we introduce a COPU to consolidate multiple burst-mode data streams with drifting wavelength and unequalled burst powers from each PON segment and convert them to a set of stabilised WDM wavelengths with equalised burst-to-burst power for transmission over the long-reach backhaul fibre, which may be dual fibres, reusing current core or metro network fibres and may or may not include amplification. The proposed COPU, shown in Figure 5.2, is composed of an optical power equaliser followed by a wavelength converter.

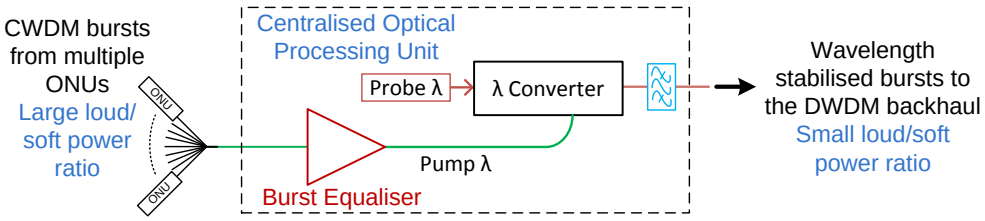

Figure 5.2 The centralised optical processing unit

The COPU is expected to meet three different requirements which are, namely, wavelength conversion, optical burst power equalisation, and transmission distance enhancement. The wavelength conversion process consolidates multiple CWDM ONUs wavelengths onto a set of fixed DWDM wavelengths for efficient backhaul transmission over a WDM optical link. Also, the unlevelled bursts coming from ONUs at different distances from the exchange will need to be equalised to reduce the receiver dynamic range requirement at the OLT. In addition, optical bursts at the intermediate exchange site would need regeneration to have a higher extinction ratio and possibly pre-chirping to enable dispersion tolerant transmission required in the long reach scenario [24], which will increase the backhaul transmission distance over an uncompensated link. The following sections will begin by explaining why the move to XPM wavelength conversion is necessary.

5.3 Wavelength Conversion techniques for 10G-PON

The principal element in the COPU is the wavelength converter. A number of wavelength conversion techniques are available, the most commonly used coherent technique is four-wave mixing (FWM); the most common incoherent (cross-modulation) techniques are XGM and XPM. The FWM wavelength conversion is coherent as it preserves the phase information as well as the amplitude information, making this conversion technique attractive as it is transparent to modulation format. However, the FWM conversion efficiency between up- and down-conversion is asymmetric and the efficiency can decrease sharply when the input signal

wavelength shift is increased [15]. The conversion efficiency is defined as the ratio between the converted signal power and input signal power [80]. As described in Section 2.3, the uncooled ONU laser wavelength is not fixed and each customer's ONU wavelength may drift in the 20nm CWDM band. The wavelength of each ONU is temperature dependent, thus a large mix of wavelengths maybe present at the exchange at any one instance. It will be almost impossible to compensate for the decrease in conversion efficiency if FWM was to be used as a wavelength converter to map multiple CWDM signals on to a DWDM backhaul. In addition, FWM is polarisation dependent which is not suitable for PON, because in PON the distribution fibres are connected to more than 32 ONUs in the customer's premise, it will be extremely difficult and costly to maintain or control the polarisation for all the fibre connections. Therefore, the remaining options are XGM and XPM wavelength conversion techniques.

Previously, a network configuration was proposed making use of a wavelength converter unit based on the XGM properties of SOA [13] for consolidation of 2.5Gb/s PON systems. A demonstration of this XGM wavelength converter was built in the laboratory, as shown in Figure 5.3. An input pump or data signal modulates the gain of the SOA forming the XGM converter, which in turn modulates the CW probe wavelength. The pump signal was filtered and the remaining signal is at the probe wavelength carrying the inverse of the original data. However, there exist some drawbacks of the XGM wavelength converter that become an issue as the access network data rate is increased to 10Gb/s.

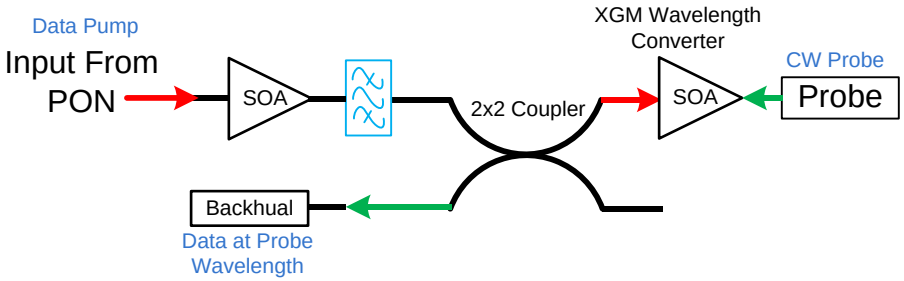

Figure 5.3 Wavelength converter based on Cross Gain Modulation in SOA

Similar to the spectral broadening effect we observed in gain saturated SOAs in Section 4.4, the gain saturation of the cross gain modulated SOA will result in increased positive chirp [44]. The chirped signal increases the impact of dispersion in long distance standard single mode fibre (SSMF) transmission, therefore, reducing the maximum error free transmission distance of the signal. As the data rate is increased to 10 Gb/s, the decreased pulse width means that the chirped signal eye will be completely closed by dispersion after 11km of SSMF. Transmission at 10 Gb/s is therefore, more sensitive to dispersion than at lower data rates e.g. 2.5 Gb/s.

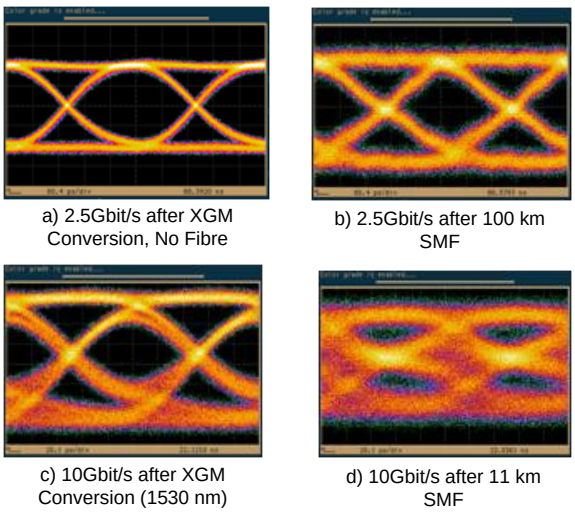

Figure 5.4 Comparing XGM and XPM wavelength converted signal at 2.5Gb/s and 10Gb/s data rate [13]

As shown in Figure 5.4, transmission of 100km is possible at 2.5 Gb/s, yet the optical eye of the 10 Gb/s XGM wavelength converted signal is completely

closed after 11km of SSMF, which means the signal is not recoverable by the receiver in the OLT without dispersion compensation.

An ideal wavelength converter should produce equal performance for conversion of the input signal from short to longer wavelengths and vice versa. However, this is not easily achieved. In XGM wavelength converters, the SOA gains are not uniform across all operating wavelengths. The longer and shorter wavelengths experience different gain variations with input power levels. Increasing the input signal power causes the SOA gain to become saturated because of the reduction in carrier injection from the bias current. The gain peak will shift towards longer wavelengths as a result of the carrier depletion due to the reverse process of the band-filling [81]. Therefore, when the CW pump is considered as a reference wavelength, the longer wavelength will experience higher gain and therefore, it will be easier for it to saturate the SOA. As a result of this effect, another drawback of the XGM conversion scheme exists; extinction ratio conservation cannot be achieved for both up and down wavelength conversion. Up converting the signal wavelength (for example from 1550nm to 1560nm) will reduce the extinction ratio of the output signal, as it is more difficult for the shorter input wavelength to saturate the SOA. Therefore, the performance of the system will be reduced when converting to longer wavelengths [82].

In order to overcome the extinction ratio degradation in XGM wavelength converters and enhancing the extinction ratio and transmission distance of the converted signal, XPM based on a dual SOA Mach-Zehnder Interferometer (SOA-MZI) [83] can be used. The XPM WC using SOAs are considered the most effective incoherent wavelength conversion technique because of its high conversion efficiency, extinction ratio enhancement and negative chirp characteristics [84]. The

XPM wavelength converters have previously been proposed previously for use in WDM enabled core and metro networks [53, 85]. In the core network, the input signal to the XPM converter is a continuous mode modulated signal with fixed wavelength, constant power and reasonable extinction ratio. As a result of the cost considerations for ONUs in access networks described in section 5.2, un-cooled, wavelength not strictly defined lasers will be used in the ONUs, thus the temperature dependent input signal wavelength to the XPM wavelength converter is no longer precisely controlled. Burst mode signals are also expected instead of continuous mode as is common in the core network. Wavelength and power differences between bursts are also expected. Therefore, aside from wavelength conversion, the XPM converter is expected to handle wavelength drifts and would ideally provide extinction ratio improvement to the equalised bursts.

An integrated XPM wavelength converter was used in our experiment, as shown in Figure 5.5. This scheme operates by using the input signal to modulate the carrier density in the active region of the SOA, which in turn modulates the refractive index. The result is phase modulation of the CW probe signal. The interferometer configuration of the SOA transfers the phase modulation into amplitude modulation due to the constructive and destructive interference depending on the phase change. The advantage of using XPM is that the wavelength conversion is not as wavelength dependent as XGM within the SOA operating range. Up-conversion in XGM has a 6dB extinction ratio degradation, for both up- and down- conversion, the penalty remained less than 0.5dB over a 26nm range [86], therefore, it will be possible to conserve the extinction ratio when converting from any wavelengths within the converter's CWDM operating band. This greatly benefits the ONU design requirement, because it enables wavelengths from low cost,

colourless ONUs to be converted to a tightly controlled pump wavelength, allowing the use of DWDM in the backhaul section of the PON while maintaining simplicity for ONUs in the customer's premises.

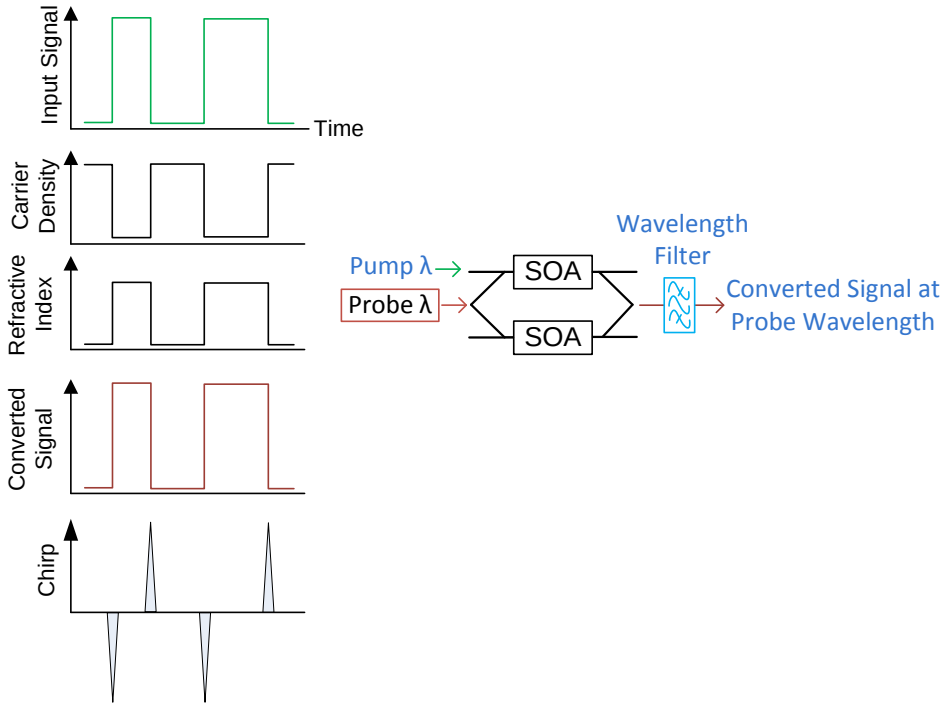

Figure 5.5 Wavelength converter utilising cross phase modulation, using the integrated SOA-MZI device to perform XPM under non-inverting mode operation [82]

The XPM scheme also requires smaller gain variation to perform the conversion. Hence, the effect of chirp is reduced and therefore, it allows transmission at more than 10Gb/s and over longer distances. The ability to bias the phase shifter in the XPM converter allows the interferometric SOA converter to operate either on the positive or negative slope of the interferometer. The positive slope of operation will generate negatively chirped non-inverting converted signals which may enable transmission of 10Gb/s signal over long distances of standard SMF. It is necessary to characterise the SOA-MZI device to find out the basic input and output operating power condition required for good conversion performance. Furthermore, the network conditions in access networks such as wavelength drift and the "loud/soft" input burst powers are not the same as in core network where this

device is typically used as a signal regenerator. It is also useful to take advantage of the negative chirp that this device could generate to maximise backhaul transmission distance using standard SMF, the characterisation can reveal the operating points that can be used generate such negative chirp.

5.4 Characterisation of the SOA-MZI device

Figure 5.6 shows an internal schematic of the SOA-MZI device for the following experiments. It was a prototype device supplied by CIP photonics packaged as an integrated all-optical regenerator, which is used as a XPM wavelength converter in this work.

5.4.1 Characterisation of the phase shifter voltage

The SOA-MZI has integrated thermo-optic phase shifters on each SOA arm. When voltage is applied to a phase shifter, it heats up which results in a refractive index change of the waveguide in one arm of the MZI [80], thus the phase bias point of MZI can be electronically controlled. When the light from the upper and lower arm of the SOA-MZI interfere in the output coupler, their phase difference causes the output light to re-direct from one port to the other, this phase difference can be adjusted by the phase shifter in either arm of the SOA-MZI. The result of the adjustment can result in two modes of operation: the **Non-inverting mode** where the output binary bits have the same polarity as the input, and the **Inverting mode**, where the output binary bit is inverted with respect to the input. As illustrated in Figure 5.6, a CW laser and two power meters were used to characterise the phase shifter control voltage, giving us the operating points needed for the operating modes.

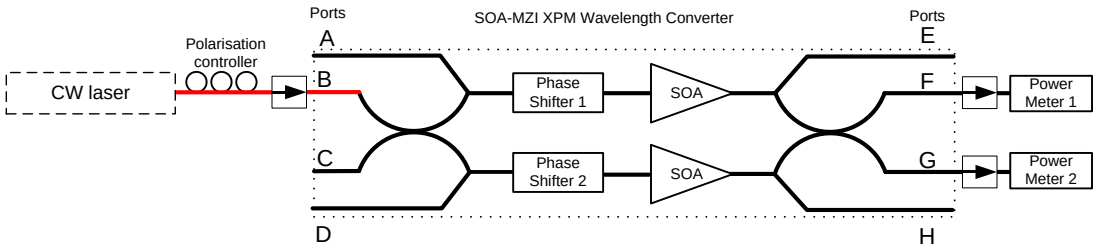

Figure 5.6 Block diagram of the characterisation of phase shift control voltage

The CW laser source fed a -5dBm probe signal at 1555nm into port B, which was coupled to both arms of the SOA-MZI device. Both SOAs are biased at the typical operating current of 360mA, the top and bottom SOAs have an unsaturated gain of 23.6dB and 20.1dB respectively at this bias values. Sweeping the phase shifter voltage (V_{PS}) from 0 to 25V showed that the largest power difference between port F and G occurs at 15V. The probe polarisation is mechanically controlled via the polarisation controller, in order to compare the effect of the CW probe polarisations, a polarisation state was chosen based on a quantifiable value, in this case the output power of port G. First, the polarisation controller of the input CW tuneable laser was adjusted so that output power of port G was at its maximum, 8.43dBm. At the same time the power of port F then became -3.07dBm. At this setting, the power difference between the two ports was the largest. Optical isolators were also used at the connected input and output ports to prevent reflected light and ASE noise from interfering with SOA operation. The bottom arm phase shifter was grounded and the top arm phase shifter voltage was adjusted at 0.5V steps to obtain the result in Figure 5.7.

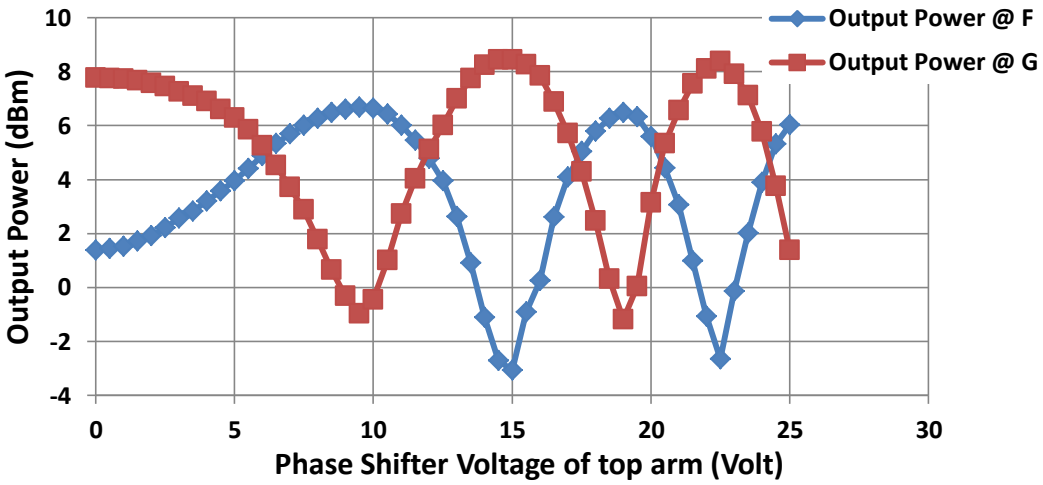

Figure 5.7 Output power at port F and G as a function of phase shifter voltage

The output ports F and G produced similar signal performance with a complementary relationship as expected. The largest peak-to-null power differences are 9.74dB and 9.61dB for port F and G respectively. The output power at port G is 1.5~2dB higher than port F at similar points in the plots such as the peaks and nulls. We suspect this higher output power is due to the lower optical coupling loss of port G. Therefore, in all future works port G will be used to ensure the converted signal power is as high as possible.

When a 10Gb/s data signal was fed into port H, with V_{PS} set on the rising slops, i.e. V_{PS} = 11.2V or 20.7V, a non-inverted output signal was observed at port G. On the other hand, the inverted signal was observed when the phase controller voltage is biased on the falling slope, that is when V_{PS} = 16.6V or 24.1V.

It is observed that the SOA-MZI device is sensitive to changes in the probe signal polarisation. Considering an opposite polarisation state, where the input probe polarisation controller was adjusted so that at V_{PS} = 15V, the output power of port G was at its minimum, 2.35dBm, then the corresponding power of port F became 4.97dBm. The top arm phase shifter was adjusted at 0.5V steps again to produce Figure 5.8.

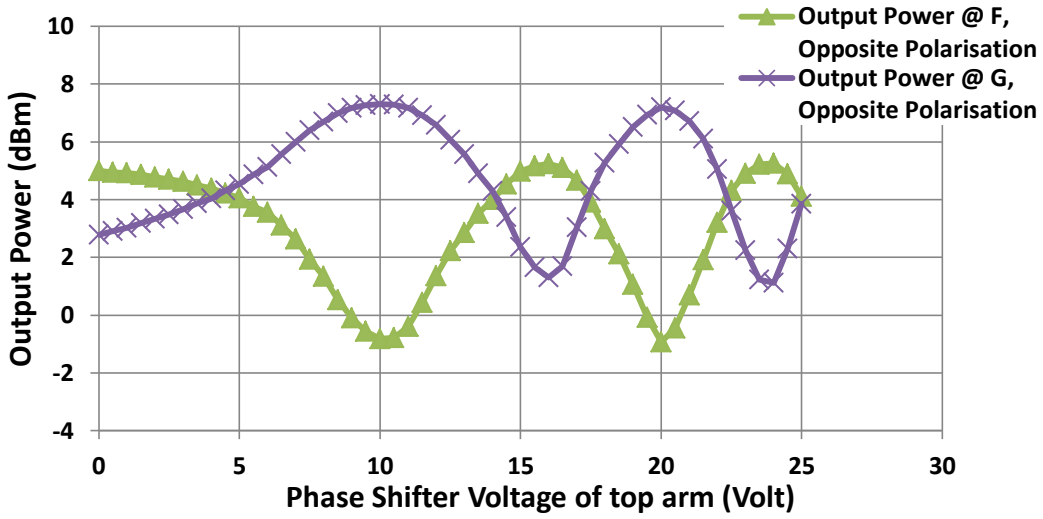

Figure 5.8 Output power at port F and G as a function of phase shifter voltage, with a opposite polarisation state

As a result of the polarisation change, the port F and G output power peaks and nulls are reversed, but with a reduced power difference between the peak and null powers. The new peak-to-null power is 6.16dB and 5.65dB for port F and G respectively. Also, the peaks and nulls undergo a shift to the right on the x-axis. In this characterisation only one CW source is used, therefore, the peak-to-null power difference is the maximum change in output power caused by the refractive index change in the phase shifters. When the peak-to-null power difference is decreased, it can be expected that, in the opposite polarisation state, the maximum amplitude change as a result of the SOA cross-phase modulation will also decrease. Therefore, at V_{PS} = 15V, the 1st polarisation state where the power of the port G is highest is expected to be the best polarisation state for port G, which makes the opposite polarisation, where the power of port G is lowest, the worst case polarisation state.

The effect on wavelength converting performance of the best and worst polarisation state can be measured. When a 10Gb/s, 1551.7nm pump signal was connected to port H, it modulates the refractive index of the lower SOA. When the converted signal is filtered at 1555nm it can be seen that its amplitude does depend

on the probe signal polarisation states. As shown in Figure 5.9, the optical eye height, ER, Q-factor were measured using the DCA. When the SOA-MZI was operating in the non-inverting mode, the converted signal eye (A) with 1.5mW eye height, 15.9 Q-factor and 15.1dB ER was observed for the best polarisation state. It is much better than the quality of the eye (B) observed for the worst polarisation state, which has 1.12mW lower eye height, 6.15 Q-factor and 13dB lower ER. For the inverting mode at the best polarisation state, the converted signal eye (C) with 2.2mW eye height, 14.3 Q-factor and 6dB ER was observed. While the quality of the eye (D) in the worst polarisation state has 1.2mW lower eye height, 9.37 Q-factor and 2.3dB lower ER, showing that the polarisation dependency is not as strong as in the non-inverting mode. The performance comparisons between the inverting and non-inverting mode will be further investigated in the next section.

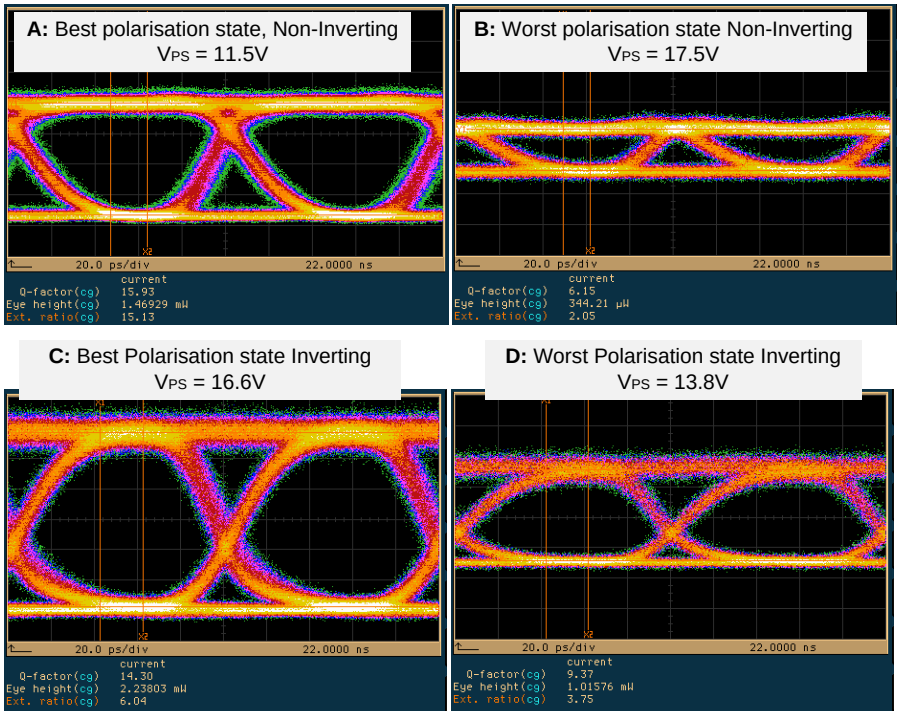

Figure 5.9 The eye of the non-inverting output signal, at opposite polarisation states.

The above results showed that it is possible to obtain non-inverting and inverting mode operation in opposite polarisation states, thus the polarisation of the

probe signal need to be optimised so that the highest ER, eye height and Q-factor is available for the converted signal. The term "worst polarisation state" used here is only relative to the best polarisation state, where a clear converted signal can be observed. The real "worst" polarisation condition will be when the two signals from the top and bottom arm of the MZI structure are not aligned, in between the above mentioned best and worst polarisations that completely corrupts the eye of the converted signal.

As the CW probe is physically located with the SOA-MZI it could be packaged together with the SOA-MZI device. Therefore, once the polarisation for the probe is optimised it is not expected to change. In the following experiments, the optimal probe polarisation will be used. After characterising the power and polarisation operating points, the performance of the WC will also need to be characterised, finding an optimal operating point for the WC.

5.4.2 Comparison between different operation modes

The SOA-MZI device is bi-directional, which allows the pump and probe signal to be in either co-propagation or counter-propagation configurations. This experiment aims to compare the wavelength conversion performance between the co-propagating and counter-propagating setups, using different possible signal input ports. Ports A and D are for co-propagating signals; E and H are for counter-propagating signals, as shown in Figure 5.10. The non-inverting and inverting operation performance of the SOA-MZI device was also compared.

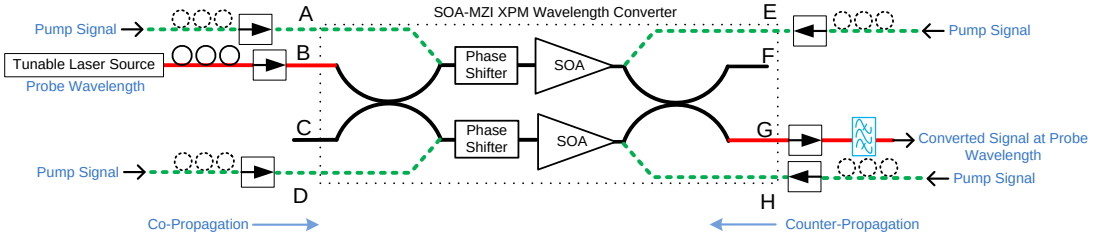

Figure 5.10 Four possible propagation configurations with pump signal input ports at A,D,E,H

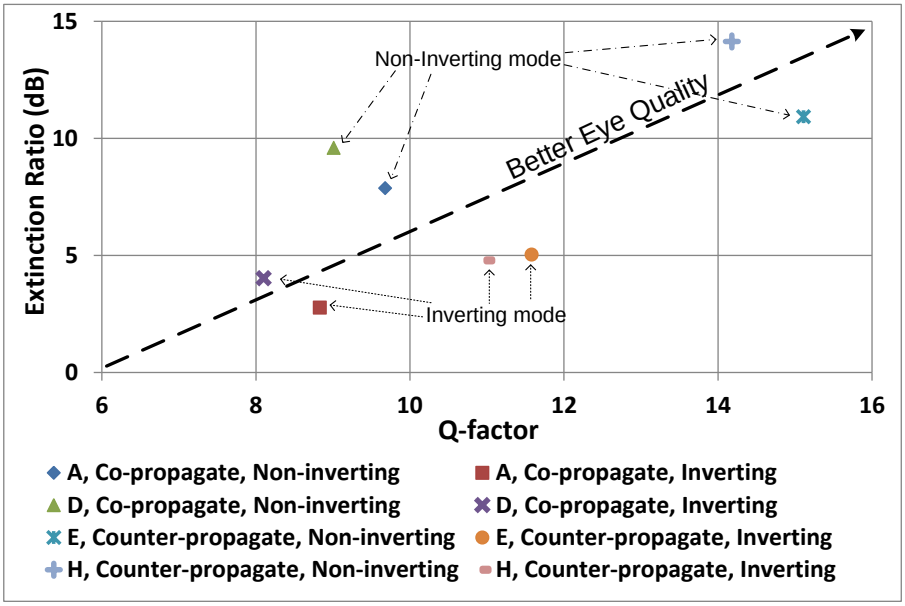

Switching from Co- to Counter-propagation	Operating mode	Q-factor increase	ER increase
Switching from Port A to E	Non-inverting	5.43	3.05 dB
	Inverting	2.75	2.26 dB
Switching from Port D to H	Non-inverting	5.17	4.55 dB
	Inverting	2.89	0.76 dB

Figure 5.11 Wavelength conversion performance (Q-factor and ER) comparison between different SOA-MZI configuration

Results of the comparison are shown in Figure 5.11. This is a back-to-back performance comparison, therefore, the BER performance for all the measurement points are better than 10^{-12}. The converted signal quality in terms of ER and Q-factor were measured. It is shown that when the CW light and data signal propagate in opposite directions (counter-propagating), they always generate better converted signal performance compare with the co-propagating configuration.

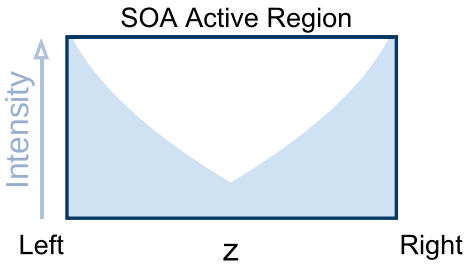

Figure 5.12 Light Intensity in a SOA active region under counter-propagation configuration

The reason for the differences in performance between the counter-propagation and co-propagation configurations are due to the non-uniform distribution of carriers in the SOA and the increasing amplification of the signal towards one end of the SOA active region. Consider a SOA active region under the counter-propagation setup, its light intensity profile will be similar to the illustration in Figure 5.12. The CW probe is input from the left and amplified towards the right side of the SOA, the amplified CW light depleted more carries towards the right side of the SOA, leaving more free carriers at the left side of the active region. While the counter-propagating data signal is input from the right and amplified towards the left side of the SOA active region, which had more free carriers, these free carriers are modulated by the amplified data signal. Since the refractive index modulation is almost linearly dependent on carrier density modulation [87], the counter-propagation is thus more efficient than the co-propagation setup for XPM wavelength conversion. The amplified co-propagating signal can only modulate the carriers that are depleted by the amplified CW light, therefore, it produces lower ER and Q-factor than the counter-propagation setup. The following experiments all used port H under counter-propagating configuration for best performance. Another advantage of the counter propagating scheme is that it allows penalty free same wavelength conversion. This is particularly useful for consolidating wavelengths from multiple ONUs on to a single fixed wavelength, which could be at the same wavelength as the probe. Since the input signal propagates in the opposite direction, the input signal will not interfere with the output converted signal as it does in the co-propagating mode.

Although the inverting mode of operation has 2dB higher average optical power, the results showed that the non-inverting operation performs better producing

wider eye openings and less patterning effect at the rising and falling edge of the signal. This is evident by the higher Q-factor and Extinction Ratio (ER) of the non-inverting signal in both the co- and counter- propagating configuration. It is seen that the inverted output signals have higher output powers but are noisier than the non-inverted signals.

5.4.3 Probe power characterisation for up and down wavelength conversion

The probe source is a CW laser that provides the seed wavelength for the wavelength conversion. The probe power cannot be too high as it will saturate the SOAs, nor too low otherwise the ASE noise in the SOA will dominate, leading to a low signal to noise ratio (SNR) of the converted signal that will decrease performance. The experimental configuration is shown in Figure 5.13, with the probe wavelength and power varying so that the optimum probe power dynamic range could be measured. This characterisation will show the wavelength dependency of the device, because in a DWDM arrangement, a range of probe wavelength spaced at 100GHz could be assigned as the probe wavelengths. There should not be significant performance difference or penalty within the assigned probe wavelength range, otherwise the device would not be suitable as a COPU. The probe power dynamic range will show the probe power range required to achieve good BER performance with in the assigned wavelength range. This characterisation was carried out in continuous mode, since the probe CW source is expected to have constant power during normal operation, the operating point deduced from this can also be used under burst mode operation.

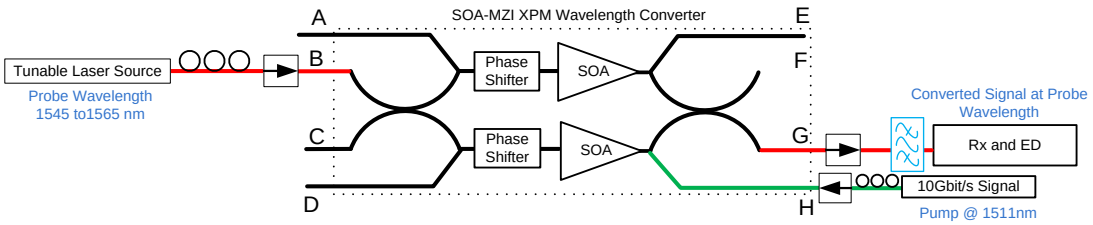

Figure 5.13 Experiment setup for probe power characterisation

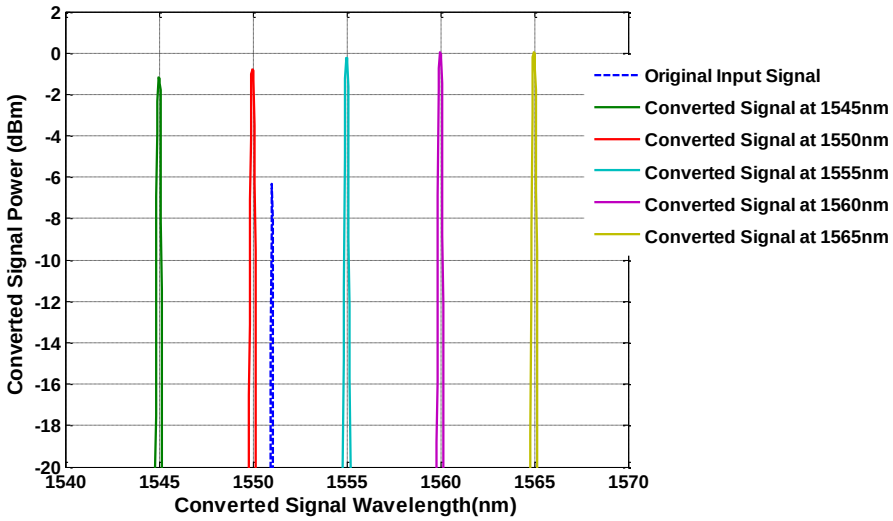

Figure 5.14 Spectrum of the converted signal, the blue dash line is the original pump (input data) signal at 1551nm

The pump data input signal was at 1551nm wavelength with a power of -6.32dBm. The probe wavelength was tuned from 1545nm to 1565nm so that both the up and down conversion of the pump signal was tested in this experiment. Figure 5.14 shows the overlapped spectrum of the converted signal output power at port G of the SOA-MZI. The wavelength band from 1260 to 1280 nm was selected for the XG-PON1 upstream [2], characterised by low chromatic dispersion. The prototype device used in this experiment cannot operate at the XG-PON1 wavelength band because it was initially designed to be used in the C Band (1530 to 1565 nm) of core and metro networks. When using SOA-MZI devices in an actual XG-PON or 10GEPON system, they would need to be manufacture according to the XG-PON or 10GEPON wavelength band selection and standard.

After 3dB loss in the optical coupler and another 3dB loss in the filter, the peak power variation of the converted signal across the 1545 to 1565nm range is small. The highest peak power is 0.1dBm at 1565nm probe wavelength and the lowest is -1.2dBm at 1545nm. The largest difference in the probe peak power is 1.3dB between the 1545nm and 1565 nm wavelengths.

The probe power dynamic range was characterised based on BER performance of the wavelength converted signal. The probe power dynamic range is the maximum change in probe power without compromising the BER performance of the wavelength converted output signal. A 10Gb/s PIN receiver and a Bit-Error-Rate Tester (BERT) were used to measure the received signal BERs performance after the wavelength conversion. At the input, a 10Gb/s optical signal was generated from a DFB laser with an integrated EAM modulator, which, was modulated by a 2^{31}-1 PRBS signal from the PPG of the BERT. The phase shifter voltage was adjusted using the 1560nm probe wavelength as a reference. The optical power of the probe was at -4dBm during the phase shifter voltage and polarisation controller optimisation. The probe power was then varied from 0 to -8dBm for each probe wavelength, Figure 5.15 shows a 3dB probe power dynamic range can be achieved with an error free output signal (BER=10^{-12}) and with a fixed phase shifter voltage, for all probe wavelengths from 1545 to 1565nm. A 4dB dynamic range can also be achieved if the GPON target performance (BER=10^{-10}) is used. For individual wavelengths, the dynamic range is 1 to 2dB wider due to a small change in polarisation as the tuneable laser changes the wavelength. The 1560nm wavelength used to optimise the polarisation has the widest, 5dB error free dynamic range.

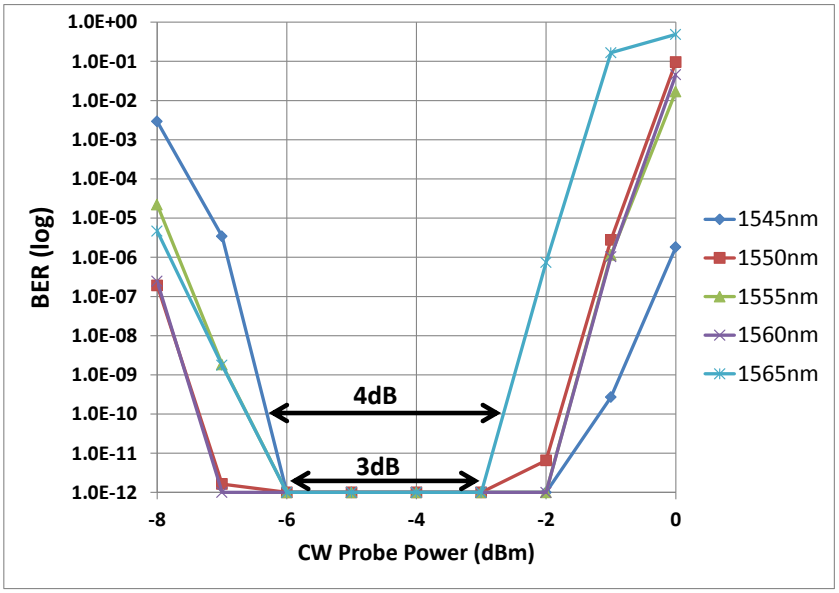

Figure 5.15 Probe power and wavelength optimisation without phase shifter adjustments

The minimum 3dB error free dynamic range allows at least 20nm wavelength tolerance when the phase shifter voltage is fixed. Besides, the probe as a seed wavelength source is expected to have stable power and is temperature controlled. Therefore, a one-time polarisation, phase shifter voltage and probe power level is required, and then the wavelength converter configuration can operate in its designed wavelength band without re-adjustment.

If different probe powers are required, possibly due to network upgrade or different network conditions, the phase shifters in the SOA-MZI device can be electronically adjusted to optimise the probe power, giving an extended dynamic range.

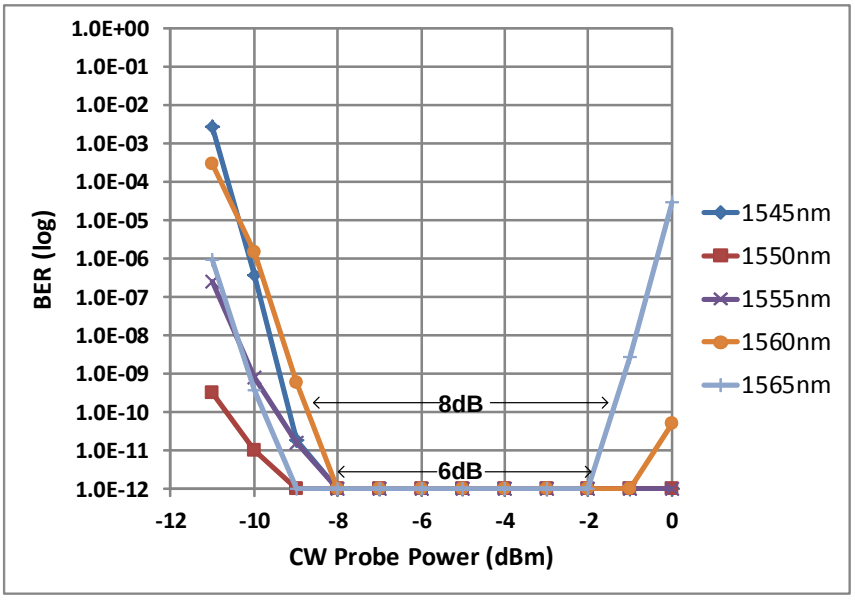

Figure 5.16 Extended probe power dynamic range by allowing phase shifter voltage adjustment

With a maximum phase shifter adjustments of ±1V from the V_{PS} = 11.2V non-inverting operation mode, the results in Figure 5.16 shows that the probe power dynamic range can be widened to 6dB achieving error free operation (BER=10^{-12}) and 8dB if the target BER is 10^{-10}. At -4dBm probe power, the tolerance to phase shifter voltage change is the highest for any wavelengths within the 20nm band, the phase shifter voltage can be ±0.7V from the fixed point (11.3V) for the system to remain error free.

5.4.4 Chirp and Dispersion of the inverting and non-inverting modes

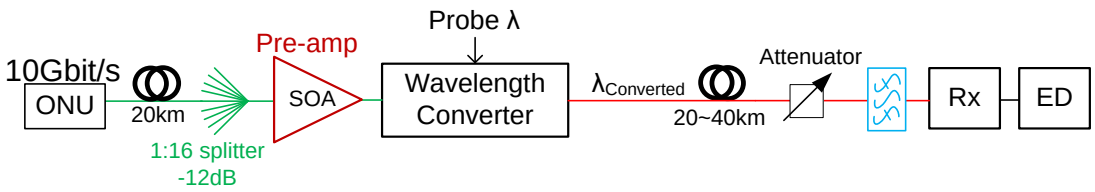

Figure 5.17 Schematic of a wavelength converted PON with un-amplified 20m and 40km backhaul

The next generation of access network with a long-reach backhaul can enable aggregation of the access network and metro network over a larger area than today's standard PON. Therefore, long-reach backhaul transmission performance needs to be studied as long distance transmission penalties can limit the maximum transmission

distance of the PON upstream signal. The main penalties of long distance transmission are due to optical power loss and dispersion in the SSMF. The combined effect of chirp on the converted signal and dispersion can lead to pulse broadening when the signal is transmitted through a non-dispersion-shifted (NDS) fibre [82]. Figure 5.17 is the schematic of the experiment used to evaluate the transmission distance penalty of the XPM wavelength converter. The signal from the ONU at 1551nm is first transmitted over a 20km PON distribution section with the splitter represented by a -12dB attenuator to simulate the loss of a 1:16 split ratio. The probe wavelength is at 1560nm, on to which the data is converted. For the SOA-MZI device used in this experiment, it was observed that the input pump power to the SOA-MZI needs to be above -8.5dBm for the wavelength converter to produce sufficient phase modulation that achieves error free converted signal performance. There is also an extra 3dB loss in the input coupler and up to 1.8dB loss in the fibre to device coupling, the -8.5dBm input signal power will be attenuated to -13.3dBm as it reaches the SOA. The ONU signal power after transmission through 20km of fibre and 1:16 splitter is already at -15.5dBm, which is lower than the minimum required pump power of the SOA-MZI device, and therefore, an optical amplifier is required to boost the signal power so that it is sufficiently high for the wavelength converter.

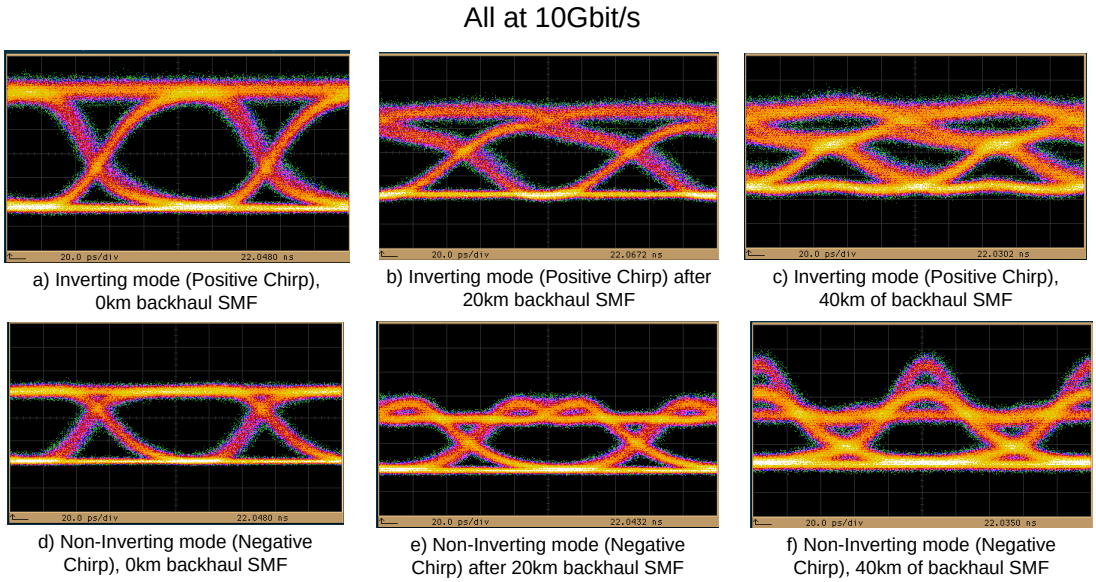

Figure 5.18 Non-inverting and Inverting mode 10Gb/s signal transmission distance comparison

Example eye diagrams of the received signals after 0, 20, 40km of backhaul transmission are shown in Figure 5.18. The top row is the inverting operation mode which induces positive chirp; and the bottom row is the non-inverting mode of operation, which induces negative chirp [82]. The negative chirp is essentially red-shifting on the leading edge of the pulse and blue-shifting on the trailing edge. In a NDS fibre, because of fibre dispersion, the leading edge of the pulse travels slower than the trailing edge, initially compresses the pulse before dispersion eventually broadens the pulse to enable longer transmission distance. As discussed in section 5.3, the penalty as a result of the pulse broadening will be more severe as the bit rate is increased to 10Gb/s, because the pulse width will decrease and the pulse broadening will cause inter-symbol-interference at shorter transmission distance.

From Figure 5.18 a) to b), then to c), the eye closure due to pulse broadening seen here is getting worse as the inverted output signal travelled through the fibre. This is similar to the eye closure observed previously with the positively chirped XGM wavelength converted signal that was transmitted through SSMF. However, in XPM wavelength conversion, the inverting signal that travelled 40km can still have a

BER of 1.62×10^{-10} while the XGM converted signal only travelled 11km. This is because the XPM conversion produced much less positive chirp than the XGM conversion and therefore, the XPM converted signal is less sensitive to fibre dispersion.

The non-inverting mode counterparts d) e) and f) show wider eyes and less pulse broadening at each backhaul distance. In order to present a quantitative comparison between the two operating modes, the power penalties for distances from 0 to 40km were measured. The power penalty is the additional power required to maintain a BER of 10^{-10} which in this cases is mainly due to fibre loss, which increases linearly with distance. The measurement of further than 40km transmission distance is limited by the receiver sensitivity and the optical power of the converted signal.

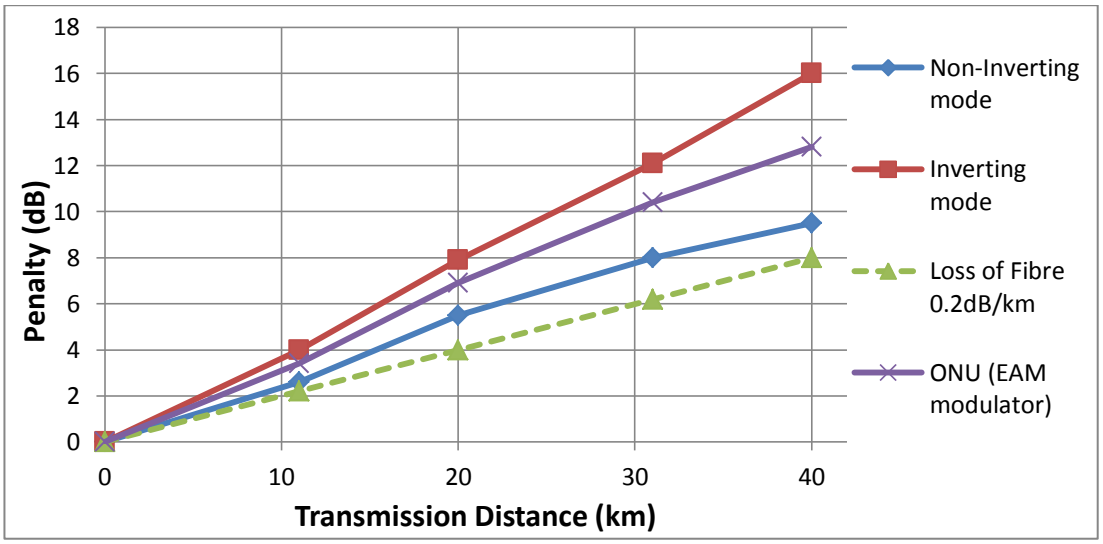

Figure 5.19 The power penalty in 0 to 40km backhaul distance transmission

As shown in Figure 5.19, for the same transmission distances, the positively chirped inverting output signal resulted in larger power penalty than the negatively chirped non-inverting signal, with the power penalty difference between the inverting mode and non-inverting mode increased from 2.4dB at 20km to 6.5dB at 40km. The power penalty difference between the non-inverting mode and the fibre

loss reference line remains <1.8dB from 20km to 40km. The power penalties of the ONU, which has an integrated EAM modulator (denoted ONU only), were also measured for reference purpose and there was only backhaul fibre between the ONU and the receiver. This shows that the positive chirp generated by the SOA-MZI device in inverting mode is larger than the ONU's EAM modulator chirp which has a chirping parameter of less than 1 [44]. 6.5dB extra power is required to boost the inverted output signal at 40km to achieve the same BER performance. The XPM wavelength converter output chirp was shown to be determined by the device properties and the intensity of the input signal, regardless of input signal chirp parameter [88]. Which means the converted signal chirp can still be negative under non-inverting mode, even when the signal from the ONU carries positive chirp. As for the non-inverting signal, the negative chirp allowed it to travel up to 50km and still maintain a received BER below 10^{-10}.

The introduction of negative chirp as a result of biasing the SOA-MZI on the positive slope of operation means that the converted signal pulse can travel longer distances in a SSMF, because this type of pre-chirped signal is dispersion tolerant.

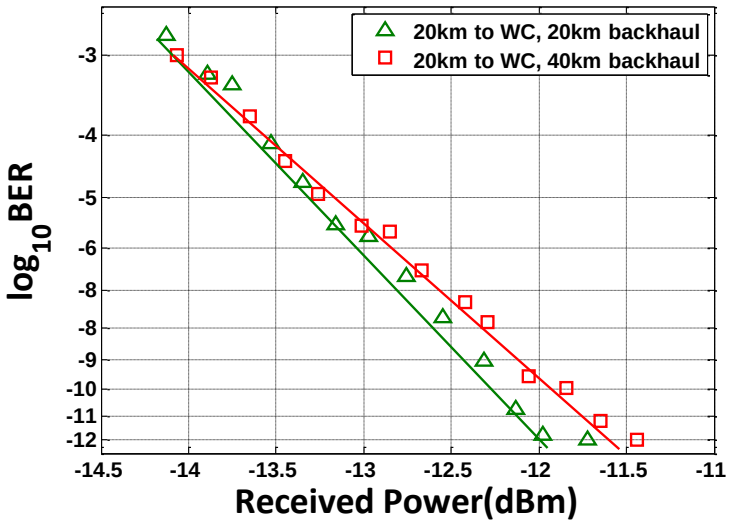

Figure 5.20. BER performance for 20km and 40km backhaul transmission distance

After transmission through a 20km distribution fibre, the signal is wavelength converted, and then it travelled thought another 20 or 40km backhaul fibre. The received non-inverting signal BER performance for the 20 and 40km un-amplified backhaul are shown in Figure 5.20. Although the signal after 20km backhaul has 4dB higher average optical power, when they were attenuated to the same received power level, the 40km backhaul has <0.5dB variation in BER performance compared to the 20km backhaul transmission distance.

After 40km of backhaul SMF the non-inverted signal is still error free. However, after 20km distribution fibre, the WC, and then a 60km backhaul the signal power is reduced to -13.6dBm which is too low to maintain error free performance. A booster SOA was required to amplify this signal resulting in the new schematic shown in Figure 5.21 for long-reach transmission.

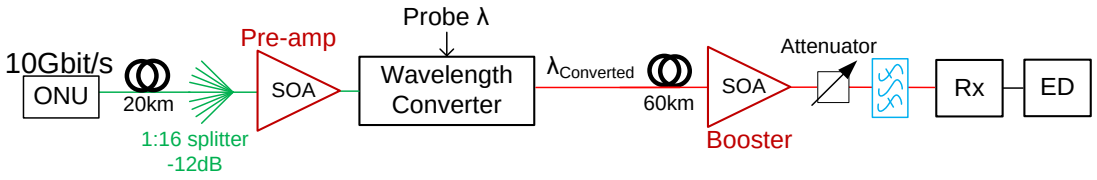

Figure 5.21. Schematic of a wavelength converted PON with 60km backhaul section, with an amplifier before the receiver to boost the signal power level

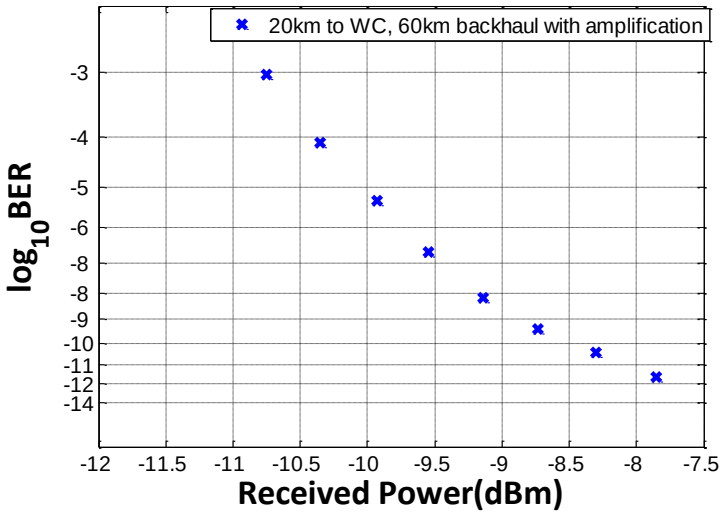

Figure 5.22 BER performance for 60km backhaul transmission distance

After 60km backhaul, when the signal power is amplified, it is still error free, but there is an error floor likely due to the ASE noise from the SOA used before the OLT, the total transmission distance from the modelled ONU transmitter to the OLT receiver is 80km.

This section has shown that the combination of negative chirp and dispersion results in longer possible transmission distances. The chirp in a XPM wavelength converter is small compared to the chirp generated in the XGM process, because smaller gain modulation is required to produce a phase change of π radians which is necessary for the modulation of the probe wavelength. The non-inverting mode of operation requires the converter to operate on the positive slope of the interferometer [82]. This mode of operation has the benefit of generating negative chirp. The pre-chirped converted signal reduces the impact of dispersion and allows the signal to travel a longer distance in a SSMF free of error. The chirp in the inverting mode of operation is positive, therefore, the inverting signal, like the XGM converted signal, is impacted more by dispersion after long distance SSMF transmission, and hence the transmission distance for the inverted signal is limited.

5.5 Input Power Dynamic Range of the SOA-MZI Wavelength Converter

The XPM wavelength converter operates by converting gain variations into phase variations in one arm and then combining the signal from both arms, where the signals interfered constructively and destructively depending on the phase difference between the two arms. This makes the device very sensitive to input power variations, because a small change in input power can change the phase of the signal by more than π radians, thus changing the interference pattern which leads to an inversion of the signal, causing large number of errors. Generally, XPM based WCs

have a limited input power dynamic range (IPDR) of about 3-4dB at 10Gb/s [89]. The IPDR is defined as the maximum range of input power that can produced a certain BER (10^{-10} or error free, depending on system requirements) at the output of the WC or at the receiver. In a burst mode PON, having a large IPDR is necessary, because it determines the ability of the device to handle loud and soft input bursts (i.e. high and low input optical powers).

In the SOA-MZI prototype device used in this work and under normal operating conditions, as shown in Figure 5.23, the IPDR is 1dB for error free operation and 3dB at a BER of 10^{-10}. Through the use of a pre-amp SOA to amplify the ONU optical signal power and a second booster SOA operating in the saturated regime to equalise the burst power, the overall error free IPDR can be enlarged to 8dB (10dB for 10^{-10} BER). The difference in burst power is equalised by the cascaded SOAs, the power going into the wavelength converter is also stabilised due to the saturated output power from the booster SOA, and therefore, the overall IPDR is increased.

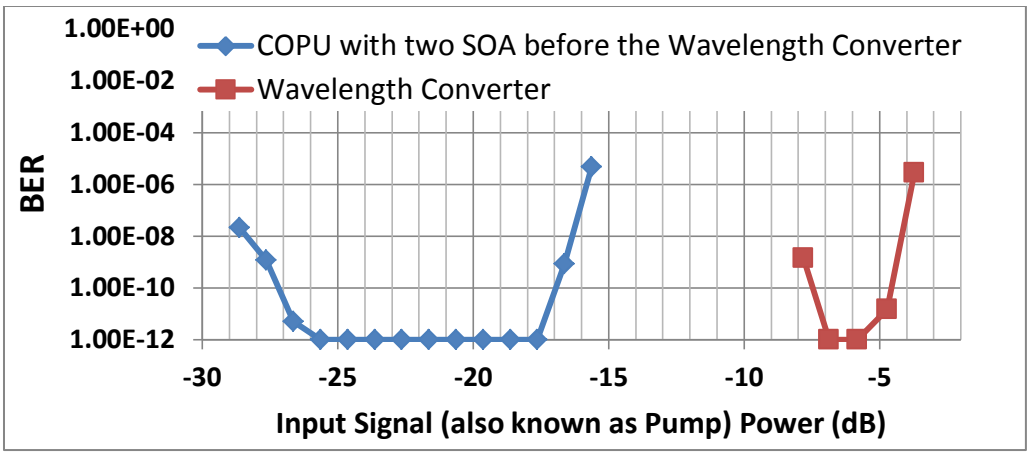

Figure 5.23 The Input dynamic range performance measured by received BER after WC

Figure 5.23 shows the BER performance across a range of ONU input signal powers. The IPDR measured demonstrates the range of input powers which result in an output BER above certain levels. The IPDR has increased from 2dB to 8dB at the

reference BER of 10^{-12} (error free), while the IPDR is 10dB if a reference BER of 10^{-10} is used. This IPDR was achieved without any adjustment to the phase shifter voltage or the bias current to the SOAs, the pre-amp and booster SOA bias current were fixed at 200mA, their normal operating current for a typical gain of 21.7dB and 12dB respectively.

The gain saturation induced signal distortion starts to affect the amplified signal performance at input signal powers above -10dBm, while the input power of the signal becomes too deteriorated at -30dBm, so that the amplified signal do not produce enough gain modulation to drive the cross phase modulation in the WC.

The advantage of this system, observed from the results of Figure 5.23, is that the required power after the PON distribution section can be as low as -26dBm for the wavelength converted signal to be error free, potentially allowing higher split ratios such as 1:256 (24dB attenuation) or 1:512 (27dB attenuation), thus it will be possible to serve a larger number of ONUs in the PON distribution section.

5.6 Performance of the Centralised Optical Processing Unit (COPU)

5.6.1 Gain and Saturation Characteristics

The input/output CW power characteristic of the COPU is shown in Figure 5.24. The output power saturates at 11.1dBm for the pre-amp SOAs when the input power is high at -5dBm, the combined pre-amp and booster also saturates at 11.1dBm, but the cascaded SOAs begin to saturate at lower input power of -15dBm. The polarisation dependent power penalty is less than 0.5dB in the pre-amp and booster SOAs. For the whole COPU that contains two SOAs and a WC, the output power saturates at 1.61dBm when the input power is -5dBm, but at -20dBm input power, the output power already begins to saturate.

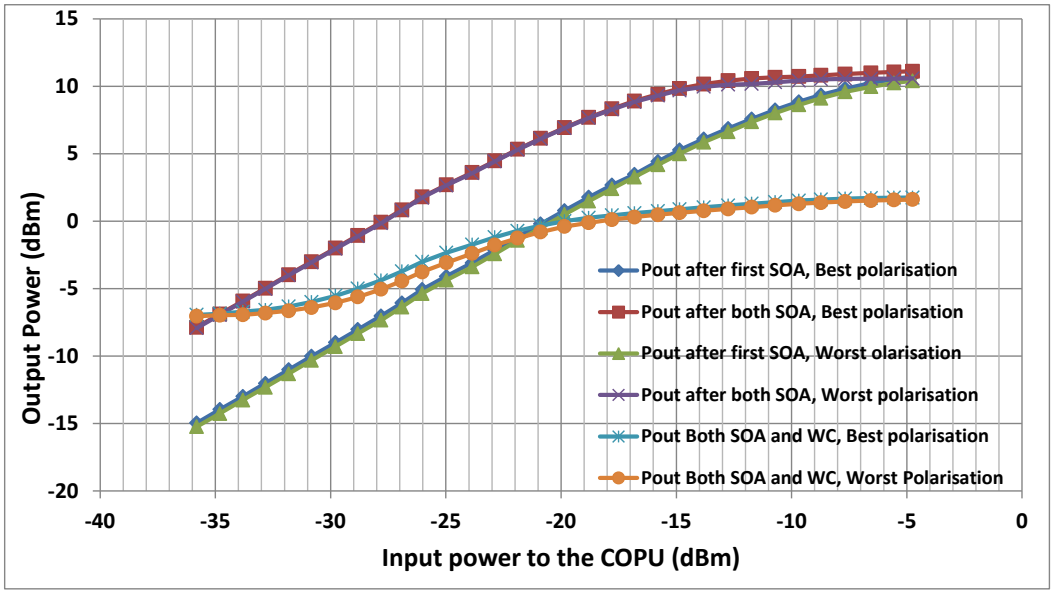

Figure 5.24 COPU input and output power characteristics

The output power of the COPU mainly depends on the amplified probe power, at the probe wavelength while the pump wavelength was cut-off by the optical filter. The pump and probe power both saturate the SOA in the WC, while there are also intrinsic losses of 3dB in each one of the SOA-MZI couplers, limiting the overall input and output power level. For a PON with 1:32 split ratio, if the ONU power is at 0dBm, the 15 dB loss in the splitter limits the COPU input power to a maximum of -15dBm. An ONU signal from 15km away and going through a total split ratio of 1:512 will be at -30dBm when it reaches the input of the COPU. For this input power range of -15 to -30dBm, the output power ranges from 1dB to -6dB, with a static COPU pump power polarisation dependent gain of 1dB. This compression in the power range can be used to reduce the loud/soft ratio of the optical bursts.

5.6.2 The two SOA saturation chirp and the SOA-MZI chirp

As shown previously in Figure 5.23, by using a pre-amp SOA to amplify the ONU input signal power, and a second saturating booster SOA to equalise the signal so that it has stable power at the WC input, the overall IPDR of the WC can be

enlarged. However, saturation of the booster SOA also produces un-wanted chirping of the ONU signal. The chirp generated can caused severe signal distortion due to the saturation induced self-phase modulation [42]. Overall, the power equaliser degrades the extinction ratio and also exhibits patterning effects in dynamic mode. On the other hand, these effects are compensated due to the regenerative properties of the nonlinear transfer function of the SOA-MZI WC. This is because the transfer function of the MZI structure has non-linear amplitude to phase response. The gain induced phase shift and the output signal amplitude has a sinusoidal relationship. When the induced phase shift is near π radians, the input amplitude noise induced phase shift will be compressed [90]. Therefore, after the distorted signal has passed through the WC it will be reshaped.

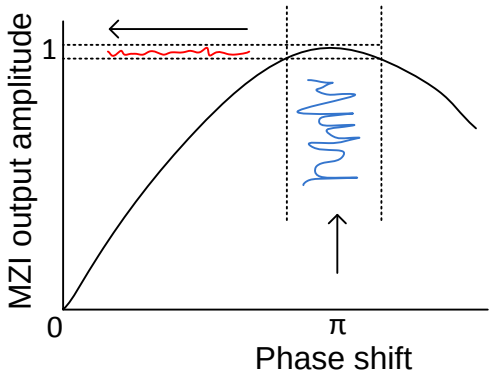

Figure 5.25 Relative SOA-MZI output amplitude as a function of induced phase shift in the SOA. The amplitude noise is compressed when the phase shift is near pi radians [90].

Three example eye diagrams are presented in Figure 5.26 showing the shape of the eyes at critical points in the system. The chirping in the cascaded SOA stage causes severe signal gain distortion and amplitude noise at the input to the WC, closing the eye as seen in Figure 5.26-(A). However, the distortion does not affect the converted output signal (B), which is demonstrated by the fact that the Q-factor has increased from 2.48 before the reshaping to 15.95 after the reshaping. The non-inverting output signal still has negative chirp, allowing the signal to travel the 40km backhaul while retaining a clear eye (C) and error free BER performance. We

therefore, conclude that the chirping induced by the pre-amp and booster does not affect the output chirp of the wavelength converter. This observation agrees with the characterisation of chirp in SOA-MZI wavelength converters presented in [88].

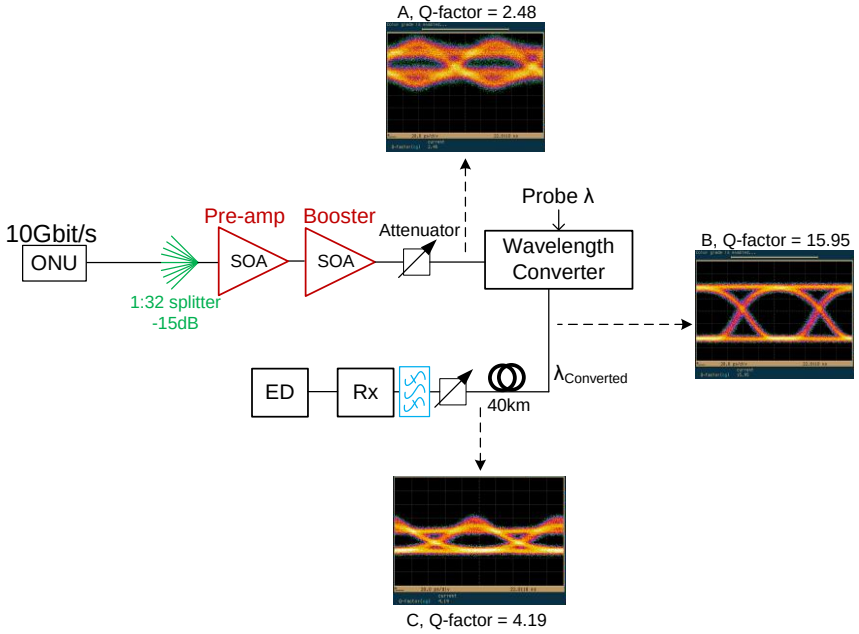

Figure 5.26 Cascaded SOA lead to signal gain distortion and wavelength conversion regenerates the chirped equalised signal

Figure 5.27 shows a spectral comparison between the equalised signal (chirped) and the wavelength converted signal (reshaped).

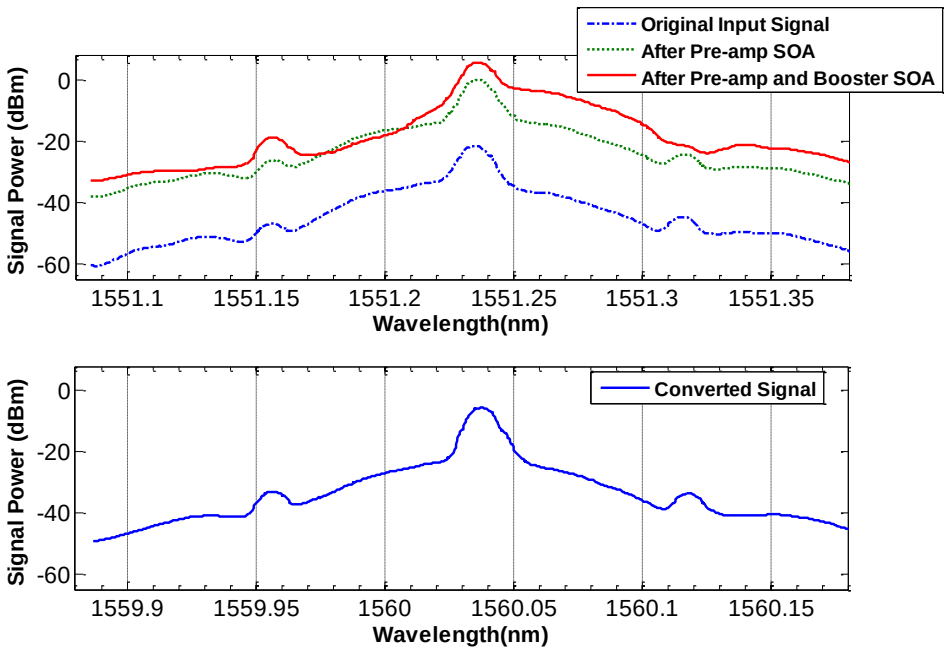

Figure 5.27 Spectrum comparison between the original signal, SOA saturation chirped signals and the wavelength converter regenerated signal

The chirp induced by the cascaded SOA causes spectral broadening in the input signal. The broadening is a shift in frequency of the chirped component of the signal away from the centre peak frequency which is the un-chirped component of the signal. As the signal passes through the SOA-MZI wavelength converter, the output signal is wavelength converted as well as regenerated. The converted signal spectrum shows that the spectral broadening and frequency shift was restored. If wide deployment is required, there could also be cost benefits and performance gain from the monolithic integration of the two SOAs and the SOA-MZI regenerator into a single device for centralised optical processing. In the following experiment, the term Centralised Optical Processing Unit (COPU) is used for this configuration.

5.6.3 IPDR and Backhaul Distance

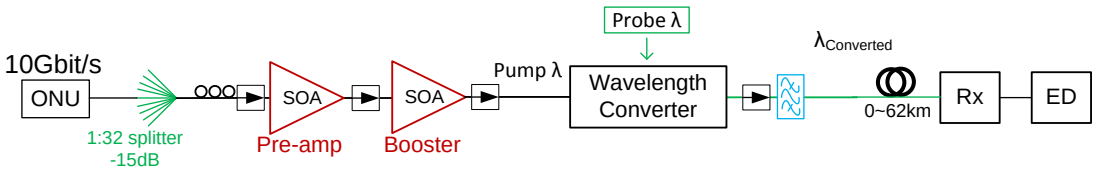

Figure 5.28 Experiment setup for the reach assessment of IPDR

The effect of a long-reach backhaul on the IPDR is studied, which reflects the maximum loud/soft power ratio of the signal entering the COPU. The distribution fibre was not used, because dispersion may affect the signal quality resulting in a lower IPDR. Backhaul SSMF distances of 0km, 22km, 40km, 62km were used in this experiment, the IPDR at each backhaul distances was measured. In the result of the IPDR measurement shown in Figure 5.29, the signal power loss in the 62km un-amplified backhaul was approximately 13dB. The IPDR shrinks significantly, the best BER performance was at 10^{-10}, observed at -20dBm input power.

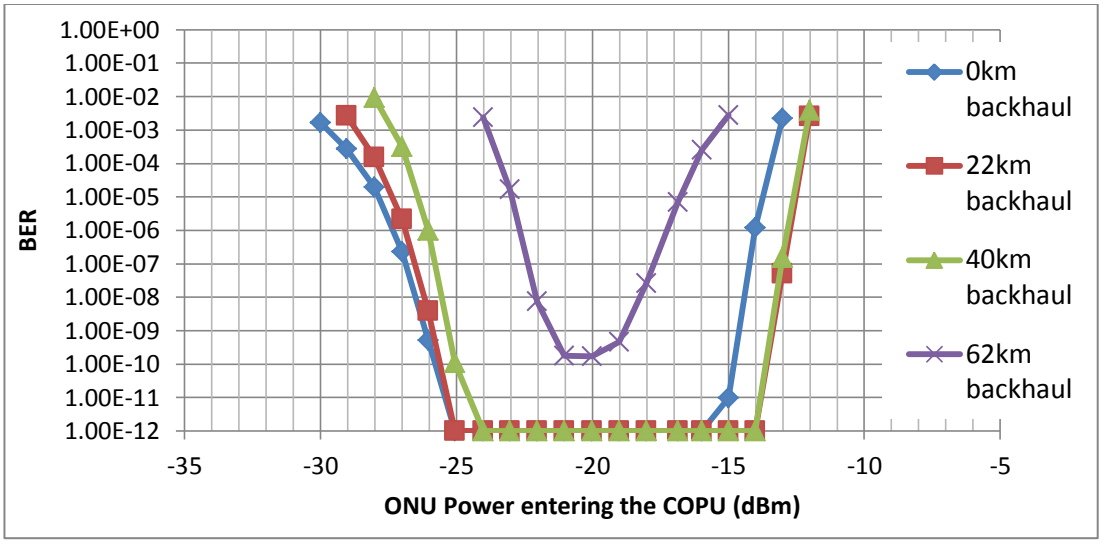

Figure 5.29 IPDR when the signal has transmitted through 0, 22, 40 and 60km backhaul SMF.

Excluding the 62km backhaul, the minimum IPDR was 8dB (BER at 10^{-12}) or 10dB (BER at 10^{-10}) for up to 40km backhaul transmission. The IPDR is determined by two factors, the low input power end (near -25dBm) of the dynamic range is due to fibre loss in the backhaul closing the eye, resulting in worse BER performance. This explains that the 0 and 22km backhaul received BER is at 10^{-12} with -25dBm input power, but the 40km backhaul BER is only at 10^{-10} at the same input power. On the contrary, the high input power end (near -14dBm) will need to be explain by the transfer function of the SOA-MZI and the eye of the signal. The gain induced phase shift and the output signal amplitude has a sinusoidal relationship, therefore, the π radians phase change in one SOA arm produces the best extinction ratio at the output.

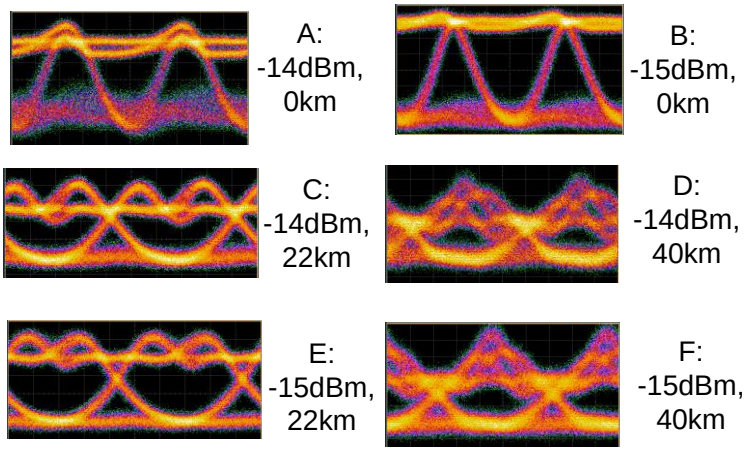

Figure 5.30 Received signal eye at high ONU power, on the right of every eye (A-F), the burst power entering the COPU and the burst travelled backhaul distance is shown.

When the input signal power was above -15dBm, the SOA will be saturated by the pump and resulting in a larger than π radians phase change which will reduce the extinction ratio of the signal. As shown in Figure 5.29, the BER performance gets worse as the input power to the COPU increases. At 0km backhaul, it can be seen in Figure 5.30 (A and B) that at -14dBm input power the "1s" of the output signal begin to reverse and there is significant noise in the "0s", introducing errors. As the signal propagates through 22km and then 40km of SSMF (Figure 5.30, C to F), the loss in the fibre lowers the "0s" noise floor and dispersion broadens the pulse, the signal eye is more open resulting in between 1 and 2 dB gain in BER performance.

5.6.4 The impact of differential dispersion

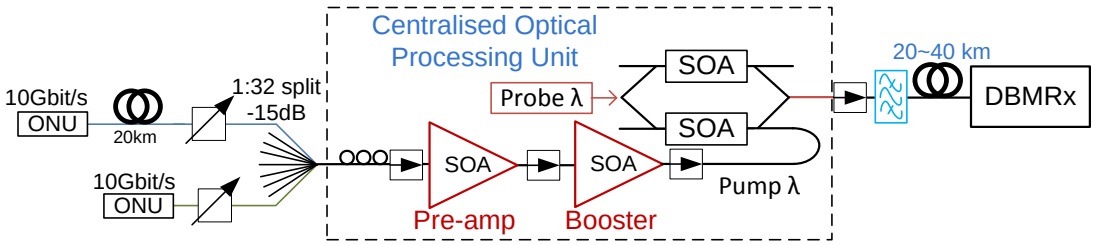

Figure 5.31 Experiment to look at the differential dispersion introduced by difference in distribution fibre distance

The ONU signal may go through different distances of PON distribution SSMF before it reaches the COPU, with the different length of fibre introduces

different amounts of dispersion. In this section the impact of dispersion is assessed using continuous-mode operations.

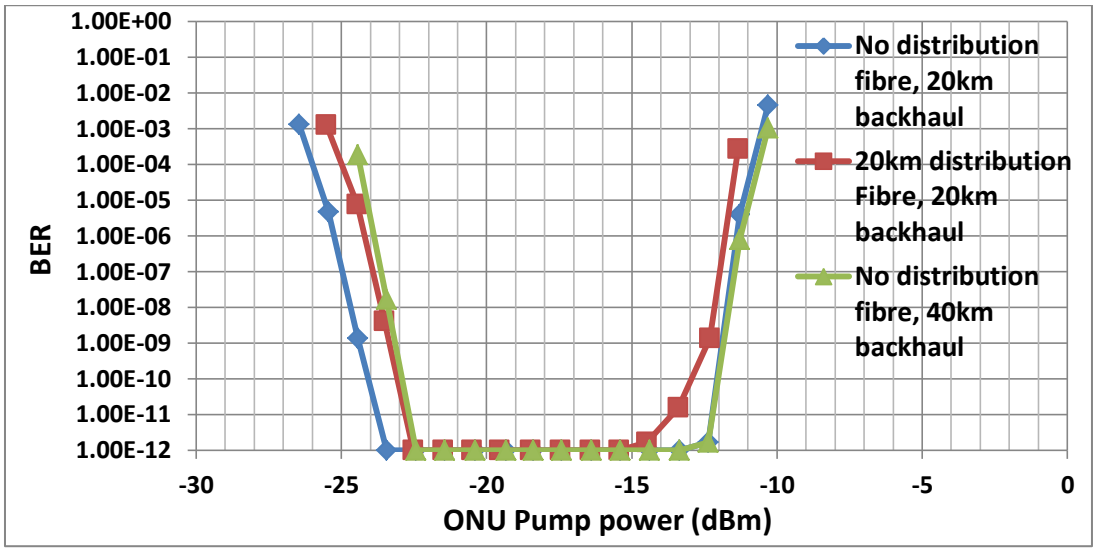

Figure 5.32 IPDR difference between 0 and 20km distribution fibre distance

The results in Figure 5.32 show that the IPDR (ONU pump power range that produced 10^{-10} BER) of the wavelength conversion system has been reduced from 12dB to 10dB with the addition of 20km distribution fibre, when the same 20km backhaul is used. When no distribution fibre was used, the optical power loss equivalent to the 20km fibre was compensated by 5.7dB attenuation of the input signal. The upper limit of the IPDR has been reduced by 1dB and the lower limit of the IPDR has been reduced by 1dB. This can be explained by the broadening in the output signal eye shown in Figure 5.33 below. The IPDR with a 40km backhaul was also shown, so that the total length of the SSMF travelled is the same as the 20km distribution plus 20km backhaul case. When the distribution fibre distance is 0km, extending the backhaul distance from 20km to 40km did not reduce the upper limit of the IPDR while the reduction of the lower bound of the IPDR of 1dB is due to loss in the fibre.

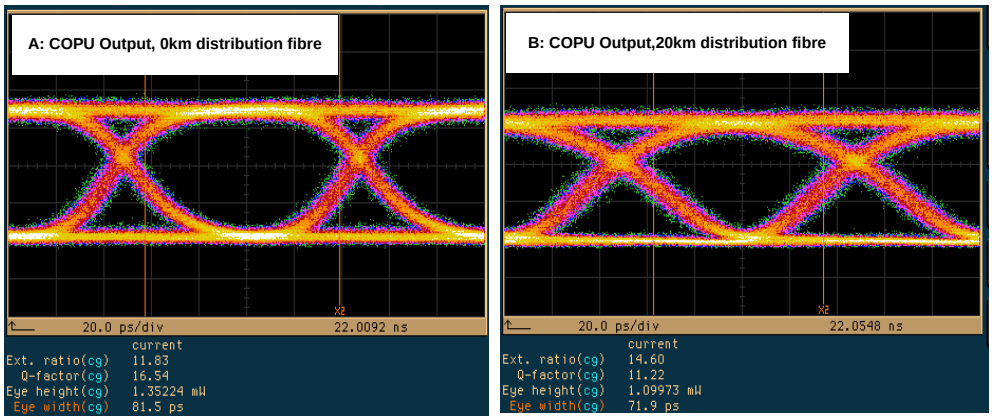

Figure 5.33 Eye of the COPU output signal, A:0km distribution SSMF, B: 20km distribution SSMF

The pulse broadening is visible in the eye diagram of the wavelength converted signals shown in Figure 5.33-B. Dispersion in the 20km PON distribution section has reduced the COPU output signal Q-factor from 16.54 to 11.22, while the shape of the output pulse is also broadened and the eye width reduced from 81.5ps to 71.9ps. When the ONU power is high, the output signal's "0s" are shorter; when the ONU power is low, the broadened signal is weaker because the peak of the pulse amplitude is reduced by the broadening, resulting in a reduction in the received BER performance.

5.6.5 ONU Wavelength Drift

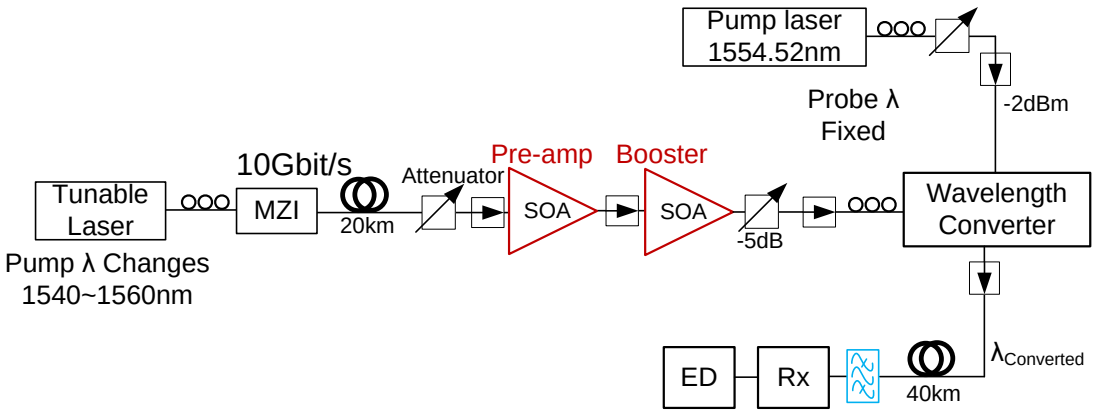

Figure 5.34 Detailed experiment schematic for measuring the effect of input ONU signal wavelength drift

This section investigates the possible wavelength drift that occurs in an uncooled ONU and its impact to the COPU and the WCOAN performance after long

backhaul transmission. Building on the setup used in the previous section, a more detailed schematic for this experiment is shown in Figure 5.34. Instead of modelling the ONU using a temperature controlled DFB laser with integrated EAM modulator, the ONU here is modelled by a tuneable laser with a Mach-Zehnder external modulator so that we can simulate the wavelength drift of an un-cooled ONUs. The tuneable wavelength ONU model was adjusted so that it has nearly identical eye height and ER as the fixed wavelength ONU. The eye diagrams of the two modelled ONU are shown in Figure 5.35.

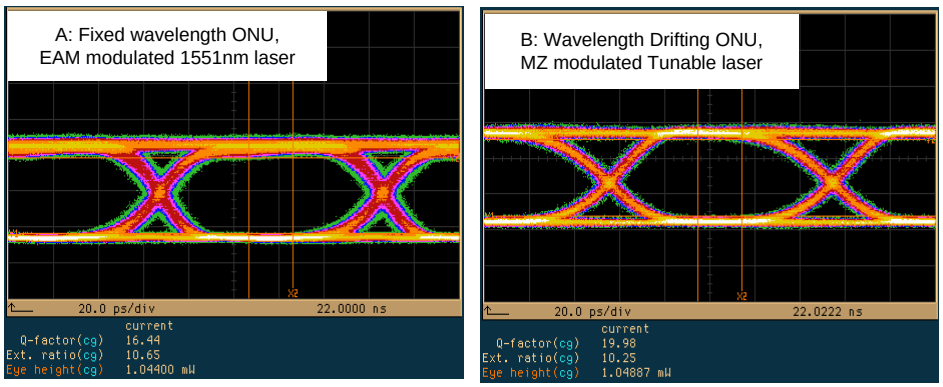

Figure 5.35 The eye diagram of a fixed wavelength ONU and a tuneable wavelength ONU, the eye height and ER were adjusted so that they are as similar as possible.

In order to ensure the wavelength tuneable ONU matches the fixed wavelength ONU in performance, the MZ modulator bias voltage and the RF input gain of the MZ modulator was adjusted so that their output power are the same, the eye height difference is 5 μW, the ER difference is 0.4dB and the Q-factor difference is 3.54. The high level in the eye produced by the MZ modulator (B) is clearer than the high level in the eye produced by the EAM modulator (A), this increases the probability of detection a one, hence increasing the Q-factor. Isolators were again used to prevent reflected light and ASE noise in the SOA from interfering with the original signal and the SOA operation. The power of the ONU signal at the input to the pre-amp SOA was changed while BER measurements were taken from the receiver at the OLT. These measurements aim to find out the input power levels as

well as wavelengths at which the wavelength converted signal output can remain error free, after a 40km backhaul. A -5dB attenuator was used to prevent the high power signal after two stages of amplification from saturation the SOA-MZI wavelength converter. When the tuneable laser is tuned to another wavelength, the signal polarisation is slightly changed, since the MZ modulator depends on the signal polarisation, the MZ modulator must be re-aligned each time the wavelength was changed, before the start of each set of IPDR measurements. The wavelength converter used in this experiment is a prototype device which is polarisation sensitive to the pump signal. This polarisation dependency can account for up to 2 dB power penalty. Since polarisation insensitive SOA-MZI wavelength converters are available [91], to minimise the effect of polarisation, the polarisation controller at the input to the WC was optimised so that the output signal eye is at their best Q-factor and ER.

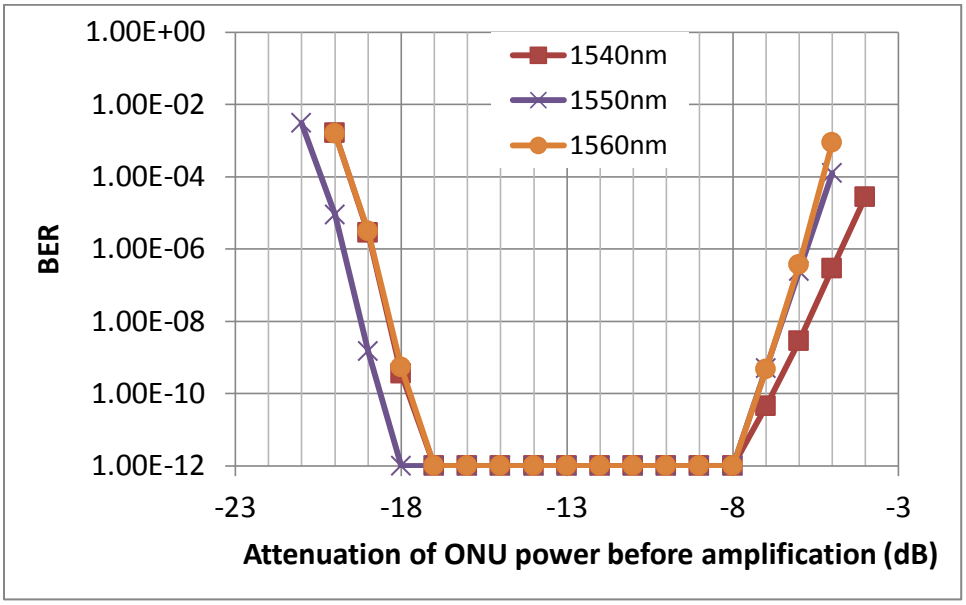

Figure 5.36 The effect of pump signal wavelength drift on IPDR measured in terms of BER performance.

The result in Figure 5.36 shows that wavelength drift does not change the system IPDR by more than 1dB when the pump signal wavelength is detuned to ±10nm from the starting wavelength at 1550nm. The IPDR is largest at the centre

wavelength of 1550nm, with a variation of 10dB in the power from the ONU possible. The IPDR decreases to 9dB (10^{-12} BER) or 10dB (10^{-10} BER) as the wavelength is tuned to 10nm away from the centre. This is because the centre wavelength of 1550nm was used as a reference to setup the system, and is the point at which the probe power was optimised for maximum pump power IPDR. Due to the non-flat gain profile of the cascaded SOAs, a small shift in pump power at ±10nm wavelength can decrease the overall system IPDR. The phase shifter voltage was also optimised for operation at 1550nm and remains unchanged throughout the experiment, because under burst mode operation, the phase shifter voltage cannot be changed manually at micro-second speed to re-optimise the system for each burst power.

The scale of the ONU power stabilisation due to saturation in the SOAs can be seen from the following result. Average pump power measurements were taken before the pump signals were injected into the wavelength converter. In keeping with the above IPDR measurements, the BER results here were measured at the receiving end. After the signal was equalised in the cascaded SOAs, the 9dB (error free) system IPDR shown in Figure 5.36 has now been reduced to less than 1.5dB, as in Figure 5.37, which is less than the inherent 3dB IPDR of the WC.

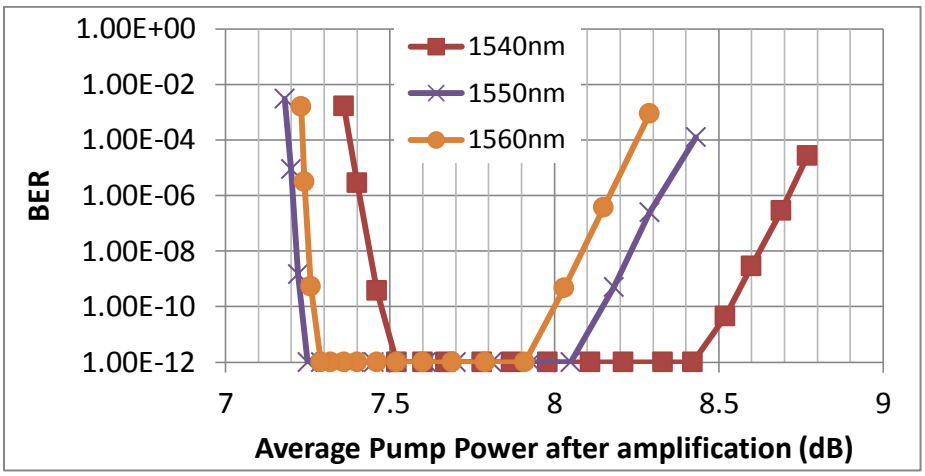

Figure 5.37 Average pump power variation at the input to the WC

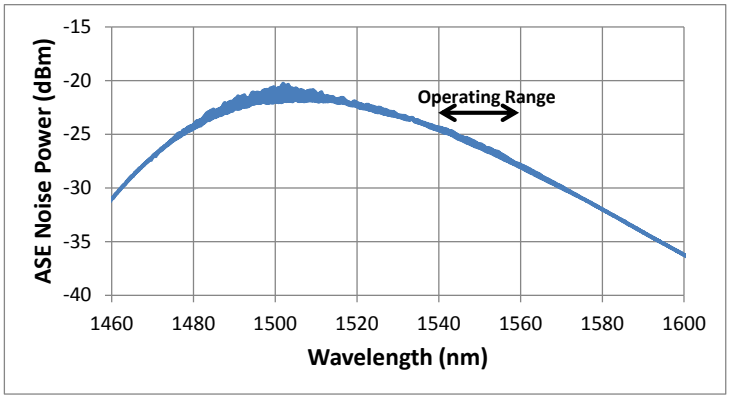

Figure 5.38 ASE noise profile of the pre-amp and booster SOAs formed equaliser

Another issue which must be considered is that the SOA ASE noise is not flat across all wavelengths. Figure 5.38 shows that the SOA ASE noise is much higher towards the gain peak at 1500nm. In the lower wavelength range (1540nm), the SOA ASE noise is higher adding to the average pump power, shifting the pump power up by 0.5dB. At the centre and higher wavelengths 1550nm and 1560nm, the ASE noise power is 2 to 3dB less and therefore, the signal power dominates and the average pump power is 0.5dB less.

5.6.6 Burst Equalisation and Wavelength Conversion

An experiment was built to test the burst equalisation and wavelength conversion of the COPU using the standard PIN receiver. The setup is shown in Figure 5.39.

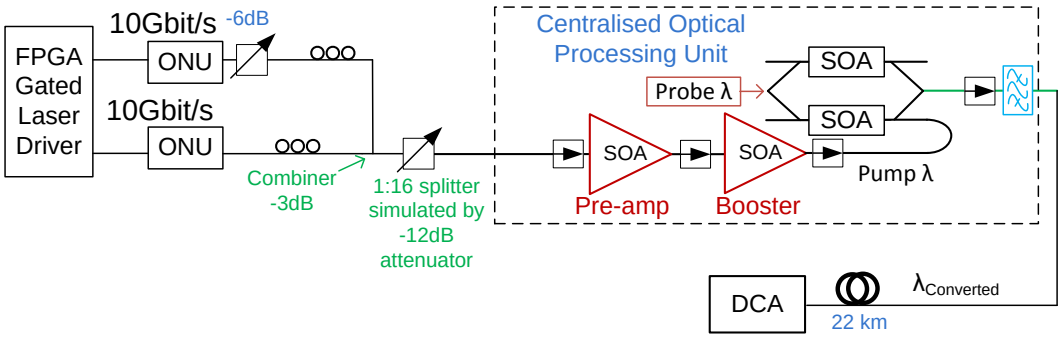

Figure 5.39 Experiment setup for burst mode equalisation and wavelength conversion performed in a COPU

The ONUs were modelled by EAM modulated DFB lasers, with a 10Gb/s 2^{31} PRBS pattern loaded onto both ONUs. The FPGA and gated laser driver together generated alternating gating currents that turn the DFB lasers on and off, resulting in alternating 125μs bursts with 500ns guard times between the bursts. A quick switch to continuous mode operation is available, leaving either one of the ONU running at continuous mode so that their BER or eye diagram can be monitored individually using the BERT. In order to create the difference in burst power, a 6dB attenuator was used at one of the ONU outputs. The ONU powers, when measured individually in continuous mode, have 0dBm and -5.53dBm optical powers respectively. The DCA was triggered using the gating signal, therefore, bursts are visible on the DCA display, Figure 5.40 shows the ONU bursts at the combiner and the bursts observed after the COPU output. It can be seen that their power differences are reduced, with their signal powers measured in the continuous mode after 22km of backhaul fibre being -4.86dBm and -5.40dBm. The power difference is reduced from 5.53dB to 0.54dB. Both converted signals showed an error free BER of 10^{-12} when monitored under continuous mode using the BERT.

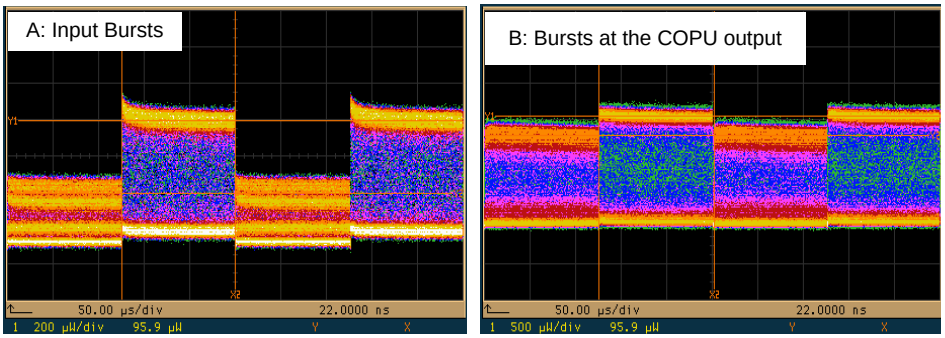

Figure 5.40 Bursts at the input and at the COPU output. Vertical scale are different, A:200μW/div, B:500μW/div

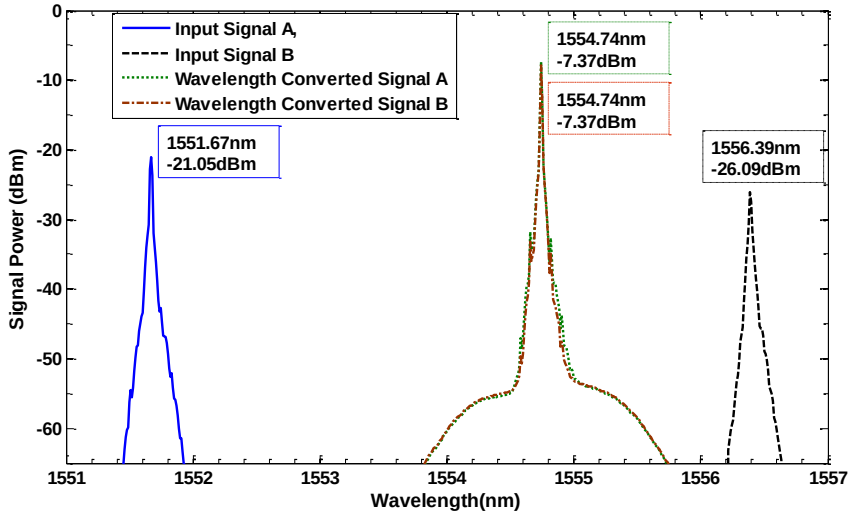

Figure 5.41 Spectrum of the input signals and the converted signal at the COPU output, showing wavelength conversion of the two signals to the same fixed wavelength

The combined spectrum showing the two input ONU signals and their converted output signals are presented in Figure 5.41. It shows that the two ONU signals at 1551.67nm and 1556.39nm wavelength were both converted to the same probe wavelength at 1554.74nm. These spectrums were measured in the continuous mode which reflects the "on" state spectrum of the burst. Under burst mode operation, the laser power fluctuates and the spectrum will exhibit adiabatic chirp generated during on/off laser switching. The 500ns guard time used between the bursts allows on/off switching and laser power stabilisation, so that the power fluctuations and adiabatic chirp do not introduce intensity noise during the burst transmission.

5.6.7 Digital Burst-mode Receiver

The standard receiver used in the experiments so far is a DC-coupled PIN receiver with clock synchronisation and data recovery in continuous mode operations provided by the BERT. Under burst-mode condition, the fibre transmission introduces optical delay of the signal, a burst-mode receiver or at least the burst mode clock and data recovery function will be required to measure the burst BER. A

10Gb/s burst-mode receiver was not available for this experiment, but there is an alternative solution, which is the digital burst-mode receiver (DBMRx) [78] developed by José Manuel Delgado Mendinueta in the optical networks group at UCL. The DBMRx is based on a DC-coupled PIN photodiode, a fast ADC, and has digital clock and data recovery capabilities realised in software.

The receiver used a standard DC-coupled PIN photodiode and an integrated trans-impedance amplifier (TIA) to convert the optical signal to electronic signals. Then a Tektronix oscilloscope containing fast ADCs at 25GS/s was used to digitise the signal for subsequent Digital Signal Processing (DSP) in MATLAB. The DSP stage determines the line-rate and recovers the clock and data from the bursts [78].

5.6.8 Burst-mode System Performance

The implementation of the DBMRx changes the gating mechanism slightly. Instead of using a continuous PRBS pattern in the PPG, a fixed length repeated PRBS pattern containing two burst sequences 65536bits (6.6μs) long with 2048bits (204ns) guard times was loaded on to the PPG. The PPG triggered the laser drivers, which gate the laser. The fixed payload of the loud and soft burst will allow the DBMRx to determine the errors in each burst and through post-processing determine the BER of the individual bursts.

Although the length of the burst payload here is constrained due to the limited PPG memory available, in a real NG-PON, the burst mode receiver will only use less than 512ns information in the preamble and delimiter of a burst to set the decision threshold, therefore, a 6.6μs burst length is sufficient to analyse the performance of the system. At longer burst length, the threshold set should be the same as the one set by a 6.6μs burst in out experimental system. In NG-PON, the burst length can be more flexible than the GPON burst size and no longer limited to

125μs per burst, in order to allow more efficient use of the upstream bandwidth. XGPON bursts have a physical synchronisation block upstream (PSBu) followed by a variable number of FEC codewords along with parity check bits, but the payload size is not fixed, the last FEC codeword is shortened to ease the loss of bandwidth caused by odd-sized bursts[2]. The 10G-EPON implementation is similar, it has a laser synchronisation pattern and a fixed 66 bit burst delimiter pattern at the beginning of each burst, followed by a start of frame preamble to signal the start of the FEC codewords. At the end of the payload there is also a 66 bit block of burst terminator pattern of alternating ones and zeros [92].

In the DBMRx, the DSP process in MATLAB compares the recovered data from the ADC captured traces with the burst patterns in the PPG to determine the detection threshold of the DBMRx and calculate the BER [78].

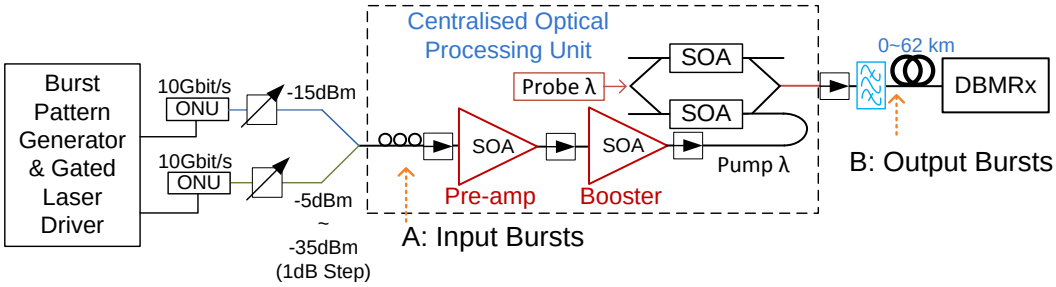

Figure 5.42 Burst-mode characterisation experiment setup with COPU and DBMRx

Figure 5.42 shows the experimental setup used to characterise the burst-mode performance of the COPU. Two ONUs were modelled with two externally modulated DFB lasers at different wavelengths (1553.5 and 1556.3nm), with an extinction ratio of 14dB. In this COPU, the probe and pump signals are in a counter-propagation configuration, as described in Section 5.4.2 this arrangement generates a better signal performance in terms of higher extinction ratio and Q-factor. The probe, onto which the upstream traffic is converted, was a CW laser at 1554.7nm As this is a proof- of- concept experimental demonstration only commercially available C-

band devices were available in our laboratory. Wavelength conversion from 1.3 μm to 1.5 μm using 1.3 μm SOAs has been previously demonstrated [68]. Both up and down wavelength conversion were tested using this experimental setup and no significant difference between the two was observed. Optical isolators were also used at the ports to prevent reflected light interfering with SOA operation.

In real world applications the polarisation of the burst coming from the ONU is random. The SOAs used in the equalisation stage have less than 0.5dB polarisation dependent gain, but the SOAs inside this prototype SOA-MZI device had a stronger polarisation dependent gain (PDG). The PDG changes the signal power in one arm of the SOA-MZI, which affects the bias point of the WC and can result in an up to 2.5 dB dynamic polarisation penalty for the received BER sensitivity. It is expected that a production grade SOA-MZI device will be used in the real system, which will have an optimised SOA active region and is polarisation insensitive [91]. Therefore, the bias point of a polarisation insensitive SOA-MZI device will not be affected by the random polarisation of the ONU bursts.

The following procedure was used to adjust the ONU polarisation, i.e., the WC bias point, to overcome the polarisation penalty of this prototype device. Two bursts of -15 (loud) and -25 dBm (soft) were generated and then three COPU optimisation cases, named A, B, and C, were chosen. These cases are illustrated in Figure 5.43 for a backhaul transmission distance of 22 km, where the soft burst eye was superimposed on the loud burst eye. The loud burst eye exhibits a nonlinear distortion due to patterning-generated additional optical power before the SOA-MZI sinusoidal transfer function, which contrasts with the characterisation of Figure 5.24, where no eye overload is noticeable in static CW mode. In case A, the optical eye diagram of the loud and soft bursts was equalised as much as allowed. Ideally, this

would be the case for the real system with a polarisation insensitive SOA-MZI device. Case C is the opposite and so the amplitude of the loud burst is maximised and the power of the soft burst is minimised. Case B is a compromise between cases A and C.

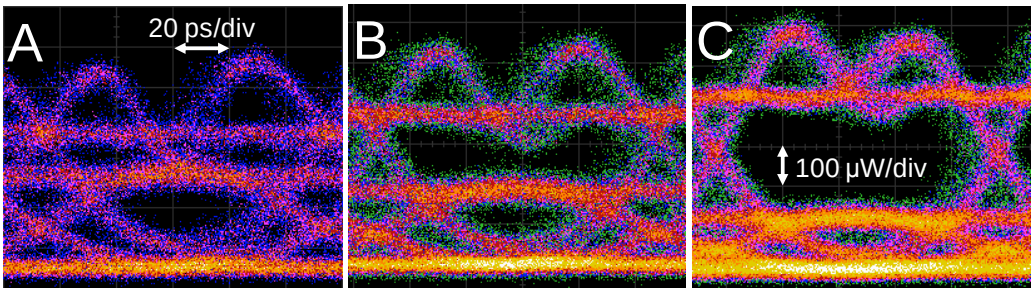

Figure 5.43 COPU output signal eye diagrams after 22 km of fibre for (a) polarisation case A, (b) polarisation case B, and (c) polarisation case C.

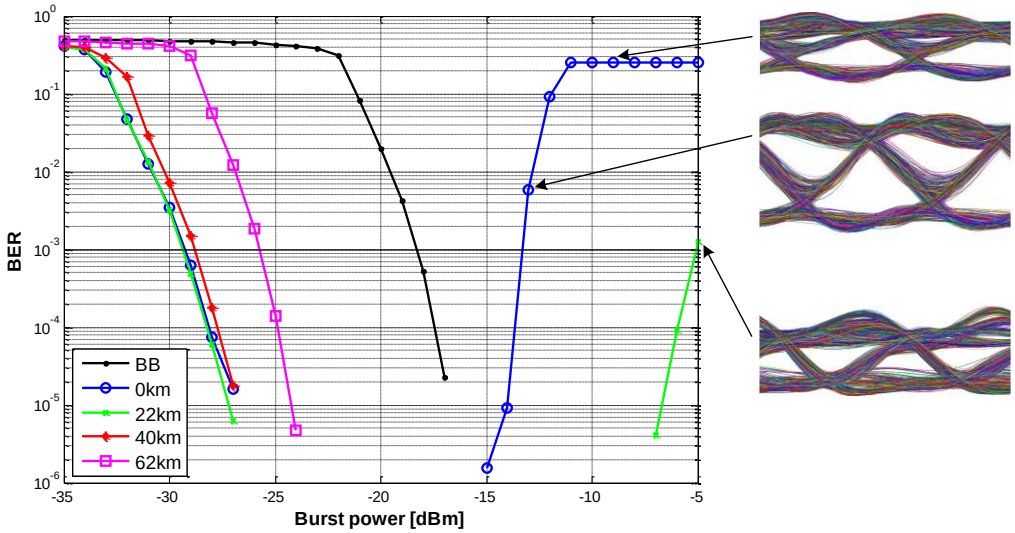

Figure 5.44 Soft burst BER performance of the received signal in burst-mode operation at 0km, 22km, 40km and 62km fibre length.

Figure 5.44 shows the soft burst BER performance in burst-mode operation for COPU optimisation case B, which keeps the overload point above -15dBm and has the minimum sensitivity. At the overload points, the selected electrical eye diagrams as seen by the digital receiver are also shown. In these measurements, the attenuators were configured in such a way that the optical power of the 'loud' burst was fixed at -15dBm, in order to simulate the 32-way splitter losses, while the power

of the 'soft' burst was swept from -5dBm to -35dBm in 1dB steps. For each step, 32 traces were captured and processed offline with MATLAB so as to obtain BER measurements with acceptable confidence intervals. The back-to-back (BB) result in Figure 5.44 indicates the DBMRx sensitivity in burst-mode operation and was measured by connecting the burst-mode transmitter straight into the DBMRx. The sensitivity is defined as the minimum soft burst power that produced a BER below the 10^{-3} reference, which is the FEC limit. Implementing the COPU has contributed to the digital receiver sensitivity by allowing 12dB lower input burst power to achieve the same BER as the BB case, as well as performing wavelength conversion. The sensitivity of the digital receiver is maximal for the 0km case and diminishes with transmission distance due to fibre losses and dispersion. When the input burst power is higher than -15dBm, the overshoot of the receiver is worse for the 0km case, and improves with longer backhaul transmission distance. The SOA-MZI device operating in non-inverting mode has the benefit of generating negative chirp. The pre-chirped converted signal reduces the impact of dispersion, and so the results show that the overshoot improves when fibre distance increases from 0km to 22km. Three electrical eye diagrams shown in Figure 5.44 illustrate this effect at the receiver side. For -9dBm burst power and 0km fibre transmission distance the received eye is completely closed. By comparing this eye with the one at -13dBm burst power we observe the fast eye degradation as input burst power increases, for 0km transmission distance. However, for -5dBm burst power and 22km of fibre the eye is reasonably open, its BER is below 10^{-3}. On the other hand, the BER of the loud burst was also monitored and it is always below the 10^{-3} FEC limit.

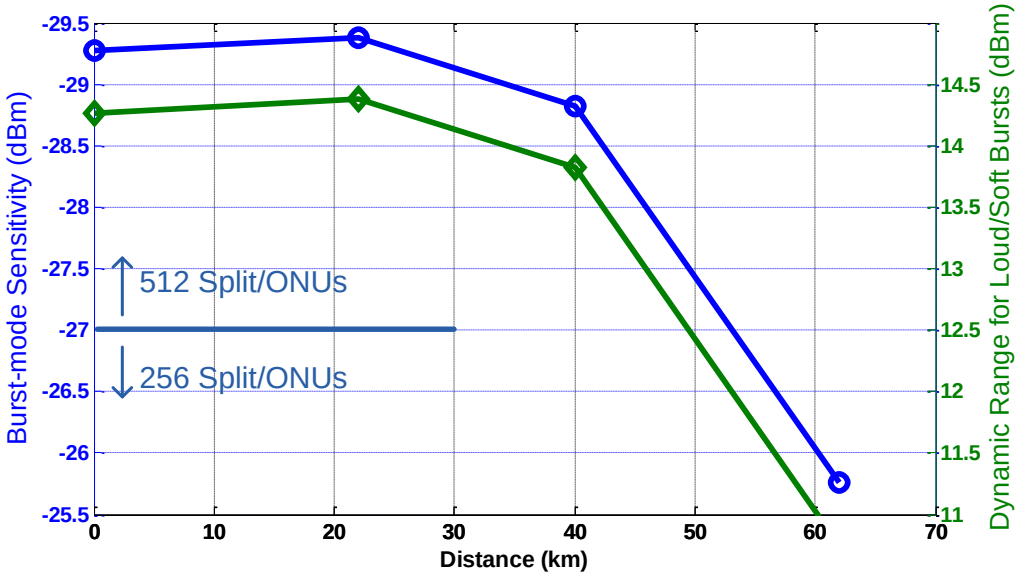

Figure 5.45 OLT sensitivity of bursts and loud/soft bursts dynamic range, at a 10^{-3} BER reference.

The minimum sensitivity and dynamic range of the burst-mode receiver are shown in Figure 5.45. The minimum sensitivity is the lowest soft burst power at the input to the COPU for a received BER below 10^{-3}. The dynamic range is defined as the maximum power difference between the loud burst (in this case at -15dBm) and soft burst, when they are successfully received, i.e., both bursts BER are below 10^{-3}. It showed that the overall system with COPU and the PIN photodiode based DBMRx can support up to 512-way splitter loss (or 512 ONUs) over a maximum 53km distance, at BER below 10^{-3}. At longer backhaul distances, the dispersion in the fibre begins to dominate, and the dynamic range decreases to a value as low as 10.8 dB at 62km from a maximum of 14.3dB directly after the COPU. This dynamic range reduction is also due to loss in the fibre and the decrease of the sensitivity. The system sensitivity at 60km backhaul distance can still support 256 ONUs of a PON segment at the distribution section.

5.7 Conclusions

In this chapter a new architecture to integrate multiple 10Gb/s CWDM PON into a DWDM long-reach backhaul was introduced and described. The essential element of this architecture is the Centralised Optical Processing Unit, which contains a burst power equaliser stage and a wavelength conversion stage based on a XPM WC. The WC's power, polarisation and phase voltage bias were characterised. It was found that by biasing the phase shifter, an inverting mode that generated positive output signal chirp or a non-inverting mode that generated negative chirp can be selected. The performances of the co- and counter- propagation modes were also compared and it was concluded that counter-propagation generates 3dB higher extinction ratio and 5.43 more signal SNR for this SOA-MZI based WC.

For the first time an experimental, upstream access network transmission system using the XPM WC was demonstrated. The BER performance at 20km, 40km and 60km backhaul distances were compared and an error free (10^{-12} BER) total transmission distance of 80km (20km distribution, 60km backhaul with optical amplification) was achieved.

The overall Input Power Dynamic Range (IPDR) of the COPU was characterised, the IPDR is larger than 10dB (10^{-10} BER) for transmission distances up to 40km. The ONU wavelength drift within a 20nm wavelength window did not change the IPDR by more than 1dB. However, the dispersion caused by a 20km distribution fibre in the PON section can reduce the IPDR by 2dB due to pulse broadening and power loss.

A proof-of-concept, full burst-mode long-reach wavelength converting optical access network upstream that utilised the COPU was also experimentally demonstrated for the first time. The BER performance at 22, 40, and 62 km backhaul

distances were compared and a sensitivity penalty of -0.1dB, 0.6dB, and 3.6dB were found, respectively. The same penalties were found in input burst dynamic range for the aforementioned transmission distances. For this COPU that contained a prototype SOA-MZI device, there is a less than 2.5dB overall polarisation-dependant penalty.

Chapter 6. Conclusions

In this thesis, the design and performance aspects of the next generation optical access network are investigated, they include interferometric noise in ring based access networks as well as a novel intermediate stage optical processing technology for the integration of multiple PON with a DWDM long-reach backhaul. Theory, simulation and new experimental demonstrations were used to characterise the performance in these 10Gb/s systems, it allows for a better understanding of the operating range and merits of the proposed systems and their impact on performance. Access network specific issues such as the temperature dependent source wavelengths and burst-mode transmission have also been considered during the investigations, the results obtained from these are significant, as similar techniques used in the core network scenarios assumed fixed wavelength and continuous-mode transmission.

WDM backhaul and wavelength stacking of multiple PONs is expected to be used in next generation access networks, as well as optical amplifications, which can

be used to enhance capacity and extend the network reach beyond 20km. In Chapter 2. The conditions of burst-mode transmission in passive optical network was also describe in Chapter 2, along with the benefit of using all-optical processing, such as burst equalisation, wavelength conversion and other techniques for achieving burst mode levelling, access/metro network aggregations, DWDM backhaul integration and reach extension.

In future ring based access networks with OADMs, interferometric noise may arise from the interference of normal data signal and parasitic crosstalk, as a result of the low cost OADM used. Previous core network studies in this area assume fixed wavelengths, but in access, wavelength tolerance is a key factor and was considered for the first time. In Chapter 3, current studies on the topic of burst equalisation methods and the effects of interferometric noise (IN) in ring based access network were reviewed. In the simulation and experiment presented in Chapter 3, the BER performance characteristics for up to 0.08nm (10GHz) detuned wavelengths at several interferer attenuation levels (18 to 40 dB) were shown. Using standard 10Gb/s PIN receivers with an 11GHz internal filter 3dB bandwidth, reducing the interferer signal power or detuning its wavelength away from the data signal can produced better BER performances in the received data signal. When the interferer attenuation is at 20dB, 4 orders of magnitude better BER performance were observed by detuning the interferer wavelength by 0.08nm (10GHz). The addition of an electrical filter with a bandwidth of 7.5GHz after the receiver produced better performance than using the receiver alone, it is most significant at > 5GHz detuned frequencies. These observations lead us to simulate and develop a model to analyse the BER performance characteristics at various electrical filtering bandwidths, while also taking wavelength tolerance into account. This investigation showed by

narrowing the receiver filter bandwidth and/or increasing the frequency detuning of interferer, the amplitude and thus impact of IN is reduced. However, a less than 6GHz filter bandwidth can also lead to ISI, which will worsen the BER performance. This is a significant and key conclusion for OLT design, it showed the impact of receiver filter choice on BER performance, in ring access network with the presence of IN. The simulation results were also compared and validated with the experimental ones, the largest difference between the results is less than 1.5 orders of magnitude of BER. The model is validated to be accurate in most results, except when the distribution of filtered IN noise is half way between Gaussian and arc-sine distributed, at 0.04nm (5GHz) detuned interferer wavelengths.

PON uses burst-mode transmission, the near-far ranging of ONUs produces different power bursts in the upstream. In Chapter 4, the idea of using SOA as a limiting amplifier in an optical burst equaliser was explained and demonstrated, in order to ease burst-mode receiver dynamic range requirements for the OLT. SOA models were developed and compared based on the ability to simulate real SOA characteristics under normal and more importantly deep SOA saturation. It was suggested that using an effective carrier lifetime instead of a constant lifetime can give more precise results at SOA high saturation. A saturated SOA model was created with carrier lifetime adjustments, which was validated by experimental measurements. This new model was used to study the burst equalisation system's output signal BER performance, as well as the SOA saturation induced time and frequency distortions in the equalised signal, which have not been previously studied in this context. The experimentally verified model's ability to simulate frequency distortion alongside gain distortion is significant, as these effects are interlinked and it showed that saturated SOA will chirp the equalised signal. Frequency chirping can

harm the equaliser output signal performance, a better technique was implemented and presented in Chapter 5 to tackle this issue, in order to reduce or eliminate the SOA saturation induced gain and frequency distortions.

A proof of concept experimental dual SOA optical burst equalisation system was presented for the first time, it levelled a 5dB difference in input burst power, this is equivalent to 25km distance between two ONUs, which is 5km more than the standard defined 20km maximum distribution fibre length. Optical filtering was suggested to reduce the effect of spectral broadening caused by the non-linear effect in SOA saturation. When the power difference between the two burst is at 2dB, we observed 5 orders and 9 orders of magnitude increase in BER performance for the filtered-equalised loud and soft power burst in simulation, respectively. As the soft burst is attenuated to 11dB below the loud burst, the initially error free filtered-equalised soft burst BER increase to 10^{-6}. A 2dB increase in extinction ratio and 4 orders of magnitude increase BER performance was also observed in the experiment, as the impact of chirped signal distortions was reduced by the optical filtering. Power balancing the two SOAs by adding 3.6dB attenuation between them was shown to increase the loud burst ER by 1dB, this is useful for high ONU input powers that oversaturates the booster SOA.

In order to solve the signal distortion shortcoming of the two SOA burst equalisation system as well as addressing the wavelength drift and extension of reach in future access networks, Chapter 5 presented and first experimentally demonstrated a new solution to integrate multiple up to 10Gb/s CWDM PON into a DWDM long-reach backhaul through the use of a novel Centralised Optical Processing Unit (COPU). This essential element contains a burst power equaliser stage followed by a

wavelength conversion stage based on a XPM WC. This solution has the capability to level burst power, stabilised wavelengths and extend transmission reach.

For the first time, a XPM based wavelength converter was demonstrated in a burst-mode access network system that considers wavelength drift and wavelength stabilisation, the performance of it at 20km, 40km and 60km backhaul distances were compared. An error free 10Gb/s total transmission distance over 80km SSMF was achieved owing to the pre-chirped WC output. Furthermore, the XPM WC was also able to regenerate so that the spectral broadened and gain distorted signal from the burst equaliser is restored for backhaul transmission. At the same time, the burst levelling stage stabilises the input power to the XPM WC, therefore, its overall error free Input Power Dynamic Range (IPDR) increased from 3 to 10 dB when measured just after the COPU. The ONU wavelength drift within a 20nm window did not change the IPDR by more than 1dB. However, the dispersion in 20km of distribution fibre before the COPU can reduce the error free IPDR by 2dB due to pulse broadening and loss. The significance of this result is that it showed that the IPDR of the COPU is insensible to reasonale wavelength drift and it is only affected in the extreme cases of dispersion, therefore, the COPU is robust enough to tolerate ±10nm wavelength drift and supports ONU distribution distance up to 20km with a maximum 3dB combined dynamic range penalty.

Continuous-mode and full burst-mode demonstration of a long-reach wavelength converting optical access network architecture was presented and demonstrated for the first time, incorporating this novel COPU. The BER performance at 22, 40, and 62 km backhaul distances were compared. At 22km, loud burst power and soft burst power entering the COPU at -15dBm and -29.3dBm were both received and below 10^{-3} BER (FEC limit), which is equivalent to an input burst

dynamic range of 14.3dB. In terms of split size and ONU numbers, this system supports 512 ONUs at 53km SSMF backhaul distance and 256 ONUs at 62km backhaul with a PIN photodiode based DBMRx, with dispersion compensation techniques and higher sensitivity receivers, the backhaul distance can be increased further. Sensitivity penalties of -0.1dB, 0.6dB, and 3.6dB were found, for 22, 40, and 62 km backhaul distances, respectively. The same penalties were found in dynamic range for the aforementioned transmission distances. Since a prototype SOA-MZI device was used in this SOA, there is a less than 2.5dB overall polarisation-dependant penalty.

In conclusion, the aim to fully exploit existing ODN infrastructure by consolidating multiple PON segments into a long-haul DWDM backhaul was achieved and experimentally demonstrated, using intermediate optical processing techniques. It has been shown that optical wavelength stabilisation, optical burst equalisation and transmission distance enhancement can address next generation access network design issues. Although the dual SOA burst equalisation alone has limitations, when it is combined with an XPM WC in the COPU, together they can level the incoming burst, thus reducing the dynamic range requirements of the OLT receiver. This allows potential cost saving to operators deploying next generation access networks. Through the use of DWDM in the backhaul, additional services can be added to the backhaul of this network without changing the existing PON distribution network. The ring access network performance in the presence of IN has also been investigated, considering the wavelength tolerance of the system and filter leakage in OADMs, specific to access network.

6.1 Suggestions for future work

A number of possible further investigations are suggested as a result of the work performed here.

A more advanced analytic model can be developed for the relationship between BER performance and the filtering characteristics in the presence of interferometric noise. This can extend the work in Chapter 3. In [93], it is found that when the interferer are at unequal power the Gaussian approximation is not the ideal model for the statistics analysis. Two particular BER assessment techniques based on the Moment Generating Function (MGF) may instead be used, they are the Saddlepoint Approximation [94] and the Modified Chernoff Bound [95].

The Further SOA model and parameters requires further adjustment and refinement. It would be ideal to add the ability to simulate multiple wavelengths and gain peak shift [81] due to laser pumping. If this can be achieved, the SOA model will be able to simulate wavelength conversion in OptSim.

For the experimental work, some investigations were carried out to investigate the IPDR of the SOA-MZI device in Chapter 5. If there is more time to study this, other methods or combinations of methods to further increase the IPDR of the COPU need to be found, thus allowing increased number of users in the distribution network. The following table included the methods found in literature to improve the input power dynamic range of the XPM wavelength converter. Electronic control and all-optical methods are available. The cascaded SOA option is similar to the burst equalisation in PON which was used in our experiment.

Methods	**Claimed Improvement on Dynamic Range**	**Pros**	**Cons**	**References**

Electronic control of phase arm voltage/ SOA bias current	5 dB/8 dB	Low cost to implement	Small dynamic range; No directly available control circuit because the control is non-linear.	[89, 96]
Electronic control of the SOA bias current and phase arm voltage together	10 to 15dB	Low cost to implement	Only suitable for slowly varying input power (~100ms) Need to measure the phase arm voltage and SOA bias current for the optimum operating inverting and non-inverting state.	[97]
Saturated EDFA	40dB	Large dynamic range	Only suitable for slowly varying input power, because of slow gain recovery(~1ms), may not be suitable for burst mode PON.	[89]
Electronic control of SOA pre-amplifier bias current	28dB	Large dynamic range, faster gain dynamics than EDFA	High noise figure at high input power (above -5dBm) because of the corresponding low SOA bias current (saturation power) required for the phase adjustment	[89]
Integrated Pre-amp	10dB	No fibre-chip coupling loss between the pre-amp and wavelength converter.	Require new fabrication or purchase of new device; Performance depends on the device quality.	[98, 99]
Cascaded SOA (similar to our burst equalisation setup)	20dB	Moderate dynamic range	Non-linear effects in the SOAs may lead to signal power penalty.	[100]
Control of SOA gain through external light injection (Tested experimentally in our setup, but did not produced as good result as the SOA equaliser)	20dB	Shortens the carrier lifetime while retaining the saturation output power; Less SOA gain distortions, than the SOA bias current control method.	Requires optimisation for the control light wavelength and detailed power characterisation; The control light power is non-linearly related to the input power and wavelength;	[84, 101]

The backhaul reach of the current system is at 62km, as this was an unamplified and uncompensated reach which resulted in a good BER performance. It is expected that this can be extended further, using APD receivers with higher

sensitivity instead of the currently PIN photo-diode based receiver or further optical amplification. Dispersion compensation fibre is another component that could be used to extend the reach, which will need to be investigated if the required components are available.

So far, our overall architecture did not consider more complex modulation schemes and higher line-rate TDM due to the limited device availability for used in experimental demonstrations. These can also be investigated in the future.

References

[1] K. Grobe, M. Roppelt, A. Autenrieth, J. P. Elbers, and M. Eiselt, "Cost and energy consumption analysis of advanced WDM-PONs," *Communications Magazine, IEEE,* vol. 49, pp. s25-s32, 2011.

[2] F. J. Effenberger, "The XG-PON System: Cost Effective 10 Gb/s Access," *Lightwave Technology, Journal of,* vol. 29, pp. 403-409, 2011.

[3] M. Hajduczenia and H. J. A. da Silva, "Next generation PON systems - Current status," in *Transparent Optical Networks, 2009. ICTON '09. 11th International Conference on*, 2009, pp. 1-8.

[4] J. i. Kani, F. Bourgart, A. Cui, A. Rafel, M. Campbell, R. Davey, and S. Rodrigues, "Next-generation PON-part I: technology roadmap and general requirements," *Communications Magazine, IEEE,* vol. 47, pp. 43-49, 2009.

[5] K. Kanonakis, I. Tomkos, T. Pfeiffer, J. Prat, and P. Kourtessis, "ACCORDANCE: A novel OFDMA-PON paradigm for ultra-high capacity converged wireline-wireless access networks," in *Transparent Optical Networks (ICTON), 2010 12th International Conference on*, 2010, pp. 1-4.

[6] T. Kamijoh, M. Kashima, H. Tamai, M. Sarashina, H. Iwamura, and G. C. Gupta, "CDM-technologies for next generation optical access networks," in *Optical Fiber Communication - incudes post deadline papers, 2009. OFC 2009. Conference on*, 2009, pp. 1-3.

[7] D. Nesset, "Network operator perspective on WDM-PON systems and applications," in *Optical Communication (ECOC), 2011 37th European Conference and Exhibition on*, 2011, pp. 1-3.

[8] D. O. Committee. (2011, 15 Dec). FTTH Handbook 2011. Available: http://www.ftthcouncil.eu/documents/Reports/FTTH-Handbook-2011-V4.1.pdf

[9] K. Tanaka, A. Agata, and Y. Horiuchi, "IEEE 802.3av 10G-EPON Standardization and Its Research and Development Status," *Lightwave Technology, Journal of,* vol. 28, pp. 651-661, 2010.

[10] M. Hajduczenia, H. J. A. Da Silva, and P. Monteiro, "Development of 10 Gb/s EPON in IEEE 802.3av," *Communications Magazine, IEEE,* vol. 46, pp. 40-47, 2008.

[11] A. Fu-Tai, K. Kyeong Soo, D. Gutierrez, S. Yam, E. Hu, K. Shrikhande, and L. G. Kazovsky, "SUCCESS: a next-generation hybrid WDM/TDM optical access network architecture," *Lightwave Technology, Journal of,* vol. 22, pp. 2557-2569, 2004.

[12] F. Saliou, P. Chanclou, F. Laurent, N. Genay, J. A. Lazaro, F. Bonada, and J. Prat, "Reach Extension Strategies for Passive Optical Networks [Invited]," *Optical Communications and Networking, IEEE/OSA Journal of,* vol. 1, pp. C51-C60, 2009.

[13] D. P. Shea and J. E. Mitchell, "Architecture to integrate multiple PONs with long reach DWDM backhaul," *Selected Areas in Communications, IEEE Journal on,* vol. 27, pp. 126-133, 2009.

[14] R. P. Davey, D. B. Grossman, M. Rasztovits-Wiech, D. B. Payne, D. Nesset, A. E. Kelly, A. Rafel, S. Appathurai, and Y. Sheng-Hui, "Long-Reach Passive Optical Networks," *Lightwave Technology, Journal of,* vol. 27, pp. 273-291, 2009.

[15] P. Ossieur, C. Antony, A. M. Clarke, A. Naughton, H. G. Krimmel, Y. Chang, C. Ford, A. Borghesani, D. G. Moodie, A. Poustie, R. Wyatt, B. Harmon, I. Lealman, G. Maxwell, D. Rogers, D. W. Smith, D. Nesset, R. P. Davey, and P. D. Townsend, "A 135-km 8192-Split Carrier Distributed DWDM-TDMA PON With 2 x 32 x 10 Gb/s Capacity," *Lightwave Technology, Journal of,* vol. 29, pp. 463-474, 2011.

[16] G. Williamson, "The challenge of the demand for access to the digital home - The Journey to an Open Access Network," in *IET Next Generation Networks Conference*, London, UK, 2007.

[17] S. Huan, K. Byoung-Whi, and B. Mukherjee, "Long-reach optical access networks: A survey of research challenges, demonstrations, and bandwidth assignment mechanisms," *Communications Surveys & Tutorials, IEEE,* vol. 12, pp. 112-123, 2010.

[18] D. E. A. Clarke and T. Kanada, "Broadband: the last mile," *Communications Magazine, IEEE,* vol. 31, pp. 94-100, 1993.

[19] D. W. Faulkner, D. B. Payne, J. R. Stern, and J. W. Ballance, "Optical networks for local loop applications," *Lightwave Technology, Journal of,* vol. 7, pp. 1741-1751, 1989.

[20] ITU-T, "Recommendation G.987: 10-Gigabit-capable passive optical network (XG-PON) systems: Definitions, abbreviations, and acronyms," ed: International Telecommunication Union, 2010.

[21] "IEEE Standard for Information technology - Telecommunications and information exchange between systems - Local and metropolitan area networks - Specific requirements Part 3: Carrier Sense Multiple Access with Collision Detection (CSMA/CD) Access Method and Physical Layer Specifications Amendment 1: Physical Layer Specifications and Management Parameters for 10 Gb/s Passive Optical Networks," *IEEE Std 802.3av-2009 (Amendment to IEEE Std 802.3-2008),* pp. c1-214, 2009.

[22] D. Breuer, F. Geilhardt, Hu, x, R. lsermann, M. Kind, C. Lange, T. Monath, and E. Weis, "Opportunities for next-generation optical access," *Communications Magazine, IEEE,* vol. 49, pp. s16-s24, 2011.

[23] D. P. Shea and J. E. Mitchell, "Long-Reach Optical Access Technologies," *Network, IEEE,* vol. 21, pp. 5-11, 2007.

[24] B. Cao, D. P. Shea, and J. E. Mitchell, "Wavelength Converting Optical Access Network for 10Gbit/s PON," presented at the The 15th International Conference on Optical Networking Design and Modeling, Bologna, Italy, 2011.

[25] M. Maier, "WDM Passive Optical Networks and Beyond: the Road Ahead [Invited]," *Optical Communications and Networking, IEEE/OSA Journal of,* vol. 1, pp. C1-C16, 2009.

[26] C. Bock, J. A. Lazaro, and J. Prat, "Extension of TDM-PON Standards to a Single-Fiber Ring Access Network Featuring Resilience and Service Overlay," *Lightwave Technology, Journal of,* vol. 25, pp. 1416-1421, 2007.

[27] J. Prat, V. Polo, J. A. Lazaro, F. Bonada, E. Lopez, B. Schrenk, M. Omella, F. Saliou, Q. T. Le, P. Chanclou, D. Leino, R. Soila, S. Spirou, L. Costa, A. Teixeira, G. M. Tosi-Beleffi, D. Klonidis, and I. Tomkos, "Demonstration and field trial of a scalable resilient hybrid ngPON," in *Optical Communication (ECOC), 2011 37th European Conference and Exhibition on,* 2011, pp. 1-3.

[28] S. Dahlfort, "Comparison of 10 Gbit/s PON vs WDM-PON," in *Optical Communication, 2009. ECOC '09. 35th European Conference on*, 2009, pp. 1-2.
[29] ITU-T, "Recommendation G.984.2 : 'Gigabit-capable Passive Optical Networks (GPON): Physical Media Dependent (PMD) layer specification'," ed: International Telecommunication Union, 2003.
[30] S. Chao, C. Lian-Kuan, and C. Kwok-Wai, "Theory of burst-mode receiver and its applications in optical multiaccess networks," *Lightwave Technology, Journal of*, vol. 15, pp. 590-606, 1997.
[31] T. Nakanishi, K. I. Suzuki, Y. Fukada, N. Yoshimoto, M. Nakamura, K. Kato, K. Nishimura, Y. Ohtomo, and M. Tsubokawa, "High sensitivity APD burst-mode receiver for 10Gbit/s TDM-PON system," *IEICE Electronics Express*, vol. 4, pp. 588-592, 2007.
[32] H. Wessing, B. Sorensen, B. Lavigne, E. Balmefrezol, and O. Leclerc, "Combining control electronics with SOA to equalize packet- to-packet power variations for optical 3R regeneration in optical networks at 10 Gbit/s," in *Optical Fiber Communication Conference, 2004. OFC 2004*, 2004.
[33] B. C. Thomsen, B. J. Puttnam, and P. Bayvel, "Optically equalized 10 Gb/s NRZ digital burstmode receiver for dynamic optical networks," *Opt. Express*, vol. 15, pp. 9520-9526, 2007.
[34] A. V. Tran, C. J. Chae, and R. S. Tucker, "Optical packet power equalization with large dynamic range using controlled gain-clamped SOA," in *Optical Fiber Communication Conference, 2005. Technical Digest. OFC/NFOEC*, 2005, p. 3 pp. Vol. 1.
[35] R. Sato, T. Ito, Y. Shibata, A. Ohki, and Y. Akatsu, "40-gb/s burst-mode optical 2R regenerator," *Photonics Technology Letters, IEEE*, vol. 17, pp. 2194-2196, 2005.
[36] W. Xing, Y. Su, L. Xiang, J. Leuthold, and S. Chandrasekhar, "10-Gb/s RZ-DPSK transmitter using a saturated SOA as a power booster and limiting amplifier," *Photonics Technology Letters, IEEE*, vol. 16, pp. 1582-1584, 2004.
[37] M. Zirngibl, "An optical power equalizer based on one Er-doped fiber amplifier," *Photonics Technology Letters, IEEE*, vol. 4, pp. 357-359, 1992.
[38] C. R. Giles, E. Desurvire, and J. R. Simpson, "Transient gain and cross talk in erbium-doped fiber amplifiers," *Opt. Lett.*, vol. 14, pp. 880-882, 1989.
[39] D. P. Shea and J. E. Mitchell, "A 10-Gb/s 1024-Way-Split 100-km Long-Reach Optical-Access Network," *Lightwave Technology, Journal of*, vol. 25, pp. 685-693, 2007.
[40] H. Xiaobin, H. Weiping, and W. Jian, "Burst mode receiver based on SOA," in *Optical Fiber Communication and Optoelectronics Conference, 2007 Asia*, 2007, pp. 324-326.
[41] S. V. Pato, R. Meleiro, D. Fonseca, P. Andre, P. Monteiro, and H. Silva, "All-Optical Burst-Mode Power Equalizer Based on Cascaded SOAs for 10-Gb/s EPONs," *Photonics Technology Letters, IEEE*, vol. 20, pp. 2078-2080, 2008.
[42] G. P. Agrawal and N. A. Olsson, "Self-phase modulation and spectral broadening of optical pulses in semiconductor laser amplifiers," *Quantum Electronics, IEEE Journal of*, vol. 25, pp. 2297-2306, 1989.

[43] L. B. Kazovsky, Sergio; Willner, Alan, *Optical Fiber Communication Systems*. Massachusetts: Artech House, Inc, 1996.
[44] F. Koyama and K. Iga, "Frequency chirping in external modulators," *Lightwave Technology, Journal of,* vol. 6, pp. 87-93, 1988.
[45] N. A. Olsson and G. P. Agrawal, "Spectral shift and distortion due to self-phase modulation of picosecond pulses in 1.5 mu m optical amplifiers," *Applied Physics Letters,* vol. 55, pp. 13-15, 1989.
[46] M. J. Connelly, "Wideband semiconductor optical amplifier steady-state numerical model," *Quantum Electronics, IEEE Journal of,* vol. 37, pp. 439-447, 2001.
[47] A. Mecozzi and J. Mørk, "Saturation induced by picosecond pulses in semiconductor optical amplifiers," *J. Opt. Soc. Am. B,* vol. 14, pp. 761-770, 1997.
[48] A. Mecozzi and J. Mork, "Saturation effects in nondegenerate four-wave mixing between short optical pulses in semiconductor laser amplifiers," *Selected Topics in Quantum Electronics, IEEE Journal of,* vol. 3, pp. 1190-1207, 1997.
[49] D. Cassioli, S. Scotti, and A. Mecozzi, "A time-domain computer simulator of the nonlinear response of semiconductor optical amplifiers," *Quantum Electronics, IEEE Journal of,* vol. 36, pp. 1072-1080, 2000.
[50] M. Fricke, "Examining the Evolution of the Access Network Topology," presented at the IEEE GLOBECOM, Honolulu, HI, 2009.
[51] D. Campi and C. Coriasso, "Wavelength Conversion Technologies," *Photonic Network Communications,* vol. 2, pp. 85-95, 2000.
[52] G. T. Kanellos, D. Petrantonakis, D. Tsiokos, P. Bakopoulos, P. Zakynthinos, N. Pleros, D. Apostolopoulos, G. Maxwell, A. Poustie, and H. Avramopoulos, "All-Optical 3R Burst-Mode Reception at 40 Gb/s Using Four Integrated MZI Switches," *J. Lightwave Technol.,* vol. 25, pp. 184-192, 2007.
[53] H. S. Chung, R. Inohara, K. Nishimura, and M. Usami, "All-optical multi-wavelength conversion of 10 Gbit/s NRZ/RZ signals based on SOA-MZI for WDM multicasting," *Electronics Letters,* vol. 41, pp. 432-433, 2005.
[54] J. C. Attard, J. E. Mitchell, and C. J. Rasmussen, "Performance analysis of interferometric noise due to unequally powered interferers in optical networks," *Lightwave Technology, Journal of,* vol. 23, p. 1692, 2005.
[55] P. J. Legg, M. Tur, and I. Andonovic, "Solution paths to limit interferometric noise induced performance degradation in ASK/direct detection lightwave networks," *Lightwave Technology, Journal of,* vol. 14, p. 1943, 1996.
[56] A. Arie and M. Tur, "Phase-induced intensity noise in optical interferometers excited by semiconductor lasers with non-Lorentzian lineshapes," *Lightwave Technology, Journal of,* vol. 8, pp. 1-6, 1990.
[57] J. L. Gimlett and N. K. Cheung, "Effects of phase-to-intensity noise conversion by multiple reflections on gigabit-per-second DFB laser transmission systems," *Lightwave Technology, Journal of,* vol. 7, pp. 888-895, 1989.
[58] M. Tur and E. L. Goldstein, "Dependence of error rate on signal-to-noise ratio in fiber-optic communication systems with phase-induced intensity noise," *Lightwave Technology, Journal of,* vol. 7, p. 2055, 1989.
[59] M. Tur and A. Arie, "Phase induced intensity noise in concatenated fiber-optic delay lines," *Lightwave Technology, Journal of,* vol. 6, p. 120, 1988.

[60] W. D. Cornwell and I. Andonovic, "Interferometric noise for a single interferer: comparison between theory and experiment," *Electronics Letters*, vol. 32, pp. 1501-1502, 1996.
[61] P. J. Legg, D. K. Hunter, I. Andonovic, and P. E. Barnsley, "Inter-channel crosstalk phenomena in optical time division multiplexed switching networks," *Photonics Technology Letters, IEEE*, vol. 6, p. 661, 1994.
[62] R. Meleiro, J. Castro, D. Fonseca, P. Andr é, and P. Monteiro, "In-band crosstalk penalties in optical networks with narrow optical and electric filtering," *Opt. Express*, vol. 17, pp. 4605-4610, 2009.
[63] P. J. Legg, "The impact of interferometric noise on the performance of optical communication networks," Ph.D Thesis, Electronic and Electrical Eng. Dept., University of Strathclyde, Glasgow, U.K., 1995.
[64] A. Arie, M. Tur, and E. L. Goldstein, "Probability-density function of noise at the output of a two-beam interferometer," *J. Opt. Soc. Am. A*, vol. 8, pp. 1936-1942, 1991.
[65] E. L. Goldstein, L. Eskildsen, C. Lin, and Y. Silberberg, "Polarization statistics of crosstalk-induced noise in transparent lightwave networks," *Photonics Technology Letters, IEEE*, vol. 7, pp. 1345-1347, 1995.
[66] T. R. Anselm Deninger. (2010, Accessed on 26 Nov 2011). 12 Orders of Coherence Control: Tailoring the coherence length of diode lasers Available: http://www.toptica.com/uploads/media/toptica_AP_1010_coherence_control_2010_03.pdf
[67] I. T. Monroy, E. Tangdiongga, and H. d. Waardt, "On the Distribution and Performance Implications of Filtered Interferometric Crosstalk in Optical WDM Networks," *J. Lightwave Technol.*, vol. 17, p. 989, 1999.
[68] M. E. V. Valkenburg, *Analog Filter Design*. Oxford: Oxford University Press, 1982.
[69] X. Yin, X. Z. Qiu, J. Gillis, J. Put, J. Verbrugghe, J. Bauwelinck, J. Vandewege, F. Blache, D. Lanteri, M. Achouche, H. Krimmel, D. van Veen, and P. Vetter, "DC-coupled burst-mode receiver with high sensitivity, wide dynamic range and short settling time for symmetric 10G-GPONs," in *Optical Communication (ECOC), 2011 37th European Conference and Exhibition on*, 2011, pp. 1-3.
[70] R. M. Jopson, T. E. Darcie, K. T. Gayliard, R. T. Ku, R. E. Tench, T. C. Rice, and N. A. Olsson, "Measurement of carrier-density mediated intermodulation distortion in an optical amplifier," *Electronics Letters*, vol. 23, pp. 1394-1395, 1987.
[71] J. Gowar, *Optical Communication Systems*. Hemel Hempstead, Hertfordshire, UK: Prentice Hall Europe, 1993.
[72] M. J. Connelly, *Semiconductor Optical Amplifiers*. Boston MA: Kluwer, 2002.
[73] G. J. Borse, *Numerical methods with MATLAB : a resource for scientists and engineers*. Boston, MA: PWS Publishing Company, 1997.
[74] J. W. John E. Carroll, Dick Plumb, *Distributed Feedback Semiconductor Lasers*. London, United Kingdom: The Institution of Electrical Engineers, 1998.
[75] R. Guti érrez-Castrej ón and M. Duelk, "Modeling and simulation of semiconductor optical amplifier dynamics for telecommunication applications," in *Computer Physics Research Trends*, S. J. Bianco, Ed., ed: Nova Science Publishers, Inc, 2007.

[76] K. Inoue, "Optical filtering technique to suppress waveform distortion induced in a gain-saturated semiconductor optical amplifier," *Electronics Letters*, vol. 33, pp. 885-886, 1997.

[77] L. N. Mads, M. Jesper, S. Jun, S. Rei, and U. Yoshiyasu, "Reduction of Nonlinear Patterning Effects in SOA-Based All-Optical Switches Using Optical Filtering," in *Optical Fiber Communication Conference and Exposition and The National Fiber Optic Engineers Conference*, 2005, p. OThE7.

[78] J. M. D. Mendinueta, J. E. Mitchell, P. Bayvel, and B. C. Thomsen, "Digital multi-rate receiver for 10GE-PON and GE-PON coexistence," in *Optical Fiber Communication Conference and Exposition(OFC)*, Los Angeles, CA, 2011.

[79] T. Katsuyam. (2009, 29 March 2011). Development of Semiconductor Laser for Optical Communication. *SEI Technical Review 69*. Available: http://global-sei.com/tr/pdf/special/69-02.pdf

[80] B. A. Moller, L. Jensen, C. Laurent-Lund, and C. Thirstrup, "Silica-waveguide thermooptic phase shifter with low power consumption and low lateral heat diffusion," *Photonics Technology Letters, IEEE*, vol. 5, pp. 1415-1418, 1993.

[81] K. Inoue, T. Mukai, and T. Saitoh, "Gain saturation dependence on signal wavelength in a travelling-wave semiconductor laser amplifier," *Electronics Letters*, vol. 23, pp. 328-329, 1987.

[82] T. Durhuus, B. Mikkelsen, C. Joergensen, S. Lykke Danielsen, and K. E. Stubkjaer, "All-optical wavelength conversion by semiconductor optical amplifiers," *Lightwave Technology, Journal of*, vol. 14, pp. 942-954, 1996.

[83] T. Durhuus, C. Joergensen, B. Mikkelsen, R. J. S. Pedersen, and K. E. Stubkjaer, "All-Optical Wavelength Conversion By SOAs In A Mach-Zehnder Configuration," *IEEE Photonics Technology Letters*, vol. 6, pp. 53-55, Jan 1994.

[84] J.-M. Kang, S.-H. Lee, J.-Y. Kim, H.-C. Kwon, T.-Y. Kim, and S.-K. Han, "Theoretical investigation of the input power dynamic range enhancement of XPM wavelength converter using a CW holding beam," *Optical and Quantum Electronics*, vol. 41, pp. 349-362, 2009.

[85] N. Yan, J. del Val Puente, T. G. Silveira, A. Teixeira, A. Ferreira, E. Tangdiongga, P. Monteiro, and A. Koonen, "Simulation and Experimental Characterization of SOA-MZI-Based Multiwavelength Conversion," *Lightwave Technology, Journal of*, vol. 27, pp. 117-127, 2009.

[86] C. Schubert, R. Ludwig, and H.-G. Weber, "High-speed optical signal processing using semiconductor optical amplifiers," *Journal of Optical and Fiber Communications Research*, vol. 2, pp. 171-208, 2005.

[87] M. Hattori, K. Nishimura, R. Inohara, and M. Usami, "Bidirectional Data Injection Operation of Hybrid Integrated SOA–MZI All-Optical Wavelength Converter," *Lightwave Technology, Journal of*, vol. 25, pp. 512-519, 2007.

[88] S. C. Cao and J. C. Cartledge, "Characterization of the chirp and intensity modulation properties of an SOA-MZI wavelength converter," *Lightwave Technology, Journal of*, vol. 20, pp. 689-695, 2002.

[89] S. L. Danielsen, P. B. Hansen, K. E. Stubkjaer, M. Schilling, K. Wunstel, W. Idler, P. Doussiere, and F. Pommerau, "All optical wavelength conversion

schemes for increased input power dynamic range," *Photonics Technology Letters, IEEE,* vol. 10, pp. 60-62, 1998.

[90] A. Poustie, "SOA-based All-optical Processing," in *Optical Fiber Communication and the National Fiber Optic Engineers Conference, 2007. OFC/NFOEC 2007. Conference on*, 2007, pp. 1-38.

[91] Y. Miyazaki, T. Miyahara, K. Takagi, K. Matsumoto, S. Nishikawa, T. Hatta, T. Aoyagi, and K. Motoshima, "Polarization-Insensitive SOA-MZI Monolithic All-Optical Wavelength Converter for Full C-band 40Gbps-NRZ Operation," in *Optical Communications, 2006. ECOC 2006. European Conference on*, 2006, pp. 1-2.

[92] R. Roy, M. Hajduczenia, G. Kramer, and H. da Silva, "10G-EPON efficiency," in *Advanced Networks and Telecommunication Systems (ANTS), 2009 IEEE 3rd International Symposium on*, 2009, pp. 1-3.

[93] J. E. Mitchell, "Beat Noise and Related Phenomena in Optical Networks," PhD, Electronic and Electrical Engineering, University College London, London, 2000.

[94] C. W. Helstrom, "Approximate Evaluation of Detection Probabilities in Radar and Optical Communications," *Aerospace and Electronic Systems, IEEE Transactions on,* vol. AES-14, pp. 630-640, 1978.

[95] J. O'Reilly and J. da Rocha, "Improved error probability evaluation methods for direct detection optical communication systems," *Information Theory, IEEE Transactions on,* vol. 33, pp. 839-848, 1987.

[96] C. Joergensen, S. L. Danielsen, T. Durhuus, B. Mikkelsen, K. E. Stubkjaer, N. Vodjdani, F. Ratovelomanana, A. Enard, G. Glastre, D. Rondi, and R. Blondeau, "Wavelength conversion by optimized monolithic integrated Mach-Zehnder interferometer," *Photonics Technology Letters, IEEE,* vol. 8, pp. 521-523, 1996.

[97] K. Joo-Youp and H. Sang-Kook, "Novel automatic control for the optimum optical gain and phase difference in SOA-MZI wavelength converter," in *Quantum Electronics and Laser Science Conference, 2005. QELS '05*, 2005, pp. 981-983 Vol. 2.

[98] L. H. Spiekman, J. M. Wiesenfeld, U. Koren, B. I. Miller, and M. D. Chien, "All-optical Mach-Zehnder wavelength converter with monolithically integrated preamplifiers," *Photonics Technology Letters, IEEE,* vol. 10, pp. 1115-1117, 1998.

[99] M. L. Masanovic, V. Lal, J. A. Summers, J. S. Barton, E. J. Skogen, L. G. Rau, L. A. Coldren, and D. J. Blumenthal, "Widely tunable monolithically integrated all-optical wavelength converters in InP," *Lightwave Technology, Journal of,* vol. 23, pp. 1350-1362, 2005.

[100] J. Y. Emery, B. Lavigne, C. Porcheron, C. Janz, F. Dorgeuille, F. Pommereau, F. Gaborit, I. Guillemot-Neubauer, and M. Renaud, "Increased input power dynamic range of Mach-Zehnder wavelength converter using a semiconductor optical amplifier power equaliser with 8 dBm output saturation power," *Electronics Letters,* vol. 35, pp. 995-996, 1999.

[101] K. Morito, "Output-Level Control of Semiconductor Optical Amplifier by External Light Injection," *J. Lightwave Technol.,* vol. 23, p. 4332, 2005.